Theoretical and Experimental Studies on the Details of Cellulose Allomorphs

Satoshi NOMURA

Hokkaido University

2020

CONTENTS

Chapter 1. General Introduction

1.1. Overview of cellulose

Cellulose is one of the most abundant polymers on earth, since most plants synthesize cellulose as a component of cell walls[1]. Continuous investigation has been conducted on this natural polymer on a large-scale for its utilization as a renewable material because of the unique physical and chemical properties. The mechanical strength of cellulose enables plants to stand. It has been reported that theoretical strength of cellulose is estimated 2 to 6 GPa [2]. Cellulose cannot dissolve into normal solvents. On the other hand, cellulose can be swollen water because of hydrophilicity. Cellulose is also environmentally friendly and non-toxic. These unique characteristics are generated from the three-dimensional solid structure of cellulose. Cellulose can construct variety of structures or properties through different process like chemical treatment such as simple alkaline treatment called mercerization, dissolution and regeneration or derivatization, or physical treatment such as milling, stretching, or rolling. In particular, Cellulose Nano Fiber (CNF) and Cellulose Nano Crystal (CNC) is expected as the next-generation materials. CNF has obtained by surface modifying of cellulose and surface modified cellulose is enhanced the dispersibility[3]. CNC has been obtained by partial hydrolysis, which can only remain acicular crystals[4]. Both of CNF and CNC have large specific surface area and relatively high crystallinity. Crystallinity and surface area have been becoming also the important topic for understanding and improving the characteristic of cellulose materials.

1.2. Crystal allomorph of cellulose

Cellulose is a liner polysaccharide that is composed of β-1,4 linked glucose units. Cellulose has three hydroxyl groups per one glucose unit and the hydroxyl groups construct intra- and inter-molecular hydrogen bonds. All hydroxyl groups are located at equatorial direction and the other axial direction is occupied by aliphatic carbon. Hydroxyl groups construct hydrophilic region at equcatorial direcition of each cellulose

molecule and aliphatic hydrogen constructs hydrophobic region at the other axial direction. Hydrophilic regions construct intra- or inter-molecular hydrogen bonds and Hydrophobic regions construct hydrophobic interaction. These interactions can thought to be the most important factors for the stability of the crystal structure of cellulose. Cellulose molecules are shaped as less twisted form by intra-molecular hydrogen bonds. Intramolecular hydrogen bonds enable cellulose molecules to construct molecular sheets of cellullose supported by intermolecular hydrogen bonds. The molecular sheets, which have hydrophobic region at equatorial direction of each molecules in the sheets, can aggregated into three-dimensional stacked structure, namely crystal structure. The crystal structure can take multiple patterns. In previous studies, four types of the crystal structure of cellulose has been reported. The structures are called as cellulose I, II, III and IV.

Plants, algae and microorganisms can produce native cellulose, that has the cellulose I type crystal structure. Cellulose I consists of two kinds of crystal allomorphs called cellulose Iα and cellulose Iβ[5–11]. Cellulose I is rigid structure, which is not possible to construct such linear chain polymers like cellulose with glucans containing other types of linkages such as β-(1-3) or α-(1-4), known as β-(1-3) glucans and amylose, respectively. Cellulose regenerated from such solvents has a crystal structure called cellulose II[12–14], which differs from the original, native cellulose structure. There is another process called mercerization that is used in the textile industry to improve luster and strength, and this process can also produce cellulose II from cellulose I. Mercerization is a process in which cellulose remains in the solid state and is soaked in strong alkali solutions (e.g., NaOH)[11]. It is impossible to make cellulose I from cellulose II, suggesting that the crystal transition from cellulose I to II is irreversible. The origin of the irreversibility is still not clear, although it can be thought that cellulose II is more stable than cellulose I[1]. Among the various cellulose allomorphs, cellulose I and II are the primary allomorphs, while other allomorphs are classified as part of the cellulose I or II family, such as cellulose III_I, III_{II}, IV_I or IV_{II}. Cellulose III_I and III_{II} are prepared from cellulose I or II, respectively, by treatment with liquid ammonia[15,16] or ethylenediamine[17,18]. Cellulose IV_I and IV_{II} are prepared from

cellulose III_I and cellulose III_{II}, respectively, by heating treatment. Cellulose III_I can revert to cellulose I or II (depending on the processing conditions)[19], whereas cellulose III_{II} and IV_{II} can only return to cellulose II[20,21]. It was reported that cellulose IV_I is identical to cellulose Iβ and the result also shows cellulose III_I can revert to cellulose I. This characteristic suggests that the main allomorphs (i.e., cellulose I and II) have specific conformational differences.

1.3. The structural difference between cellulose I and II

cellulose I is irreversibly converted to cellulose II and cellulose II have not been reverted to cellulose I with today's technology. The irreversibility of the conversion can be thought to be arisen from the structural difference between cellulose I and II. The structural difference between cellulose I and II are three differences: packing manner, C6 conformation and crystallinity.

Conventionally, the difference arising the irreversibility from cellulose I to II has been explained by packing manner. The end is divided into non-reducing end (O4 end) and reducing end (O1 end). Two types of end arise molecular orientation. X-ray structural analysis shows that the main difference between cellulose I and II is their packing manner; cellulose I packs in a parallel manner, while cellulose II packs in an anti-parallel manner[6,7,13]. The change of packing manner from pararell to anti-pararell has been thought to arise the irreversibility. The mechanism of the packing manner change has been explained as In order to explain the change in packing in the solid state, a specific mechanism for mercerization has been proposed[22–24]. In this mechanism, Na ions are intercalated among cellulose molecules and each cellulose molecule behave like single chain interacting with Na ions. As a result, unit cell of cellulose with Na ions is larger than that of cellulose I.

The important criterion influencing the chain conformation and crystal structure of cellulose is the hydrogen bonding network of the three hydroxyl groups of each anhydroglucose residue. Hydrogen bonds are important for stabilizing the molecules in the crystal structure of cellulose. One of the most important molecular

conformational differences between cellulose I and II is hydroxymethyl conformation at the C6 position (Fig. 1-1). The conformation of hydroxymethyl in cellulose I is called *tg (trans-gauche),* and of cellulose II is *gt (gauche-trans)*[25]. The difference in hydroxymethyl conformation orients the spatial O6-H bond direction differently, which changes the hydrogen bond network with other hydroxyl groups. In a molecule with a complicated hydrogen bonding network such as cellulose, it is also very important to confirm which hydroxyl group is the proton donor or acceptor. However, it is difficult to unequivocally determine hydrogen position or hydrogen bond patterns from the X-ray diffraction analysis of cellulose. The only direct detection method for locating hydrogen atoms is the neutron diffraction analysis. Nishiyama et al. revealed by neutron diffraction that there are two types of hydrogen bonding systems in cellulose I, A and B types[26,27]. Both types of hydrogen bonding systems have oxygen and hydrogen atoms associated with O3/O5' and O2'/O6 intramolecular hydrogen bonds between adjacent residues (Fig. 1-2a and 1-2b), in which the A type has O2'-H…O6 intramolecular hydrogen bonds while the B type has O2'…H-O6.

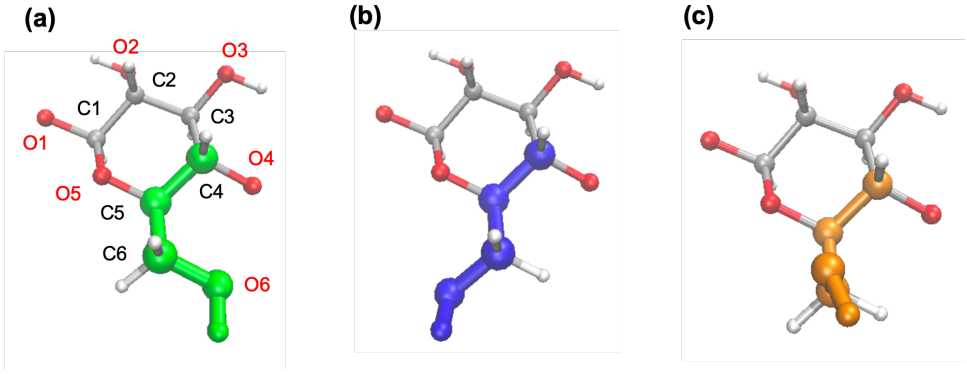

Fig. 1-1. Structure of each C6 conformation: (A) *tg*, (B) *gt*, and (C) *gg*.

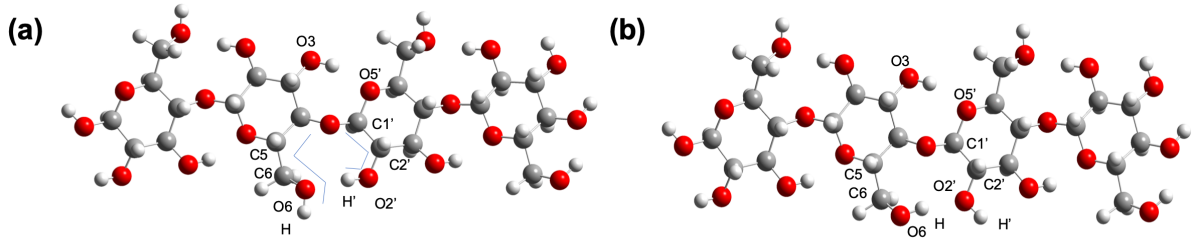

Fig. 1-2. Structure of tg-A type (a) and *tg*-B type hydrogen bond in cellulose molecules.

1.4. The crystallinity and surface structure of cellulose

It has been reported that both crystalline and coexistence of ordered and disordered regions [28].Cellulose constructs a hierarchical structure. Primary structure is a molecule which construct intra-molecular hydrogen bonds and barely twisting structure. Secondary structure is called as microfibril, which is consisted by single crystal. Microfibril was directly observed by Scanning electron microscopy or transition electron microscopy [29–31]. Finally, microfibril is aggregated and twisted to construct a ribbon.

It can be thought that microfibril is glued by adhesion of surface structure and solvents surrounded by the microfibril no longer access the glued surface. The surface is called as inaccessible surface. On the other hand, outermost surface of microfibril is always be accessed by surrounded solvents, thereby the outermost surface is called accessible surface. The schematic images of crystal core and surface structures are shown in Fig.1-3. Surface peaks in solid state ^{13}C NMR were reported by Newman et. al. [32]. Accessible surface and inaccessible surface have been reported first by Lassorn et. al. [33], with solid state ^{13}C CP/MAS NMR spectra of cellulose I. The model is correspond to cellulose in the cell wall model[34]. The surface structures of cellulose II have also been reported and hydrolysis of cellulose II by acids decreases non-crystalline region ratio accompanied by increasing crystallinity[35,36]. It has already been reported mercerization as post-treatment with low concentration of NaOH improves the crystallinity of regenerated cellulose fibers [37,38]. This report discussed that amorphous or quasi-crystal region was re-organized with constructing hydrogen bond network by the analysis using Fourier-transition infrared spectroscopy and post-treatment with low concentration NaOH is effective process for improving cellulose II assembly and mechanical structure of regenerated or mercerized cellulose material, which is composed of cellulose II crystalline and other non-negligible amount of disordered structure.

Although native cellulose shows high crystallinity and high mechanical properties, regenerated or mercerized cellulose shows less crystallinity of mechanical strength [39]. The solvents and regeneration methods used for

cellulose have been investigated previously, with the aim being to improve the overall process and the properties of the regenerated cellulose [40].

The crystallinity of cellulose is caused by separated hydrophobic and hydrophilic region of each molecule. It has been reported that hydrophobic effects between the cellulose molecules is important for the crystallization [41,42]. A more ordered cellulose is regenerated when higher polarity coagulation mediums are used (acetone < EtOH < MeOH < aqueous solutions of Na_2SO_4 and H_2SO_4). It can be thought that excessive polarity of solvents (i.e. ionic liquid) resulted in dissolution or disordering of cellulose and moderated polarity of solvents stimulates crystallization of cellulose molecules by inducing hydrophobic interaction. Artificially synthesized cello-oligomers were crystallized by inducing hydrophobic effects by adding a alkyl chain to the reducing end of the cellulose molecules, with which even cellulose I could be crystallized [43]. Moreover, the rehydration of the regenerated cellulose improves crystallinity [41,44]. Water may only interact with the hydrophilic part such as amorphous region or surface of the cellulose II crystals. The surface area is classified into accessible and inaccessible areas [35,45], and the inaccessible surface may remain, even after re-hydration. Thus, the further modifications mechanism improving the crystallinity of already prepared cellulose II are required.

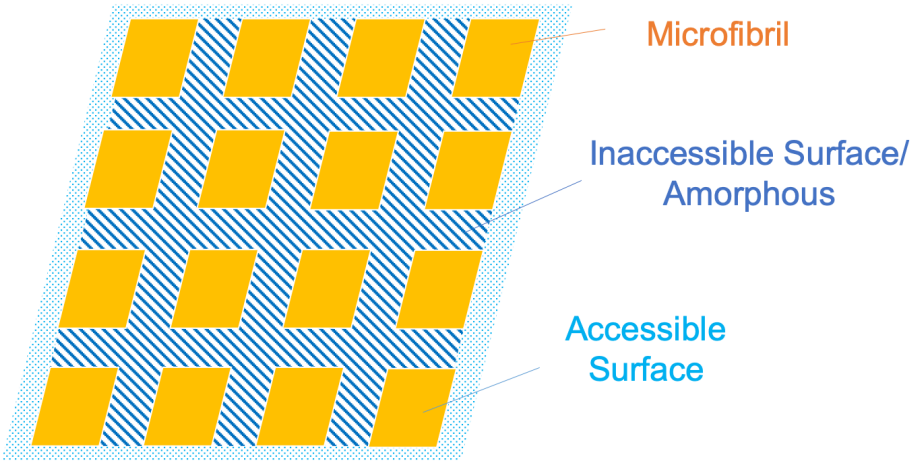

Fig. 1-3 Schematic image of cellulose ribbon consisted by microfibril (crystal), accessible surface and inaccessible surface.

1.5. Computational study of cellulose

In recent years, as the computational power of computers has increased, modeling studies have also advanced rapidly. In particular, molecular dynamics (MD) and quantum mechanics (QM) simulations with density functional theory (DFT) have become some of the most powerful methods to analyze the potential energy related to the stability of molecular structures or crystals, with many studies of MD and QM simulations on cellulose already reported[46–50]. In general, a hydrogen bond is comprised of a proton donor and acceptor as mentioned previously. Nishiyama et al. showed that the A type is more energetically stable than the B type by QM, and that the A type is suitable for cellulose Iβ by MD[26]. Based on this result, cellulose Iβ sheets or crystal structures were calculated using QM or MD with various force fields[46–48]. DFT calculations combained with sum frequency generation spectroscopy has also been researched for elucidating hydrogen bonds system and molecular conformation[51,52]. Since QM require a vast number of calculation compared to MD, various type of small models have been suggested and calculated for elucidating the stability of intra- or inter- molecular hydrogen bonds regarding cellulose I, II or III[46,53–56]. Some of the calculations revealed that cellulose Iβ structures could not maintain *tg* conformations, while other calculations indicated that at least 18 cellulose chains are necessary to maintain the *tg* conformation in cellulose Iβ crystal models [57–59] with *gt* or *gg* conformation on the surface of the crystal model[56,60–62]. These computational results suggest that the *tg* conformation has some unstable characteristics.

The change in the hydrogen bonding patterns in relation to the C6 conformation under mercerization conditions remains largely unclear. As mentioned above, intermolecular hydrogen bonds are interrupted by Na ions and each cellulose molecule behaves like single chain during mercerization. The C6 conformation and intramolecular hydrogen bonding can be changed when each cellulose molecule behaves like single chain. With the *gt* conformation, O6 (O/H) can form a hydrogen bond with O3' (O/H) of the adjacent residue, and it will be also possible that O6 and O3 in the *gt* conformation have both A type and B type hydrogen bonding systems,

similar to the *tg* conformation. From neutron diffraction analysis, cellulose II has only the A type hydrogen bonding system, whereas B type is also possible in disordered or meta-stable states[13]. MD simulations starting with the *gt*-A type conformation resulted in molecular sheets that correspond to one layer of the cellulose II crystal [54] .

1.6. Objective and outlines of the thesis

As described above, Cellulose I and II has a lot of differences. Lower crystallinity of cellulose II compared to cellulose I can be thought to be related to the surface structure of cellulose II. For improving the crystallinity of cellulose II, hydrophobic effect is a key role for comparing the crystallization process. Another difference between cellulose I and II is C6 conformation. Since C6 conformation is primary stabilized by intra-molecular hydrogen bond, intra-molecular hydrogen bond disruption is needed for rotating O6. Hydrogen bonds disruption and construction is expressed as rotating hydroxyl proton and C6 conformational change is expressed as rotation of hydroxymethyl oxygen. These rotations are related to the change of total energy of molecules.

C6 conformation is directly related to hydrogen bonding and C6 conformational change can be accompanied by hydrogen bonding reconstruction.

In chapter 1, the overview of cellulose as materials and the allomorph of cellulose were introduced. In addition, surface structure has been attracted for elucidating the crystallinity of cellulose. C6 conformation and hydrogen bonding system is also expressed as the main difference between cellulose I and II. In chapter 2, the change of surface structure caused by mercerization was analyzed. It was shown that non-crystalline region was constructed surrounding the crystal core. It was also shown that perfect mercerization was optimized for breaking cellulose I and constructing mainly non-crystalline surface structure. In chapter 3, the mechanism of improving cellulose II crystallinity by low-concentration NaOH post-treatment was analyzed by solid state ^{13}C NMR and X-ray diffraction. Improving crystallinity was caused by decreasing surface structure and increasing

crystal size. Optimization of post-treat temperature and neutralization was also carried out. In chapter 4, the C6 conformational change from *tg* to *gt* was calculated using DFT. *tg* is only stable when hydrogen bond is constructed and the structure which has no hydrogen bond around O6 was shown as transition state for constructing *gt*. It was also shown that *gt* is difficult to return *tg* because hydrogen bonds can be reconstructed rather than C6 conformation changing. It has possibility that *tg* conformation can be constructed from *gg* conformation via meta-stable *gg* state. Finally, Na ion, which is one of the most common positive ions on mercerization, was introduced in the model and it was shown that Na ion can disrupt hydrogen bond between O2 and O6. In chapter 5, the results in this study was summarized.

References

[1] D. Klemm, B. Heublein, H.P. Fink, A. Bohn, Cellulose: Fascinating biopolymer and sustainable raw material, Angewandte Chemie - International Edition. 44 (2005) 3358–3393. doi:10.1002/anie.200460587.

[2] T. Saito, R. Kuramae, J. Wohlert, L.A. Berglund, A. Isogai, An ultrastrong nanofibrillar biomaterial: The strength of single cellulose nanofibrils revealed via sonication-induced fragmentation, Biomacromolecules. 14 (2013) 248–253. doi:10.1021/bm301674e.

[3] A. Isogai, T. Saito, H. Fukuzumi, TEMPO-oxidized cellulose nanofibers, Nanoscale. 3 (2011) 71–85. doi:10.1039/c0nr00583e.

[4] Y. Habibi, L.A. Lucia, O.J. Rojas, Cellulose nanocrystals: Chemistry, self-assembly, and applications, Chemical Reviews. 110 (2010) 3479–3500. doi:10.1021/cr900339w.

[5] H. Kono, S. Yunoki, T. Shikano, M. Fujiwara, T. Erata, M. Takai, CP/MAS 13C NMR study of cellulose and cellulose derivatives. 1 . Complete assignment of the CP/MAS 13C NMR spectrum of the native cellulose, Journal of the American Chemical Society. 124 (2002) 7506–7511. doi:10.1021/ja010704o.

[6] Y. Nishiyama, J. Sugiyama, H. Chanzy, P. Langan, Crystal Structure and Hydrogen Bonding System in Cellulose Iα from Synchrotron X-ray and Neutron Fiber Diffraction, Journal of the American Chemical Society. 125 (2003) 14300–14306. doi:10.1021/ja037055w.

[7] Y. Nishiyama, P. Langan, H. Chanzy, Crystal Structure and Hydrogen-Bonding System in Cellulose Iβ from Synchrotron X-ray and Neutron Fiber Diffraction, Journal of the American Chemical Society. 124 (2002) 9074–9082. doi:10.1021/ja0257319.

[8] R.H. Atalla, D.L. VanderHart, Native cellulose: A composite of two distinct crystalline forms, Science. 223 (1984) 283–285. doi:10.1126/science.223.4633.283.

[9] A. Isogai, M. Usuda, T. Kato, T. Uryu, R.H. Atalla, Solid-State CP/MAS 13C NMR Study of Cellulose Polymorphs, Macromolecules. 22 (1989) 3168–3172. doi:10.1021/ma00197a045.

[10] A. Sarko, R. Muggli, Packing Analysis of Carbohydrates and Polysaccharides. III. Valonia Cellulose and Cellulose II, Macromolecules. 7 (1974) 486–494. doi:10.1021/ma60040a016.

[11] F.J. Kolpak, M. Weih, J. Blackwell, Mercerization of cellulose: 1. Determination of the structure of Mercerized cotton, Polymer. 19 (1978) 123–131. doi:10.1016/0032-3861(78)90027-7.

[12] P. Langan, Y. Nishiyama, H. Chanzy, X-ray structure of mercerized cellulose II at 1 Å resolution, Biomacromolecules. 2 (2001) 410–416. doi:10.1021/bm005612q.

[13] P. Langan, Y. Nishiyama, H. Chanzy, A revised structure and hydrogen-bonding system in cellulose II from a neutron fiber diffraction analysis, Journal of the American Chemical Society. 121 (1999) 9940–9946. doi:10.1021/ja9916254.

[14] H. Kono, Y. Numata, T. Erata, M. Takai, 13C and1H resonance assignment of mercerized cellulose II by two-dimensional MAS NMR spectroscopies, Macromolecules. 37 (2004) 5310–5316. doi:10.1021/ma030465k.

[15] M. Wada, H. Chanzy, Y. Nishiyama, P. Langan, Cellulose III I crystal structure and hydrogen bonding by synchrotron X-ray and neutron fiber diffraction, Macromolecules. 37 (2004) 8548–8555. doi:10.1021/ma0485585.

[16] M. Wada, L. Heux, Y. Nishiyama, P. Langan, X-ray Crystallographic, Scanning Microprobe X-ray Diffraction, and Cross-Polarized/Magic Angle Spinning 13C NMR Studies of the Structure of Cellulose IIIII Masahisa, Biomacromolecules. 10 (2009) 302–309.

[17] H. Kono, T. Erata, M. Takai, Complete assignment of the CP/MAS 13C NMR spectrum of cellulose IIII, Macromolecules. 36 (2003) 3589–3592. doi:10.1021/ma021015f.

[18] M. Wada, G.J. Kwon, Y. Nishiyama, Structure and thermal behavior of a cellulose I-ethylenediamine complex, Biomacromolecules. 9 (2008) 2898–2904. doi:10.1021/bm8006709.

[19] M. Wada, In situ observation of the crystalline transformation from cellulose IIII to Iβ, Macromolecules. 34 (2001) 3271–3275. doi:10.1021/ma0013354.

[20] J. Hayashi, A. Sufoka, J. Ohkita, S. Watanabe, The confirmation of existences of cellulose IIII, IIIII, IVI, and IVII by the X-ray method, Journal of Polymer Science: Polymer Letters Edition. 13 (1973) 23–27. doi:10.1002/pol.1975.130130104.

[21] R. Hori, M. Wada, The thermal expansion of cellulose II and IIIII crystals, Cellulose. 13 (2006) 281–290. doi:10.1007/s10570-005-9038-8.

[22] T. Okano, A. Sarko, Intermediates and a Possible Mercerization Mechanism, Jouranal of Applied Polymer Science. 30 (1985) 325–332.

[23] H. Shibazaki, S. Kuga, T. Okano, Mercerization and acid hydrolysis of bacterial cellulose, Cellulose. 4 (1997) 75–87. doi:10.1023/A:1024273218783.

[24] H. Nishimura, T. Okano, A. Sarko, Mercerization of Cellulose. 5. Crystal and Molecular Structure of Na-Cellulose I, Macromolecules. 24 (1991) 759–770. doi:10.1021/ma00003a020.

[25] F. Horii, A. Hirai, R. Kitamaru, Solid-state 13C-NMR study of conformations of oligosaccharides and cellulose - Conformation of CH2OH group about the exo-cyclic C-C bond, Polymer Bulletin. 10 (1983) 357–361. doi:10.1007/BF00281948.

[26] Y. Nishiyama, G.P. Johnson, A.D. French, V.T. Forsyth, P. Langan, Neutron Crystallography , Molecular Dynamics , and Quantum Cellulose I, Biomacromolecules. 9 (2008) 3133–3140. doi:10.1021/bm800726v.

[27] P. Chen, Y. Nishiyama, J.L. Putaux, K. Mazeau, Diversity of potential hydrogen bonds in cellulose I revealed by molecular dynamics simulation, Cellulose. 21 (2014) 897–908. doi:10.1007/s10570-013-0053-x.

[28] P. Chen, C. Terenzi, I. Furó, L.A. Berglund, J. Wohlert, Quantifying Localized Macromolecular Dynamics within Hydrated Cellulose Fibril Aggregates, Macromolecules. 52 (2019) 7278–7288. doi:10.1021/acs.macromol.9b00472.

[29] J. Sugiyama, R. Vuong, H. Chanzy, Electron Diffraction Study on the Two Crystalline Phases Occurring in Native Cellulose from an Algal Cell Wall, Macromolecules. 24 (1991) 4168–4175. doi:10.1021/ma00014a033.

[30] T. Imai, J.L. Putaux, J. Sugiyama, Geometric phase analysis of lattice images from algal cellulose microfibrils, Polymer. 44 (2003) 1871–1879. doi:10.1016/S0032-3861(02)00861-3.

[31] J. Sugiyama, H. Harada, Y. Fujiyoshi, N. Uyeda, Lattice images from ultrathin sections of cellulose microfibrils in the cell wall of Valonia macrophysa Kütz., Planta. 166 (1985) 161–168. doi:10.1007/BF00397343.

[32] R.H. Newman, J.A. Hemmingson, Carbon-13 NMR distinction between categories of molecular order and disorder in cellulose, Cellulose. 2 (1995) 95–110. doi:10.1007/BF00816383.

[33] K. Wickholm, P.T. Larsson, T. Iversen, Assignment of non-crystalline forms in cellulose I by CP/MAS 13C NMR spectroscopy, Carbohydrate Research. 312 (1998) 123–129. doi:10.1016/S0008-6215(98)00236-5.

[34] D. Fengel, Ideas on the ultrastructural organization of the cell wall components, Journal of Polymer Science Part C: Polymer Symposia. 36 (2007) 383–392. doi:10.1002/polc.5070360127.

[35] G. Zuckerstätter, N. Terinte, H. Sixta, K.C. Schuster, Novel insight into cellulose supramolecular structure through 13C CP-MAS NMR spectroscopy and paramagnetic relaxation enhancement, Carbohydrate Polymers. 93 (2013) 122–128. doi:10.1016/j.carbpol.2012.05.019.

[36] R.H. Newman, T.C. Davidson, Molecular conformations at the cellulose-water interface, Cellulose. 11 (2004) 23–32. doi:10.1023/B:CELL.0000014778.49291.c6.

[37] J. Široký, R.S. Blackburn, T. Bechtold, J. Taylor, P. White, Attenuated total reflectance Fourier-transform Infrared spectroscopy analysis of crystallinity changes in lyocell following continuous treatment with sodium hydroxide, Cellulose. 17 (2010) 103–115. doi:10.1007/s10570-009-9378-x.

[38] X. Colom, F. Carrillo, Crystallinity changes in lyocell and viscose-type fibres by caustic treatment, European Polymer Journal. 38 (2002) 2225–2230. doi:10.1016/S0014-3057(02)00132-5.

[39] C. Djahedi, L.A. Berglund, J. Wohlert, Molecular deformation mechanisms in cellulose allomorphs and the role of hydrogen bonds, Carbohydrate Polymers. 130 (2015) 175–182. doi:10.1016/j.carbpol.2015.04.073.

[40] H.P. Fink, P. Weigel, H.J. Purz, J. Ganster, Structure formation of regenerated cellulose materials from NMMO-solutions, Progress in Polymer Science (Oxford). 26 (2001) 1473–1524. doi:10.1016/S0079-6700(01)00025-9.

[41] Å. Östlund, A. Idström, C. Olsson, P.T. Larsson, L. Nordstierna, Modification of crystallinity and pore size distribution in coagulated cellulose films, Cellulose. 20 (2013) 1657–1667. doi:10.1007/s10570-013-9982-7.

[42] N. Isobe, U.J. Kim, S. Kimura, M. Wada, S. Kuga, Internal surface polarity of regenerated cellulose gel depends on the species used as coagulant, Journal of Colloid and Interface Science. 359 (2011) 194–201. doi:10.1016/j.jcis.2011.03.038.

[43] Y. Yataka, T. Sawada, T. Serizawa, Multidimensional Self-Assembled Structures of Alkylated Cellulose Oligomers Synthesized via in Vitro Enzymatic Reactions, Langmuir. 32 (2016) 10120–10125. doi:10.1021/acs.langmuir.6b02679.

[44] E. Kontturi, A. Meriluoto, P.A. Penttilä, N. Baccile, J.M. Malho, A. Potthast, T. Rosenau, J. Ruokolainen, R. Serimaa, J. Laine, H. Sixta, Degradation and Crystallization of Cellulose in Hydrogen Chloride Vapor for High-Yield Isolation of Cellulose Nanocrystals, Angewandte Chemie - International Edition. 55 (2016) 14455–14458. doi:10.1002/anie.201606626.

[45] P.T. Larsson, K. Wickholm, T. Iversen, A CP/MAS 13 C NMR investigation of molecular ordering in celluloses, Carbohydrate Research. 302 (1997) 19–25. doi:10.1016/S0008-6215(97)00130-4.

[46] P. Chen, Y. Ogawa, Y. Nishiyama, M. Bergenstråhle-Wohlert, K. Mazeau, Alternative hydrogen bond models of cellulose II and IIII based on molecular force-fields and density functional theory, Cellulose. 22 (2015) 1485–1493. doi:10.1007/s10570-015-0589-z.

[47] D.C. Glass, K. Moritsugu, X. Cheng, J.C. Smith, REACH coarse-grained simulation of a cellulose fiber, Biomacromolecules. 13 (2012) 2634–2644. doi:10.1021/bm300460f.

[48] J.F. Matthews, G.T. Beckham, M. Bergenstråhle-Wohlert, J.W. Brady, M.E. Himmel, M.F. Crowley, Comparison of cellulose Iβ simulations with three carbohydrate force fields, Journal of Chemical Theory and Computation. 8 (2012) 735–748. doi:10.1021/ct2007692.

[49] K. Mazeau, L. Heux, Molecular dynamics simulations of bulk native crystalline and amorphous structures of cellulose, Journal of Physical Chemistry B. 107 (2003) 2394–2403. doi:10.1021/jp0219395.

[50] T. Uto, S. Mawatari, T. Yui, Theoretical study of the structural stability of molecular chain sheet models of cellulose crystal allomorphs, Journal of Physical Chemistry B. 118 (2014) 9313–9321. doi:10.1021/jp503535d.

[51] M. Makarem, C.M. Lee, K. Kafle, S. Huang, I. Chae, H. Yang, J.D. Kubicki, S.H. Kim, Probing cellulose structures with vibrational spectroscopy, Springer Netherlands, 2019. doi:10.1007/s10570-018-2199-z.

[52] C.M. Lee, J.D. Kubicki, B. Fan, L. Zhong, M.C. Jarvis, S.H. Kim, Hydrogen-Bonding Network and OH Stretch Vibration of Cellulose: Comparison of Computational Modeling with Polarized IR and SFG Spectra, Journal of Physical Chemistry B. 119 (2015) 15138–15149. doi:10.1021/acs.jpcb.5b08015.

[53] D. Hayakawa, Y. Nishiyama, K. Mazeau, K. Ueda, Evaluation of hydrogen bond networks in cellulose Iβ and II crystals using density functional theory and Car–Parrinello molecular dynamics, Carbohydrate Research. 449 (2017) 103–113. doi:10.1016/j.carres.2017.07.001.

[54] H. Miyamoto, M. Umemura, T. Aoyagi, C. Yamane, K. Ueda, K. Takahashi, Structural reorganization of molecular sheets derived from cellulose II by molecular dynamics simulations, Carbohydrate Research. 344 (2009) 1085–1094. doi:10.1016/j.carres.2009.03.014.

[55] P. Chen, M. Marianski, C. Baldauf, H-Bond Isomerization in Crystalline Cellulose IIII: Proton Hopping versus Hydroxyl Flip-Flop, ACS Macro Letters. 5 (2016) 50–54. doi:10.1021/acsmacrolett.5b00837.

[56] H. Yang, T. Wang, D. Oehme, L. Petridis, M. Hong, J.D. Kubicki, Structural factors affecting 13C NMR chemical shifts of cellulose: a computational study, Cellulose. 25 (2018) 23–36. doi:10.1007/s10570-017-1549-6.

[57] J.L. Hill, M.B. Hammudi, M. Tien, The arabidopsis cellulose synthase complex: A proposed hexamer of cesa trimers in an equimolar stoichiometryw, Plant Cell. 26 (2014) 4834–4842. doi:10.1105/tpc.114.131193.

[58] B.T. Nixon, K. Mansouri, A. Singh, J. Du, J.K. Davis, J. Lee, E. Slabaugh, V.G. Vandavasi, H.O. Neill, E.M. Roberts, A.W. Roberts, Y.G. Yingling, C.H. Haigler, Comparative Structural and Computational Analysis Supports Eighteen Cellulose Synthases in the Plant Cellulose Synthesis Complex, Nature Publishing Group. (2016) 1–14. doi:10.1038/srep28696.

[59] J.D. Kubicki, H. Yang, D. Sawada, H. O'Neill, D. Oehme, D. Cosgrove, The Shape of Native Plant Cellulose Microfibrils, Scientific Reports. 8 (2018) 4–11. doi:10.1038/s41598-018-32211-w.

[60] D.M. Harris, K. Corbin, T. Wang, R. Gutierrez, A.L. Bertolo, C. Petti, D.M. Smilgies, J.M. Estevez, D. Bonetta, B.R. Urbanowicz, D.W. Ehrhardt, C.R. Somerville, J.K.C. Rose, M. Hong, S. DeBolt, Cellulose microfibril crystallinity is reduced by mutating C-terminal transmembrane region residues CESA1 A903V and CESA3 T942I of cellulose synthase, Proceedings of the National Academy of Sciences of the United States of America. 109 (2012) 4098–4103. doi:10.1073/pnas.1200352109.

[61] T. Wang, H. Yang, J.D. Kubicki, M. Hong, Cellulose Structural Polymorphism in Plant Primary Cell Walls Investigated by High-Field 2D Solid-State NMR Spectroscopy and Density Functional Theory Calculations, Biomacromolecules. 17 (2016) 2210–2222. doi:10.1021/acs.biomac.6b00441.

[62] P. Phyo, T. Wang, Y. Yang, H. O'Neill, M. Hong, Direct Determination of Hydroxymethyl Conformations of Plant Cell Wall Cellulose Using 1 H Polarization Transfer Solid-State NMR, Biomacromolecules. 19 (2018) 1485–1497. doi:10.1021/acs.biomac.8b00039.

[63] Y. Nishiyama, Structure and properties of the cellulose microfibril, Journal of Wood Science. 55 (2009) 241–249. doi:10.1007/s10086-009-1029-1.

[64] J. Cai, L. Zhang, J. Zhou, H. Qi, H. Chen, T. Kondo, X. Chen, B. Chu, Multifilament fibers based on dissolution of cellulose in NaOH/urea aqueous solution: structure and properties, Advanced Materials. 19 (2007) 821–825. doi:10.1002/adma.200601521.

[65] J. Zhou, L. Zhang, Solubility of Cellulose in NaOH / Urea Aqueous Solution, Polymer Journal. 32 (2000) 866–870.

Chapter 2. Analysis of crystallinity change during mercerization of bacterial cellulose

2.1. Introduction

Mercerization is the method that cellulose I is converted to cellulose II by soaking cellulose I with alkaline aqueous solution. The most commonly used alkali is sodium hydroxide (NaOH) and only NaOH is used as alkali for mercerization in later discussion. Mercerization proceeds by increasing the concentration of NaOH and the degree of conversion from cellulose I to II is depend on the source of cellulose I such as plants, trees, bacteria, algae and so on. The variety of source of cellulose makes the difference of microfibril size, the ratio of Iα and Iβ or crystallinity [1]. On the other hand, the crystallinity of cellulose II is lower than that of cellulose I in general. Therefore, in mercerization process, is can be thought that crystal size decrease and disordered or amorphous part is constructed instead.

Bacterial cellulose (BC) membrane is one of ideal model compounds for investigating of the change of crystallinity or surface fraction because BC has very rigid structure and crystallinity. BC has nano-structure which is consisted of microfibril that was observed by TEM[2]. It was also reported that elementary fibril is constructed only single crystal and microfibril is constructed by aggregation of elementary fibrils. In aggregated fibrils, surface of each elementary fibril is glued and general solvents except for dissolving cellulose cannot access to the surface. That surface is called inaccessible surface and the other surface that is located at the outermost of microfibril is called accessible surface. The surface structures have been investigated mainly by solid state ^{13}C CP/MAS NMR. The spectra show distinguished C4peaks of crystal and surface [3,4] (Fig.2-1a). Another surface model was reported based on C6 conformation (Fig. 2-1b).

In this chapter, we carried out mercerization of BC with various NaOH concentration and each sample was analyzed by solid state ^{13}C CP/MAS NMR and C4 peaks and C6 peaks of the obtained spectra was obtained. Crystallinity Index of cellulose I and II, surface fraction and C6 conformation fraction was calculated from obtained peaks area. The ratio of Crystal and surface was discussed related to microfibril or elementary fibril size. The factor of decreasing cellulose II crystallinity was also discussed.

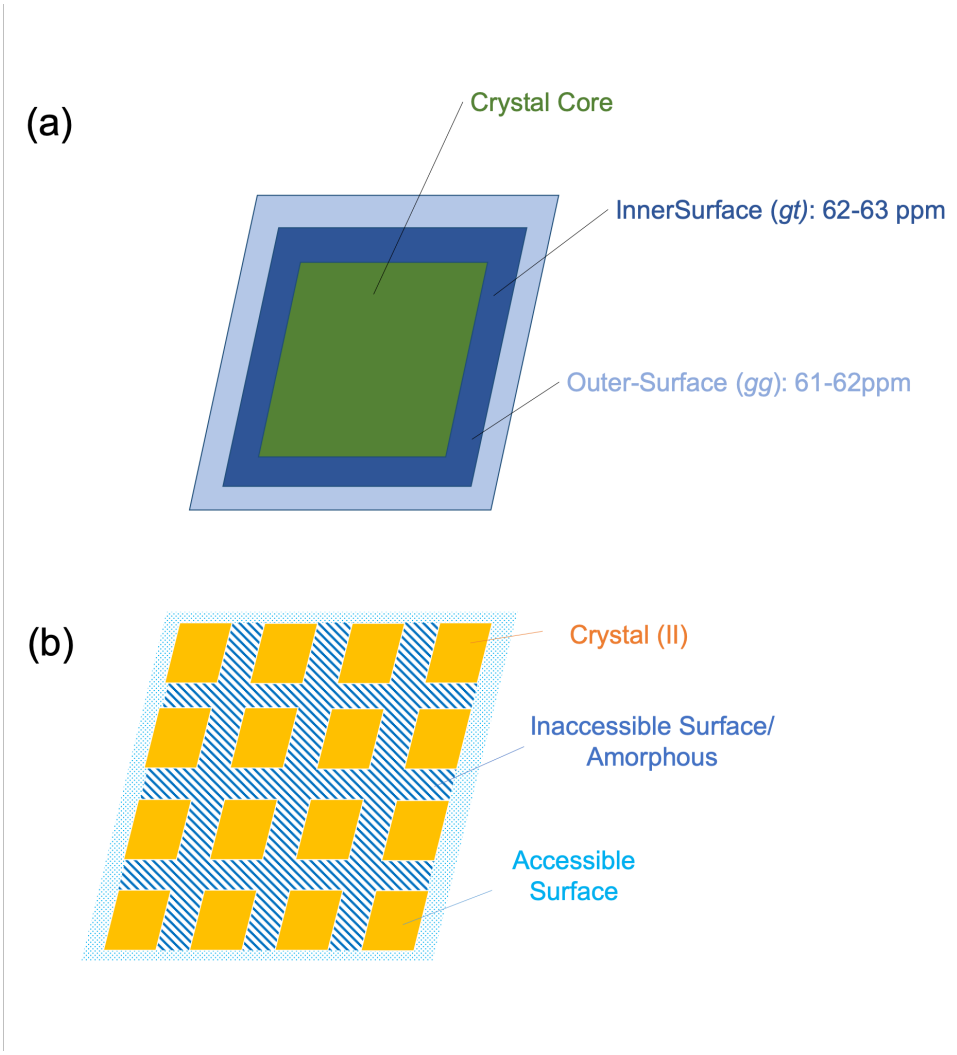

Fig. 2-1. Crystal model of cellulose obtained from Solid State 13C NMR measurement and deconvolution of C6 peaks to *tg (celllose I crstal)*, *gt(cellulose II crystal and inner surface)* and *gg (outer surface)* (a) [5]or deconvolution of C4 peaks to crystlal, accessible surface and inaccessible surface (b) [4,6].

2.2. Methods

2.2.1. Sample Preparation

Gluconacetobactre ATCC 53582 strain was used for BC production. 1.0 mL of preculture was inoculated into 20 mL of Hestrin and Schramm's medium (HS medium) and incubated at 28 ℃ for three days. The obtained culture was inoculated into 20 mL of HS medium and incubated at 28 ℃ for seven days. BC membrane produced on the culture surface was collected. Obtained BC was soaked in 1wt% NaOH aqueous solution and subsequently washed by deionized water. Purified BC was air-dried at room temperature.

Dried BC membrane was mercerized in various concentration of NaOH aqueous solution for three weeks. After mercerization, BC with NaOH aqueous solution was neutralized by 20 wt% sulfuric acid (H_2SO_4) aqueous solution up to pH 7 and subsequently washed by deionized water. Obtained samples were air-dried at room temperature.

2.2.2. Solid State ^{13}C CP/MAS NMR measurement

Solid State ^{13}C CP/MAS NMR spectra were measured using DSX 300 spectrometer (Bruker, Germany) operating at 75.48 MHz. The samples were packed in a 4.0 mm rotor and spun at a frequency of 4 kHz. All the spectra were obtained using the ^{1}H NMR 90°, which comprised the pulse length of 4.0 μs, contact time of 1.5 ms, and the recycle time of 4s. The spectra were calibrated using carbonyl carbon of glycine at 176.03 ppm as the initial.

2.2.3. Peak Fitting and Calculation method

C6 peaks fitting was obtained based on C6 conformation of *tg* (64-66 ppm), *gt* (62-63 ppm) or *gg* (60-62 ppm)[7] (see Fig. 2-2a). *tg* is only in cellulose I type crystal, *gt* is in cellulose II crystal and inner surface [5,8]

and *gg* is in outer surface or amorphous region. Inner surface, which has *gt* conformation, can be thought as para-crystalline region. Two *gt* peaks belongs to cellulose II crystal and inner surface respectively cannot be deconvoluted because they are perfectly overlapped and can define their peaks at any ratio of height and width. In addition, gg peaks are divided into accessible surface and inaccessible surface. C6 conformation fraction as Ftg, Fgt and Fgg are calculated from following equation:

$$F_{tg} = \frac{\mathrm{A}_{tg}}{\mathrm{A}_{tot}} \quad (1)$$

$$F_{gt} = \frac{\mathrm{A}_{gt}}{\mathrm{A}_{tot}} \quad (2)$$

$$F_{gg} = \frac{\mathrm{A}_{gg}}{\mathrm{A}_{tot}} \quad (3)$$

where A_{tg} is the integrated area of *tg*, peaks at 65.6, 65.2 and 65.0 ppm, A_{gt} is the integrated area of *gt* peaks at 62.9 and 62.3 ppm and A_{gg} is the integrated area of gg peaks at 61.8,61.5 and 61.0 ppm; however, Atot is the sum of A_{tg}, A_{gt} and A_{gg}.

C4peaks fitting was obtained based on the model that C4 peaks were divided into crystalline, accessible surface, and inaccessible surface/amorphous peaks, as shown in Fig. 2-2b. The peak fitting shows the model shown in Fig. 2-1. In C4 region, Crystalline peaks and surface or amorphous peaks can be divided and the fraction of crystal (i.e. Crystallinity Index, CInmr) and accessible surface and inaccessible surface including amorphous (Fas and Fis) as following equation:

$$CI_{nmr} = \frac{A_C}{\mathrm{A}_{tot}} \quad (4)$$

$$F_{as} = \frac{\mathrm{A}_{as}}{\mathrm{A}_{tot}} \quad (5)$$

$$F_{is} = \frac{\mathrm{A}_{is}}{\mathrm{A}_{tot}} \quad (6)$$

where A_C is the integrated area formed by the crystalline peaks at 89.8, 88.9 88.2 and 87.7 ppm, A_{as} is the integrated area formed by the accessible surface at 86.5 and 84.5 ppm and A_{is} is the inaccessible surface/amorphous peaks at 83.8 ppm; however, A_{tot} is formed by the summation of A_C, A_{as} and A_{is}.

Fraction division of *gt* peaks to cellulose II crystal and inner surface was calculated as following equation:

$$F_{in} = (CI_{nmr} + F_{in}) - CI_{nmr} = F_{gt} - CI^{*}_{C4} \quad (7)$$

however, since quantitativity of C4 and C6p peaks are different, CIC4* was collated value of CIC4 as following equation:

$$CI^{*}_{C4} = \mathrm{K} * CI_{C4} \quad (8)$$

$$\mathrm{K} = \frac{I_{C6}}{I_{C4}} \quad (9)$$

where K is a correction coefficient. The crystallinity of cellulose I (CI[I]) and that of cellulose II (CI[II]) was expressed as follows:

$$\mathrm{CI[I]} = F_{tg} \quad (10)$$

$$\mathrm{CI[II]} = F_{gt} - F_{in} \quad (11)$$

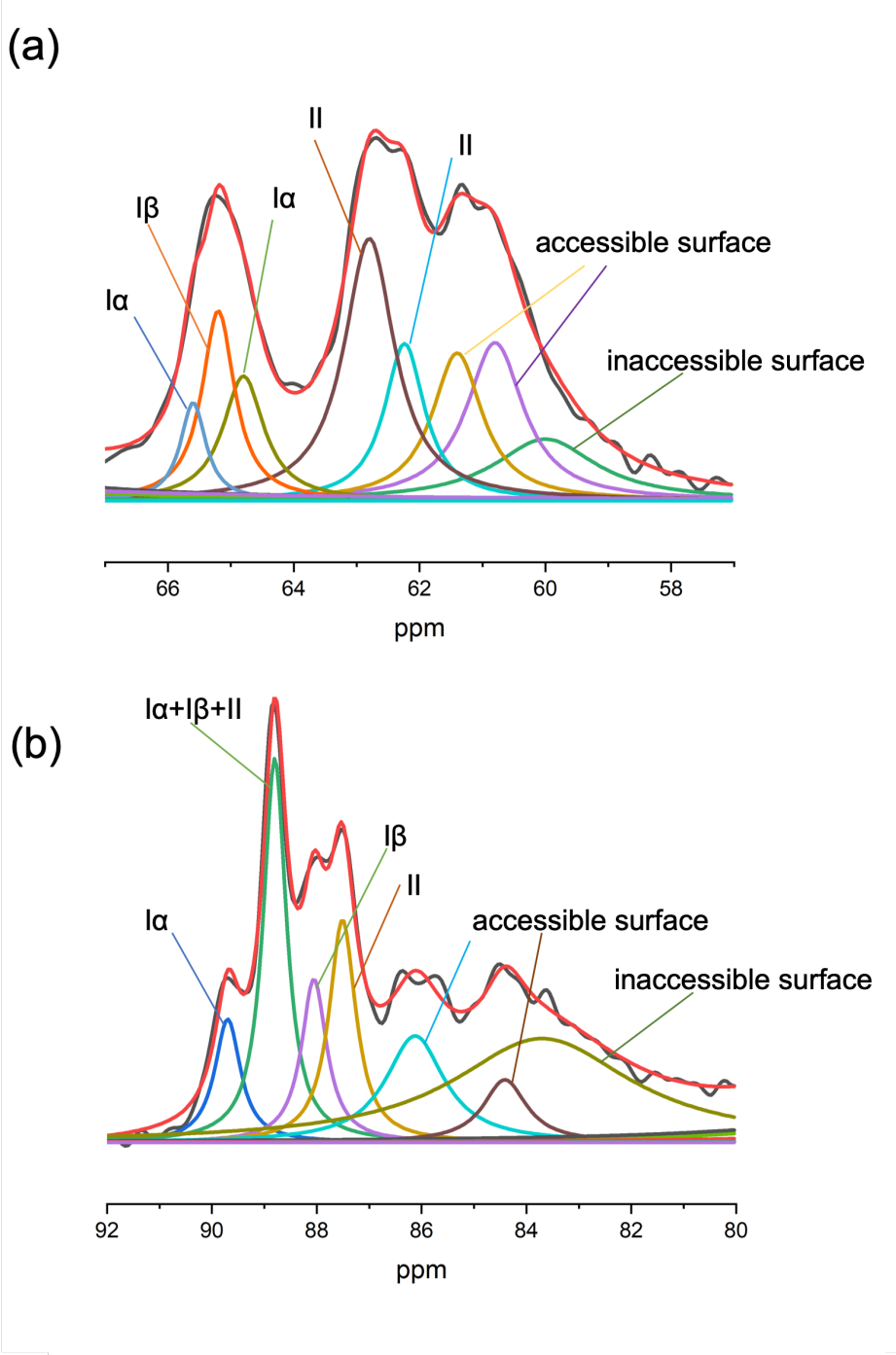

Fig. 2-2. C6 peak fitting model according to Fig. 2-1a (a) and C4 peak fitting model according to Fig. 2-1b (b).

2.3. Results and Discussion

Fig. 2-3 shows solid state ^{13}C CP/MAS NMR spectra of mercerized BC at various concentration of NaOH aqueous solution at room temperature for three weeks. The spectra show the increasing intensity of specific peaks which belongs to cellulose II as NaOH concentration increases. However, it was difficult to evaluate the change of non-crystalline signals because they show broader peaks than crystalline peaks. These qualitatively results imply the incresse of the cellulose II and therefore decrease of the cellulose I, which is consistent with previous reports. Therefore, it was decided that mercerization was successfully proceeded. For quantitatively calculating the transition from cellulose I to II and also the change of non-crystalline parts, such as accessible surface, inaccessible surface, inner surface or outer surface.

2.3.1. The change of Conformation fraction

Fig. 2-4 shows conformation fraction change with various NaOH concentration. gg and gt fraction increased with increasing NaOH concentration; whereas tg decreased. The tg fraction reached to 0% at more than 22.5% NaOH. tg fraction is directly related to the fraction of cellulose I crystal because tg is only in cellulose I crystal. On the other hand, gg is only in surface or amorphous region and gt is both cellulose II and inner crystal (or para-crysalline region). The increase of gt and gg fraction at the same time implies the increase of non-crystalline region unless almost all of gt fraciton is assingned as cellulose II. Therefore, during mercerization proceeding, the decrease of cellulose I did means not only the increase of cellulose II but also the increase of surface or amorphous fraction. For elucidating the change of crystal and surface/amorphous ratio, the change of the sum fraction of tg and gt and gg fraction divided into accessible surface and inaccessible

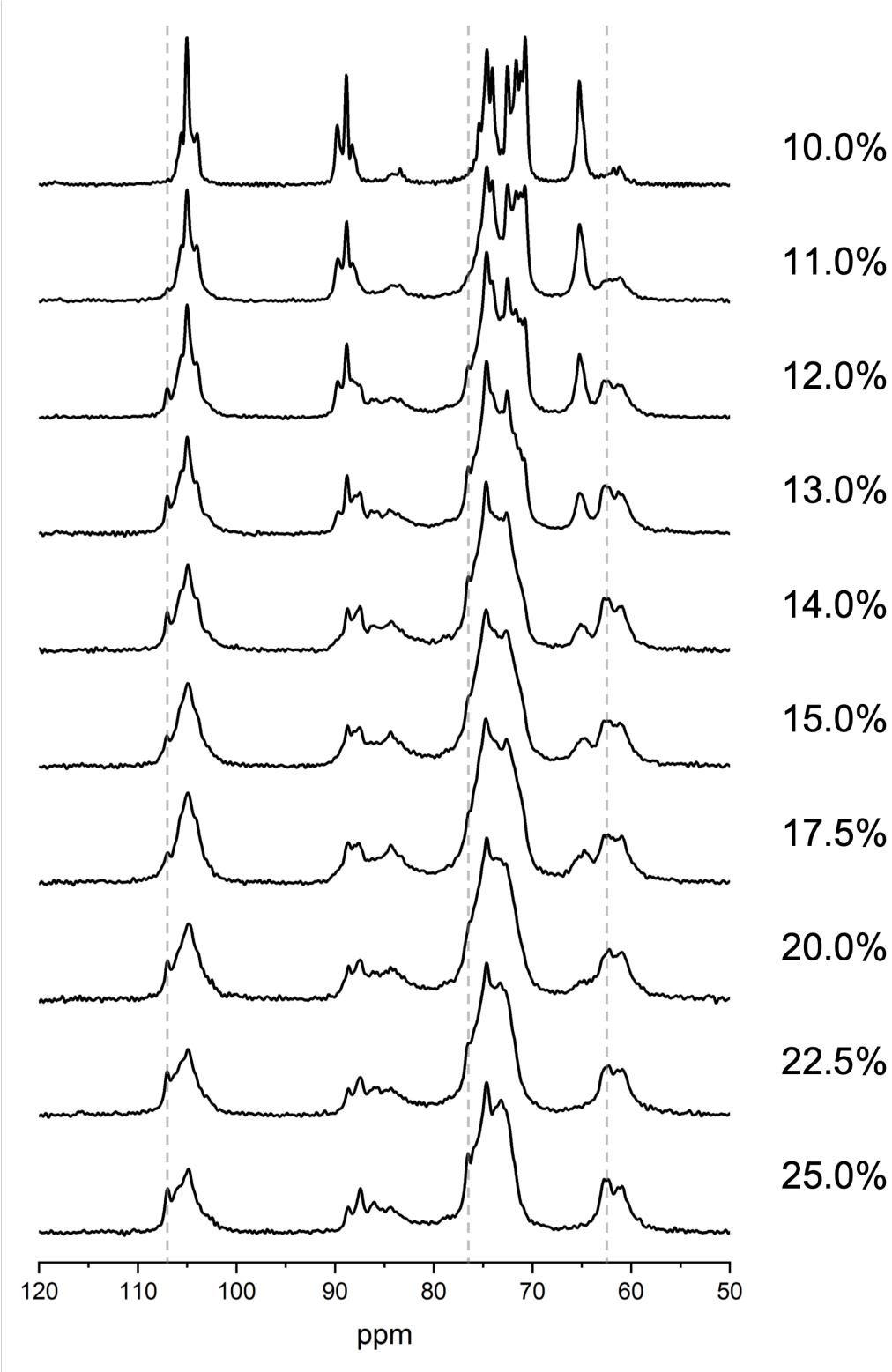

Fig.2-3. solid state ^{13}C CP/MAS NMR spectra of mercerized cellulose by various concentration of NaOH at room temperature.

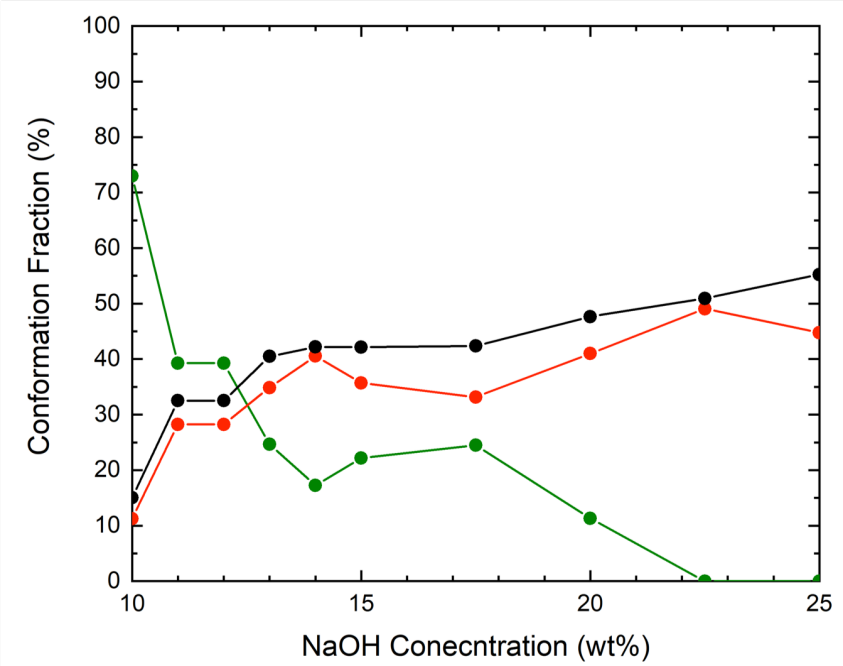

Fig. 2-4. The change of C6 conformation fraction of *tg* (*green line*), *gt* (*red line*) and *gg* (*black line*) by the change of NaOH concentration of mercerization. The values were obtained from C6 fitting results.

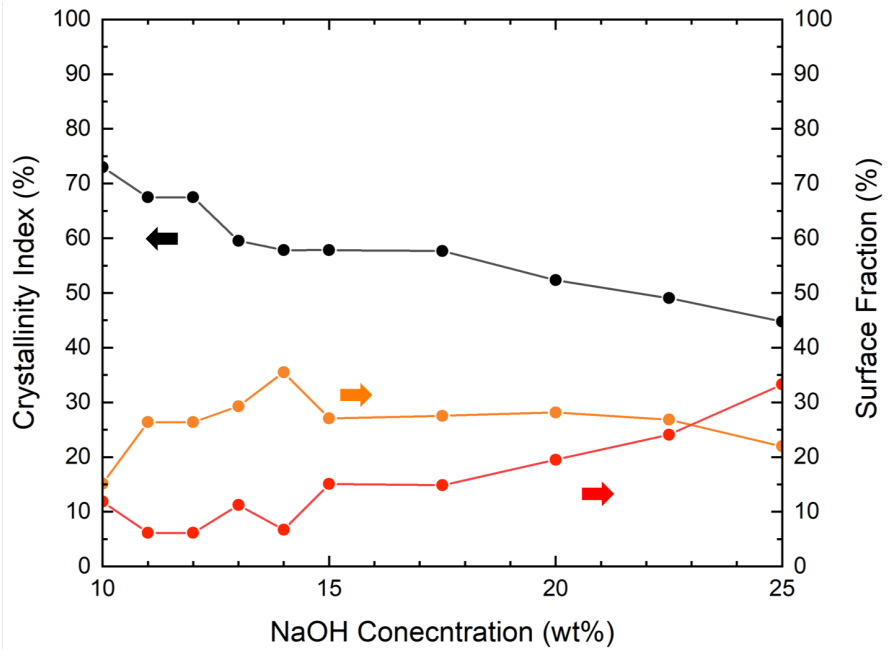

Fig. 2-5. The change of the sum of Crystal fraction and inner surface fraction (*black line*), accessible surface (*orange line*) and inaccessible surface (*red line*) by the change of NaOH concentration of mercerization. The values were obtained from C6 fitting results.

surface was plotted (see Fig. 2-5). The sum of the fraction of *tg* and *gt* shows decrease with NaOH concentration increasing; however, both accessible surface and inaccessible surface divided from gg fraction increased or did not decreased drastically. This result supported the imprement that surface or amorphous part was constructed instead of cellulose II during mercerization.

2.3.2. The change of Crystallinity and Surface Fraction

Fig. 2-6 shows the change of CI_{nmr} (CI_{C4}) and surface fraction. CInmr decreased drastically with NaOH concentration increasing from 10% to 15% and gradually decreased with NaOH concentration increasing from 15 % to 25 %. Although the tendency of decreasing CInmr is consistent wiht the

result of C6 fitting, the degree of CI_{nmr} decreasing with NaOH concentration from 10 % to 15 % is different. It can be thought the possibility that the difference is caused because *gt* fraction contains both cellulose II and inner surface. Accessible surface

fraction increased with increase of NaOH concentration from 10% to 15% and not changed severely at more than NaOH concentration of 15%. Inaccessible surface increased with increase of NaOH concentration from 10% to 15% and more than 20%. The decrease of accessible surface fraction means that total microfibril size was decreased, which sis mainly caused by elementary fibril disaggregation. The increase of inaccessible surface fraction means that crystal core of elementary fibril was down sized and disordered structure which has gt or gg conformation increased (Fig. 2-7). The result is consistent with the result from C6 peaks fitting analysis.

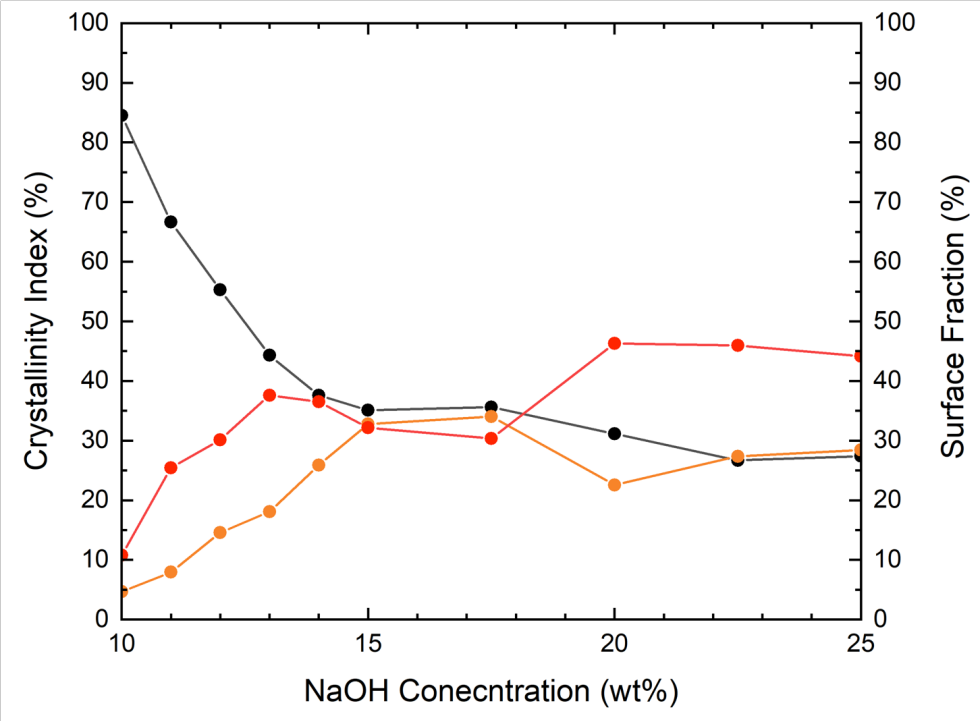

Fig. 2-6. The change of the sum of Crystallinity Index (*black line*), accessible surface (*orange line*) and inaccessible surface (*red line*) by the change of NaOH concentration of mercerization. The values were obtained from C4 fitting results.

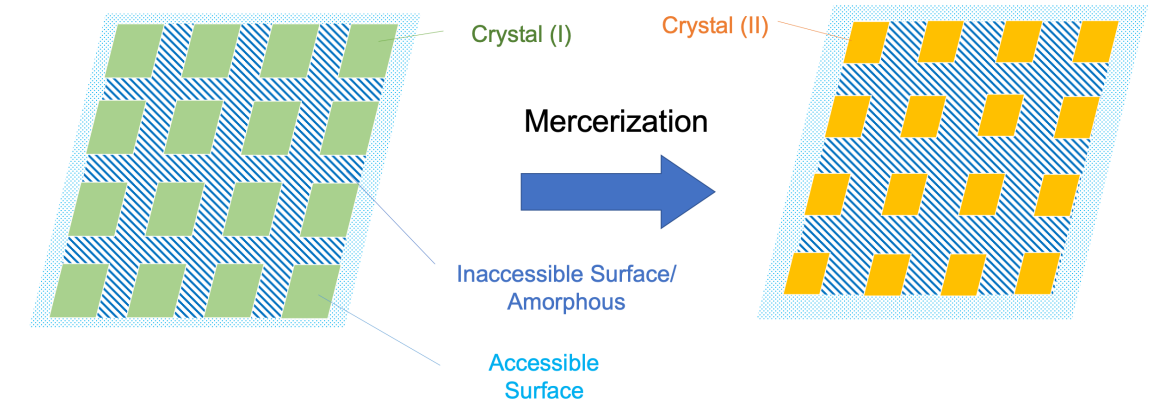

Fig. 2-7. Schematic images of the crystallinity and accessible/inaccessible surface fraction change during mercerization.

2.3.3. The change of crystal structure

Fig 2-8 shows estimated inner surface fraction contained in *gt* fraction of C6 peaks. The fraction was calculated by equation 7. Inner surface fraction was increased with NaOH concentration from 10% to 15% and unchanged largely more than 15% of NaOH concentration. On the other hand, outer surface, which has gg conformation, kept increasing with NaOH concentration increasing. Therefore, inner surface size has upper limit and outer surface is mainly constructed as the factor of decreasing crystallinity. The comparison of the CI[I] and CI[II] during mercerization is shown in Fig. 2-9. The schematic image of the result is shown in Fig. 2-10.

The crystallinity of cellulose II (i.e. CI[II]) was calculated from equation 11 and plotted in fig. 2-11. As mercerization proceeds, cellulose II was not simply increased although cellulose I was decreased. Therefore, mercerization is a process that breaks cellulose I structure and mainly construct disordered structure at the surface of elementally fibril with maintaining down-sized microfibril. Other processes is needed for obatained highly crystalline cellulose II, and mercerization of cellulose II has been reported as effective method for improving the crystallinity of cellulose II [9,10]. It can be thought the possibility that the conversion of inaccessible surface into cellulose II crystal improves the crystallinity of cellulose II and expand the utilization of regenerated or mercerized cellulose. The change of crystallinity and surface fraction was discussed in chapter 3.

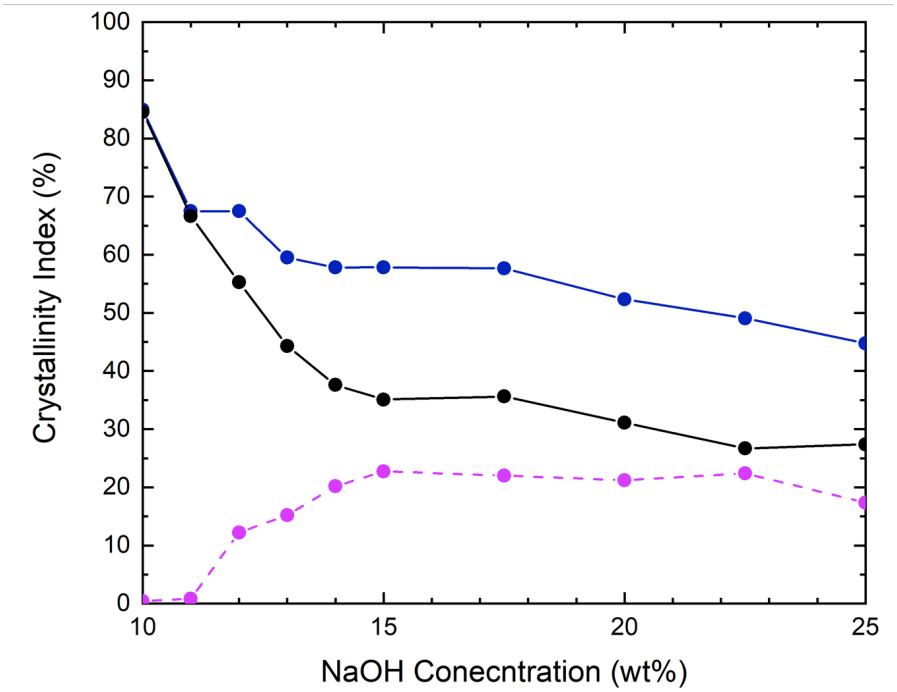

Fig.2-8 The sum of Crystal fraction and inner surface fraction (*blue solid line*), the crystallinity index obtained from C4 fitting results (*black solid line*) and the difference of them (*purple broken line*).

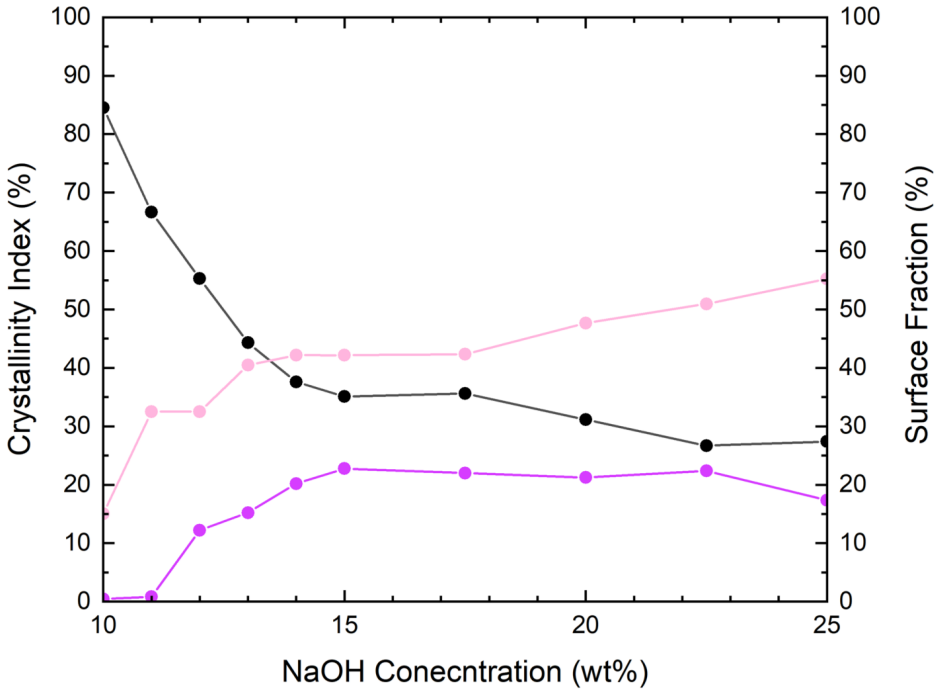

Fig.2-9. The change Crystallinity Index (*black line*), inner surface (*pink line*) and outer surface (*purple line*) by the change of NaOH concentration of mercerization. The values were obtained from C6 fitting results.

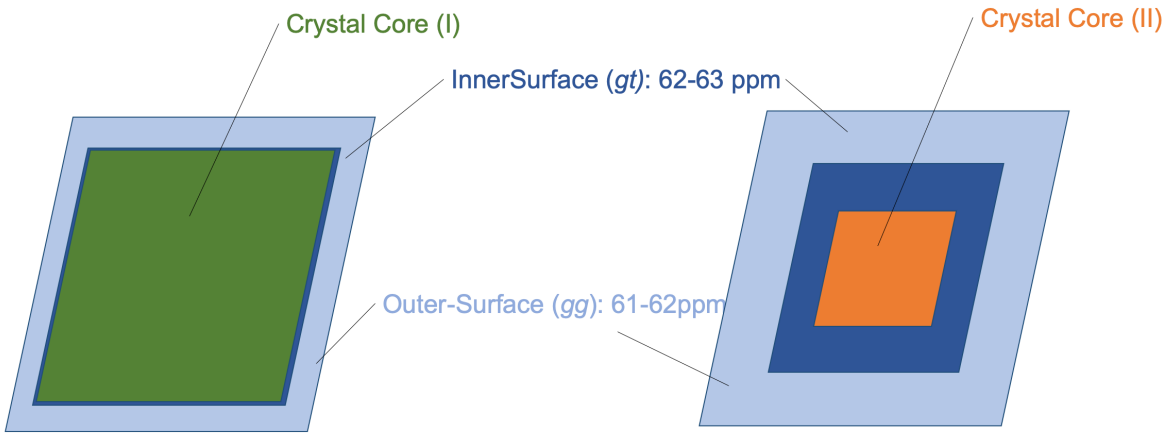

Fig.2-10. . Schematic images of the crystallinity and inner/outer surface fraction change during mercerization.

2.4. Conclusions

In this chapter, the change of crystallinity and surface fraction during mercerization was analyzed by solid state ^{13}C CP/MAS NMR measurement and peak fitting method for C4 and C6 peaks, respectively. Mercerization is conventionally used as obtaining cellulose II, however, almost two-thirds of the area in elementary fibril is converted into disordered surface structure and cellulose II is not main structure. Surface structure is classified as inner surface and outer surface, and outer surface is mainly constructed by mercerization. Outer surface is directly related to fibril aggregation and glues each elementary fibril as inaccessible surface.

References

[1] Y. Nishiyama, Structure and properties of the cellulose microfibril, Journal of Wood Science. 55 (2009) 241–249. doi:10.1007/s10086-009-1029-1.

[2] J. Sugiyama, R. Vuong, H. Chanzy, Electron Diffraction Study on the Two Crystalline Phases Occurring in Native Cellulose from an Algal Cell Wall, Macromolecules. 24 (1991) 4168–4175. doi:10.1021/ma00014a033.

[3] P.T. Larsson, K. Wickholm, T. Iversen, A CP/MAS ^{13} C NMR investigation of molecular ordering in celluloses, Carbohydrate Research. 302 (1997) 19–25. doi:10.1016/S0008-6215(97)00130-4.

[4] K. Wickholm, P.T. Larsson, T. Iversen, Assignment of non-crystalline forms in cellulose I by CP/MAS ^{13}C NMR spectroscopy, Carbohydrate Research. 312 (1998) 123–129. doi:10.1016/S0008-6215(98)00236-5.

[5] P. Phyo, T. Wang, Y. Yang, H. O'Neill, M. Hong, Direct Determination of Hydroxymethyl Conformations of Plant Cell Wall Cellulose Using 1 H Polarization Transfer Solid-State NMR, Biomacromolecules. 19 (2018) 1485–1497. doi:10.1021/acs.biomac.8b00039.

[6] G. Zuckerstätter, N. Terinte, H. Sixta, K.C. Schuster, Novel insight into cellulose supramolecular structure through ^{13}C CP-MAS NMR spectroscopy and paramagnetic relaxation enhancement, Carbohydrate Polymers. 93 (2013) 122–128. doi:10.1016/j.carbpol.2012.05.019.

[7] F. Horii, A. Hirai, R. Kitamaru, Solid-state ^{13}C-NMR study of conformations of oligosaccharides and cellulose - Conformation of CH2OH group about the exo-cyclic C-C bond, Polymer Bulletin. 10 (1983) 357–361. doi:10.1007/BF00281948.

[8] T. Wang, H. Yang, J.D. Kubicki, M. Hong, Cellulose Structural Polymorphism in Plant Primary Cell Walls Investigated by High-Field 2D Solid-State NMR Spectroscopy and Density Functional Theory Calculations, Biomacromolecules. 17 (2016) 2210–2222. doi:10.1021/acs.biomac.6b00441.

[9] J. Široký, R.S. Blackburn, T. Bechtold, J. Taylor, P. White, Attenuated total reflectance Fourier-transform Infrared spectroscopy analysis of crystallinity changes in lyocell following continuous treatment with sodium hydroxide, Cellulose. 17 (2010) 103–115. doi:10.1007/s10570-009-9378-x.

[10] X. Colom, F. Carrillo, Crystallinity changes in lyocell and viscose-type fibres by caustic treatment, European Polymer Journal. 38 (2002) 2225–2230. doi:10.1016/S0014-3057(02)00132-5.

Chapter 3. Analysis on the enhancement of mercerized cellulose II assembly with low concentration NaOH post-treatment

3.1. Introduction

In chapter 2, it was shown that mercerized cellulose has low crystallinity and surface structure which has gg conformation. It was reported that *gg* conformation makes molecular torsion [1]. Large surface area also can be seen in the solid state ^{13}C CP/MAS NMR spectra of regenerated cellulose [2]. For improving crystallinity of cellulose II, converting surface structures can be thought to be effective. It has already been reported mercerization as post-treatment with low concentration of NaOH improves the crystallinity of regenerated cellulose fibers [3,4]. This report discussed that amorphous or quasi-crystal region, which might be related to the inner surface structure, was re-organized. Post-treatment with low concentration NaOH is effective process for improving cellulose II assembly and mechanical structure of regenerated or mercerized cellulose material, which is composed of cellulose II crystalline and other non-negligible amount of disordered structure.

For discussion on the post-treatment, not only the amorphous region, but also the inaccessible surface is important and should be taken into account for the mercerization of the inaccessible surface region; this is because it is easily mercerized due to its soft structure and high mobility, but it is difficult to convert to cellulose II by employing rehydration. In addition, the effect of the mercerization temperature on partial mercerization and the selection of acid for neutralization should be considered for the cellulose II assembly; this is achieved by inducing a hydrophobic interaction with a moderate polarity.

In this study, we have carried out post-treatments with low concentrations of NaOH aqueous solutions on already mercerized or regenerated cellulose, which has cellulose II crystal structures with low crystallinity. Lower concentrations of NaOH were effective for partial mercerization and subsequent neutralization. When washing NaOH, the high polarity poor solvents may be effective for cellulose II assembly. We also focused on neutralization with H_2SO_4, CH_3COOH, and H_3PO_4, which has high polarity with various strength as acid. Solid state ^{13}C CP/MAS NMR and X-ray diffraction analyses were engaged to analyze the crystal structures, size and

crystallinity of the obtained regenerated cellulose samples, for making clear the precise mechanisms of post-treatment, namely, re-mercerization on cellulose II.

3.2. Methods

3.2.1. Sample Preparation

Cellulose II standard samples were prepared from cellulose powder supplied from Advantec Co. Ltd. (Japan) by mercerization in 25 % NaOH aqueous solution.

Regenerated cellulose was prepared according to previous reports[5–9]. NaOH, Urea and deionized water was mixed at the ratio of NaOH:Urea:Water = 7:12:81. 4 wt% of cellulose powder was dispersed into the NaOH/Urea solution and subsequently cooled at -20 ℃ with shaking once in 10 minutes for perfect dissolution. Dissolved solution was centrifuged at 5000 rpm for 10 minutes for excluding micro bubbles and casted on glass plate to obtain 1mm thick layer. The obtained layer was coagulated with 3 vol% H_2SO_4 aqueous solution for constructing hydrogel and thoroughly washed by deionized water. The hydrogel samples were kept as hydrated state.

Post-treatment on the cellulose II standard samples and the regenerated cellulose gel samples were proceeded with various concentration of NaOH aqueous solutions at room temperature or by heating with hot plate for 2 hours. The NaOH aqueous solution swelling the cellulose was neutralized with 20 wt% of H_2SO_4, H_3PO_4, or CH_3COOH aqueous solution. After thoroughly washing the neutralized NaOH solutions with deionized water, the samples were either kept in water at room temperature or air-dried.

3.2.2. Solid State ^{13}C CP/MAS NMR measurement

Solid State ^{13}C CP/MAS NMR spectra were measured using DSX 300 spectrometer (Bruker, Germany) operating at 75.48 MHz. The samples were packed in a 4.0 mm rotor and spun at a frequency of 4 kHz. All the

spectra were obtained using the ^{1}H NMR 90 °, which comprised the pulse length of 4.0 μs, contact time of 1.5 ms, and the recycle time of 4 s. The spectra were calibrated using carbonyl carbon of glycine at 176.03 ppm as the initial.

Deconvolution of the C4 peaks of the spectra were carried out with DMfit2017 line-fitting program [10]. Lorenzian was applied to each peak. Before fitting, all peak positions were decided by dinstingishing each peak top postion on the most high-resoluted spectrum.The most high-resoluted spectrum was decided as the spectra obtained from the sample which was post-treated at 10% NaOH aqueous solution at 80 ℃ for 2 hours and neutralized at room temperature with 20% H_2SO_4 aqueous solution. For elucidating peak positions, gaussian multiplicity was applied. The C4 peaks can be divided into crystalline, accessible surface, and inaccessible surface/amorphous peaks, as shown in Fig. 3-1 [11]. The crystallinity index from the NMR (CI_{nmr}) was calculated with the peak deconvolution approach by using the equation:

$$\mathrm{CI_{nmr}} = \frac{A_t - A_{am}}{A_t} \times 100 \tag{3.1}$$

where A_t is the integrated areas of the crystalline peaks at 88.5 and 87.4 ppm and accessible surface at 86.5, 85.5 ppm and inaccessible surface/amorphous peaks at 83.8 ppm, whereas A_{am} is the integrated accessible surface and inaccessible surface/amorphous peaks, respectively.

3.2.3 X-ray diffraction analysis

WAXD was performed in transmission on a Rigaku Co. Ltd., SmartLab, X-ray diffractometer equipped with a CuKα anode (λ = 1.5418 Å) powered at 45 kV. The scan range was taken the 5 – 40 ° with 0.02 ° step. The peaks were fitted using four pseudo-Voigt functions using fitting software PDXL2 (Rigaku Co. Ltd.) to obtain the peak position, peak height, and the full width at half-maximum (FWHM) for each sample.

The crystallinity index was calculated with the peak height method by using the equation, suggested by Segal et. al.[12] and Azubuikeet. al[13]:

$$\mathrm{CI_{xrd}} = \frac{I_{020} - I_{am}}{I_{020}} \times 100 \tag{3.2}$$

where I_{020} is the peak height of the (020) lattice peak (at $2\theta = 21.7°$) and I_{am} is the peak height attributed to the amorphous (at $2\theta = 16°$).

The crystallite size was calculated from obtained peak parameters from peak deconvolution by using the Scherrer equation:

$$\mathrm{t} = \frac{0.9\lambda}{\beta cos2\theta} \tag{3.3}$$

where t is the crystallite size, λ is the wavelength of the X-rays, β is the values for FWHM and 2θ is a peak position. The FWHM for each peak at $(1\bar{1}0)$, (110), and (020) was used to determine the crystallite size in the corresponding dimensions.

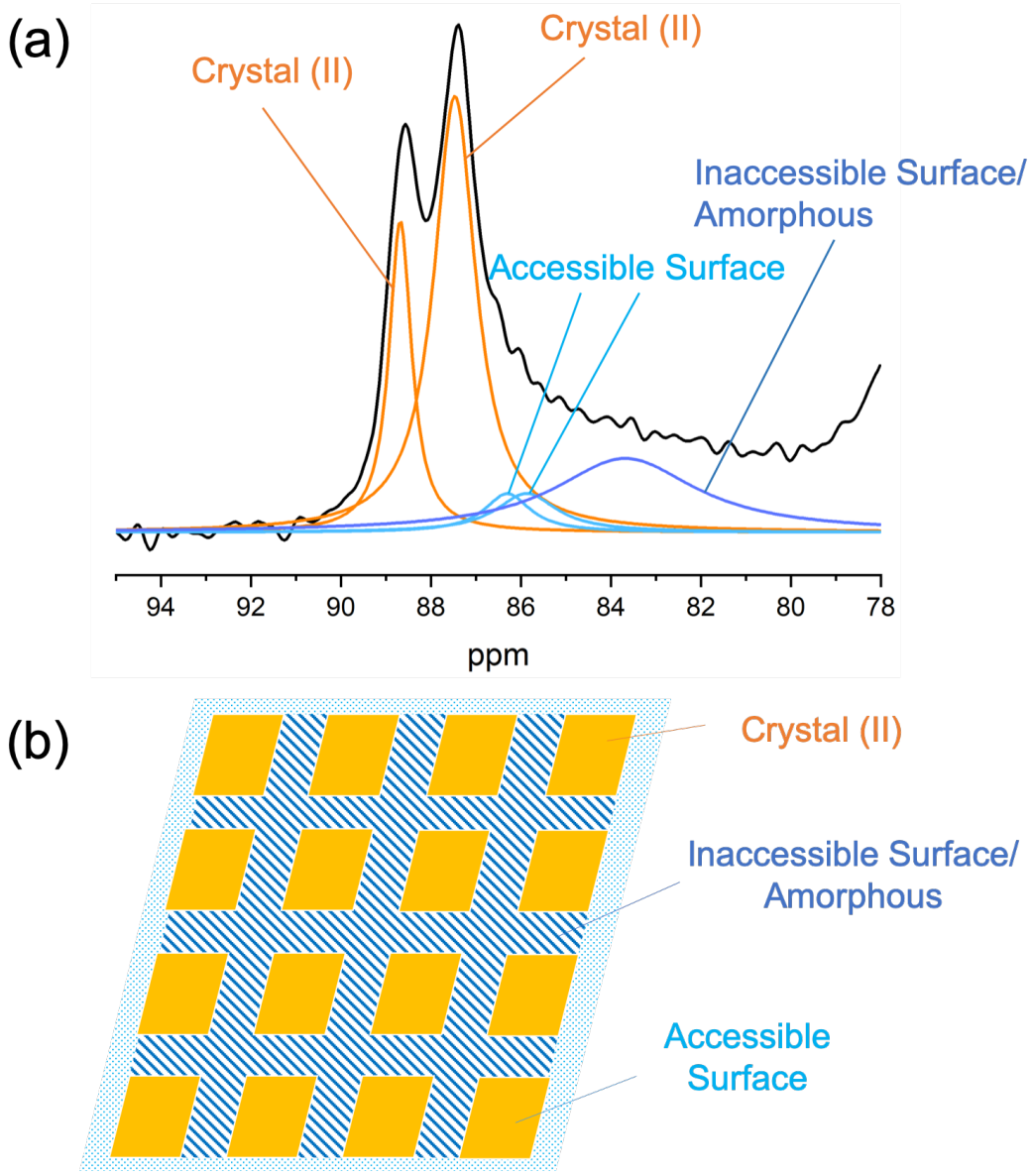

Fig. 3-1 (a) Deconvolution of solid state CP/MAS ^{13}C CP/MAS NMR C4 resonance line of cellulose II at dried state and (b) the suggested model of cellulose II assembly [11].

3.3. Results and Discussion

3.3.1 Effects of the NaOH concentration of post-treatment

3.3.1.1. Solid State ^{13}C CP/MAS NMR spectroscopy

Post-treatments, namely, re-mercerization on the starting cellulose II samples were conducted in 0 to 25 % NaOH aqueous solutions for 2 hours at room temperature. Fig. 3-2 shows the ^{13}C NMR spectrum of the hydrated state post-treated cellulose II in the 10 % NaOH aqueous solution. The spectrum of the hydrated state shows sharper peaks than the dried state, as a same in the case of cellulose I type structure [14]. The spectra show the C1 peak at 106 ppm in addition to 107.1 and 105.0 ppm. In the C2, C3, and C5 regions, four sub peaks were observed beside three main peaks. C6 peaks were divided into two crystalline peaks and one amorphous peak, as previously reported [15].

Fig. 3-3 shows the ^{13}C NMR spectra of the cellulose II post-treated by different NaOH concentration samples. The spectrum of the cellulose II sample post-treated at 10% NaOH shows sharper peaks than at the other concentration NaOH. The C4 peaks for each spectrum were fitted by the peaks of the cellulose II crystals, the accessible surface and the inaccessible surface including amorphous for calculation of each content and crystalline index, which are plotted in Fig. 3-4. As seen in Fig. 3-4, the CI_{nmr} increased with the increase in NaOH concentration from 0 to 10 %, decreased from 10 to 17.5 % and more than17.5 %, the CI_{nmr} was unchanged. It was decided that the CI_{nmr} takes optimum at 10 % NaOH concentration.

Fig. 3-4 also shows the rate of accessible surface and inaccessible surface/amorphous regions for the mercerized cellulose II samples. No remarkable change of the accessible surface cannot be seen through any concentration of NaOH, despite CI_{nmr} shows maximum at 10%, which suggests that total crystal size surrounded by accessible surface is stable regardless of NaOH in post-treatment. On the other hand, the inaccessible surface/amorphous region rate decreased with the NaOH concentration from 0 to 10 %. Increasing of the CI_{nmr} from 2.5 to 10 % was associated with the decrease of the inaccessible surface/amorphous region. Therefore, it is

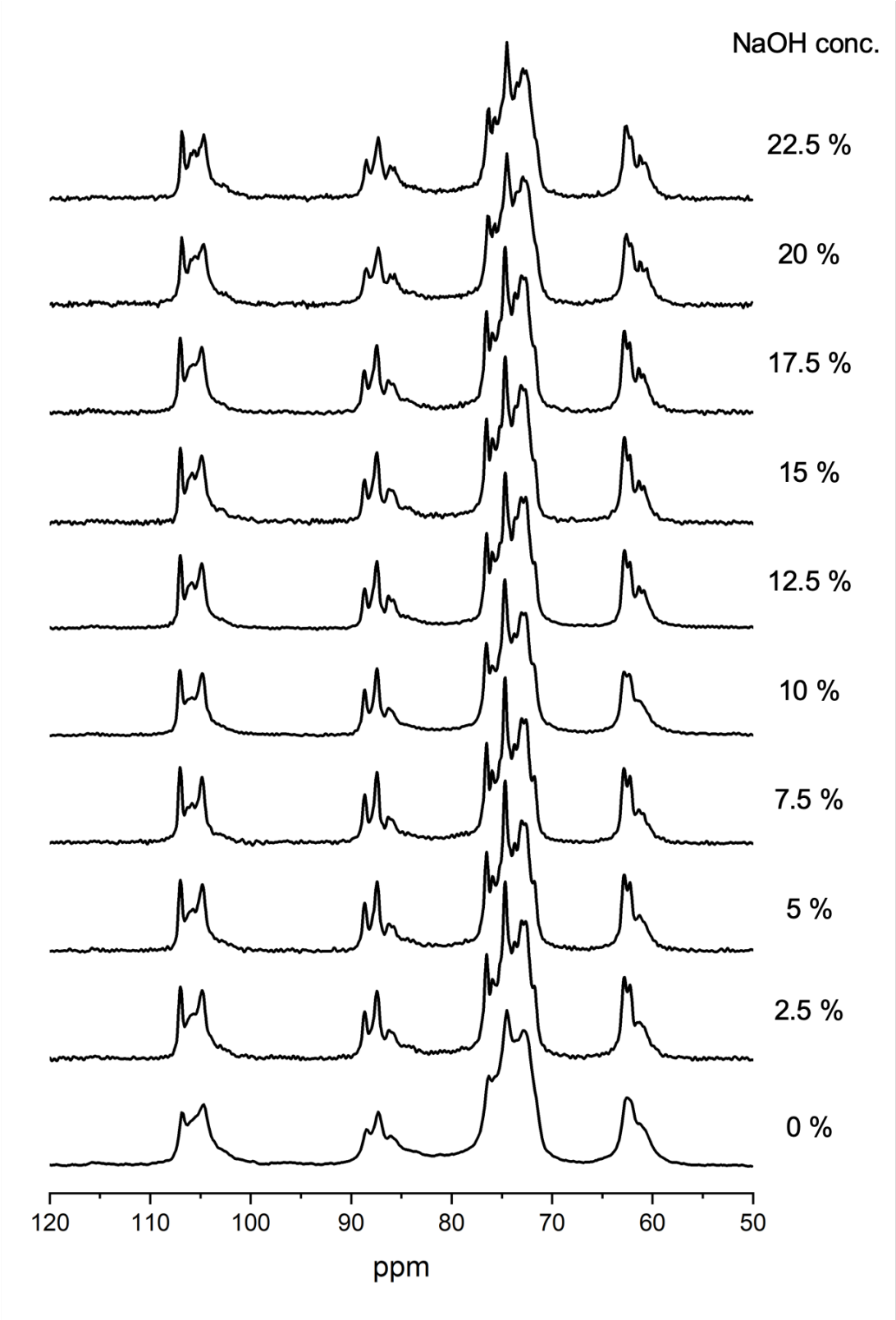

Fig. 3-2. Hydrated state ^{13}C CP/MAS NMR spectra of post-treated cellulose II standard samples with various NaOH concentration.

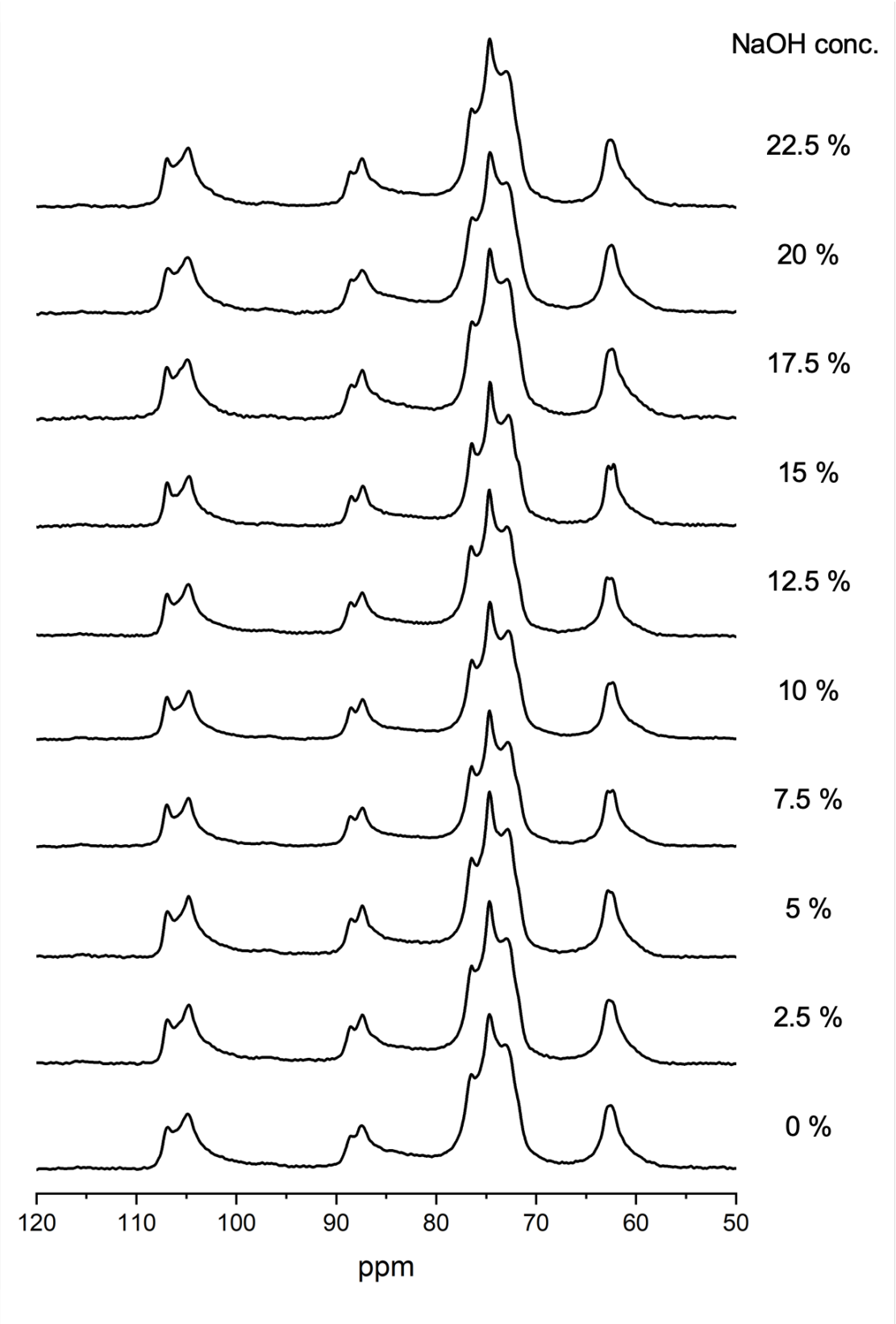

Fig. 3-3. Dried state ^{13}C CP/MAS NMR spectra of post-treated cellulose II standard samples with various NaOH concentration.

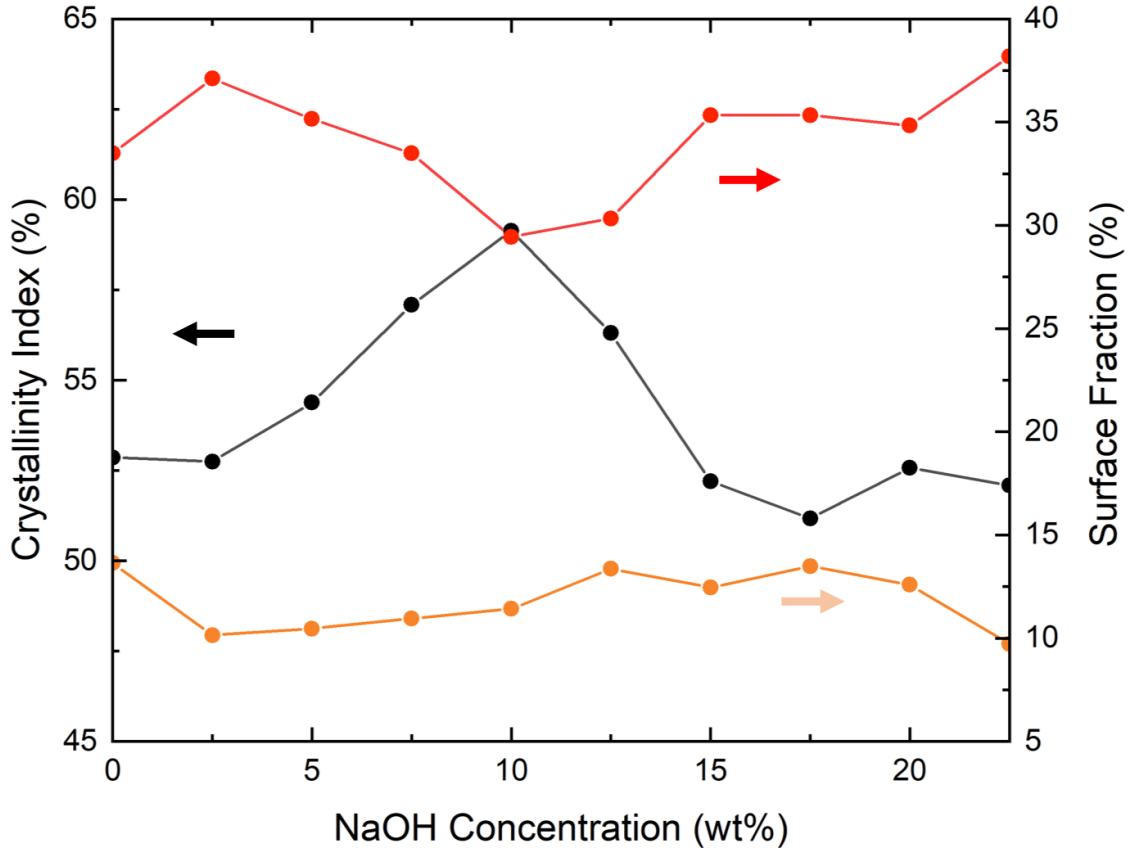

Fig.3-4. Crystallinity Index (*black line*), accessible surface fraction (*orange line*) and inaccessible surface/amorphous fraction (*red line*) by evaluated from the dried state ^{13}C CP/MAS NMR spectra (Fig. 3-3) in the post-treated cellulose from 0 to 25% concentration of NaOH aqueous solution.

thought that the inaccessible surface or amorphous region was converted to a crystal structure, in the side of crystal block with maintaining total block size at constant which is surrounded by accessible surface. The inaccessible surface/amorphous region turned to increase with the NaOH concentrations, which suggests that the decreasing cellulose II crystals resulted from the increasing inaccessible surface/amorphous region.

The NMR spectrum of the post-treated cellulose swollen with the 10 % NaOH aqueous solution before neutralization is shown as in Fig. 3-5a. Clearly, this spectrum has a component of Na-cellulose I spectrum which is added Fig.3-5d as reference, with a slight high magnetic field shift. The spectrum of cellulose II after post-treatment is plotted as Fig. 3-5b, and Fig. 3-5c is the calculated spectrum with formula α(a)-β(b) (α and β were chosen for avoiding negative value). This obtained spectrum as Fig. 3-5c is clearly similar to that of Na-cellulose I (Fig. 3-5d), which suggests that the 10 % NaOH aqueous solution partially mercerizes and the inaccessible surface/amorphous region was preferred to be mercerized and crystallized, resulting the decrease of inaccessible surface/amorphous region.

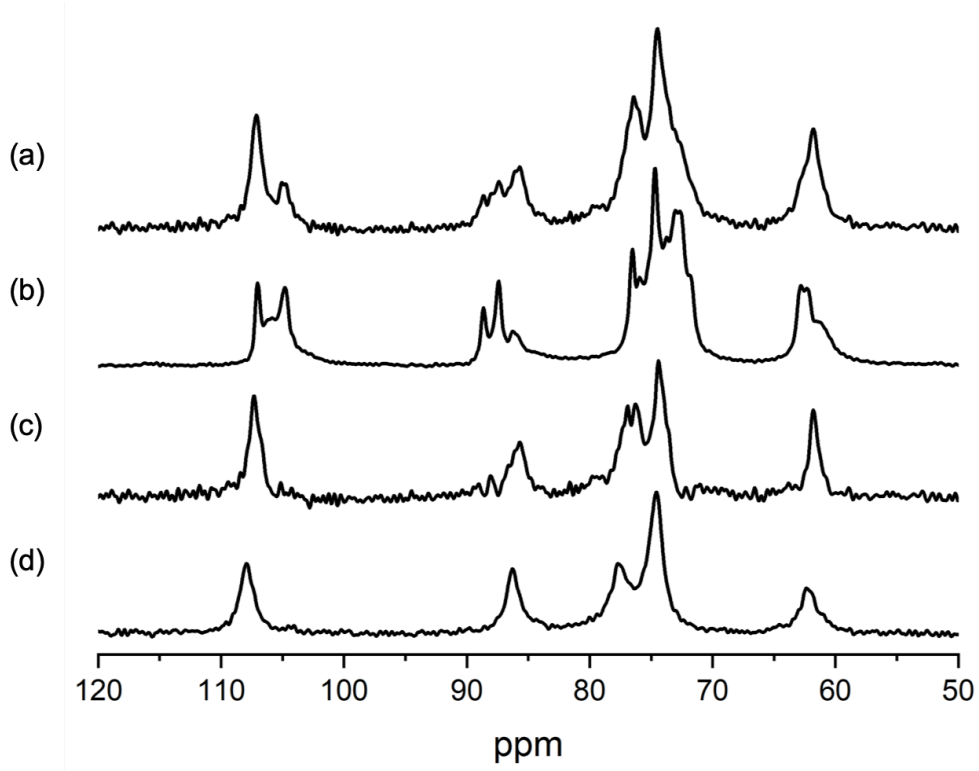

Fig.3-5. *In situ* ^{13}C CP/MAS NMR spectra of the soaked cellulose II produced by post-treatment in 10 % NaOH aqueous solution before (a) and after (b) washing NaOH, (c) calculated spectrum obtained by subtraction (see text), and (d) reference Na-cellulose I prepared from cellulose powder with 20% NaOH aqueous solution inserted for reference. Samples were dried after NaOH was removed from the samples by 20 wt% H_2SO_4 aqueous solution and subsequent deionized water.

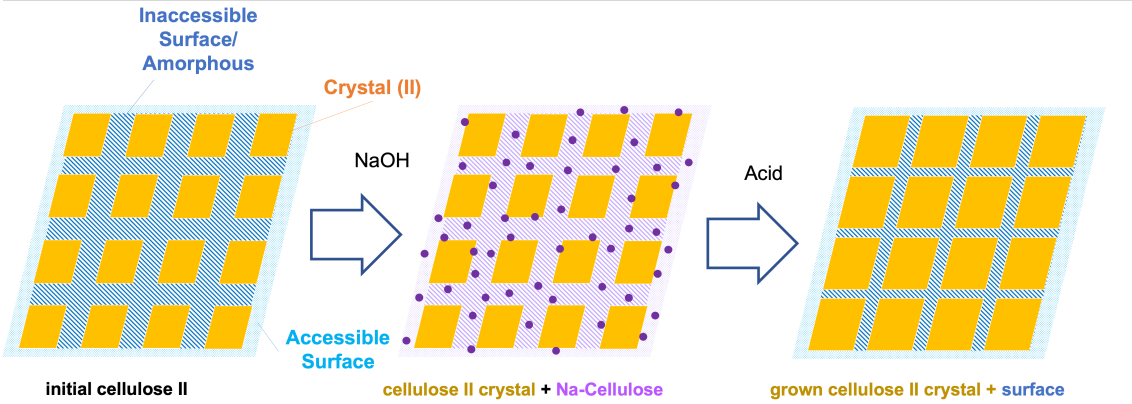

Fig.3-6. Schematic images of Na-cellulose construction during post-treatment

3.3.1.2. X-ray diffraction analysis

The XRD diffraction profiles of each post-treated cellulose II standard sample are shown in Fig. 3-6. The profile of post-treated cellulose II sample at 10% NaOH shows smaller FWHM than at the other concentration NaOH. The peak positions were referenced by planes ($1\bar{1}0$), (110) and (020), as typical peaks of cellulose II. Fig. 3-7 shows calculated crystallinity index (CI_{xrd}, *black line*) and crystalline sizes (CS, *green lines*) of each plane according to the Segal's method and Scherrer equation, respectively, as mentioned in experimental section. As seen in this Fig. 3-7, C_{Ixrd} increased with NaOH concentration from 0 to 10% and decreased from 10 to 15%, which shows the good agreement with the C_{Inmr}. More than 15%, CI_{xrd} increased although the CI_{nmr} stayed at all region of NaOH concentration. This behavior of CS (110) and CS (020) is clearly similar to that of CI_{nmr} at all region of NaOH concentration. This behavior of CS of the hydrophobic (110) and (020) planes seems to be mirror reflection of that of inaccessible surface/amorphous rate obtained from NMR spectra (Fig. 3-4, red line). More than 10% NaOH, the intercalation of Na ions to the crystal part starts and shrinks the cellulose II crystal, and the inaccessible surface increases as the results.

3.3.1.3. The mechanism of post-treatment

Based on the results by NMR and XRD, the optimum condition of post-treatment for improving the crystallinity of cellulose II is considered to be at 10 % concentration of NaOH. It can be thought if the concentration is less than 10 %, Na ions cannot penetrate to crystalline surface and if it is more than 10 %, Na ions penetrate to the crystal core. As a result, inaccessible surface decreased and crystallinity index and crystal size increased. The discussion was consistent with the report that post-treatment with a low concentration of NaOH improves the crystallinity of regenerated cellulose fibers [3,4]. There might be the possibility of alkaline

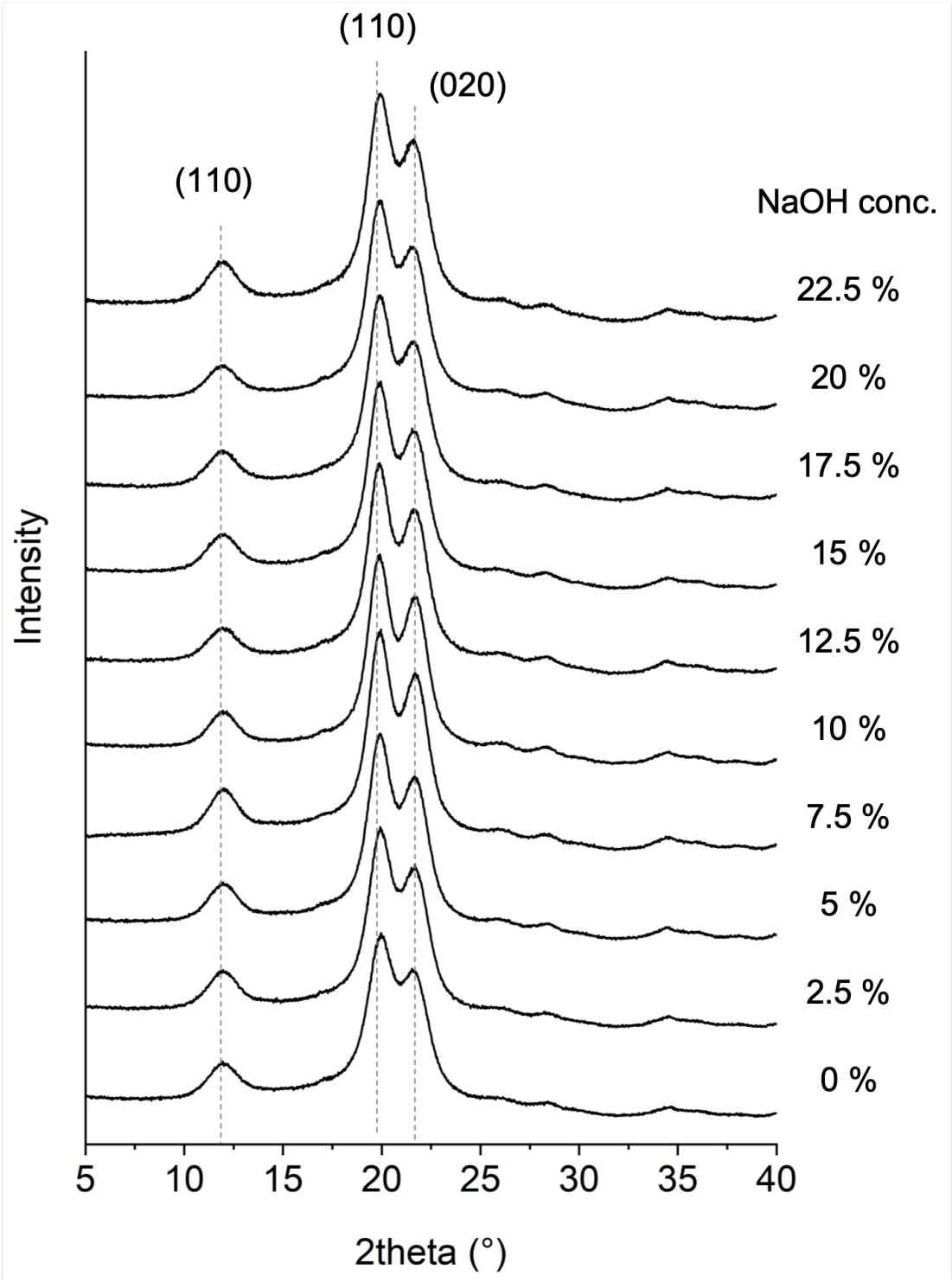

Fig.3-7. X-ray diffraction profiles of dried state post-treated cellulose with different concentrations of NaOH. Samples were dried after NaOH was removed from the samples by 20 wt% H_2SO_4 aqueous solution and subsequent deionized water.

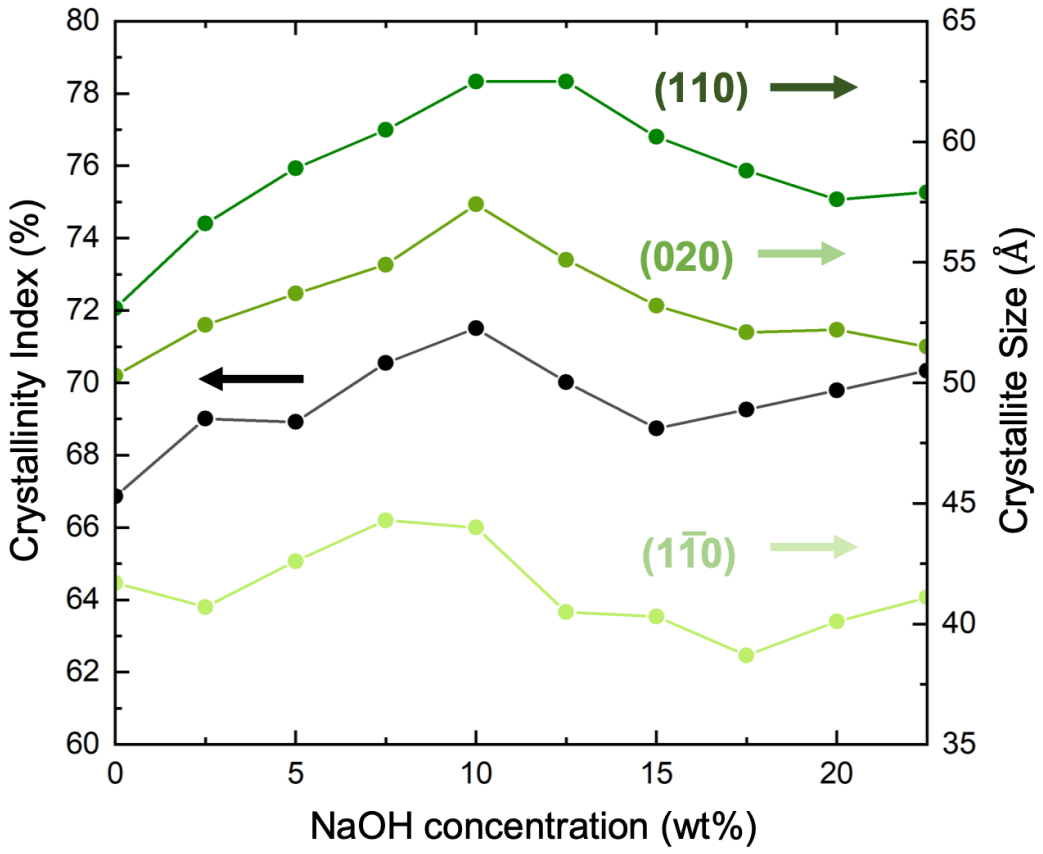

Fig. 3-8. Crystallinity index and crystal size of (1$\bar{1}$0)(*yellow green line*), (020)(*green line*) and (110) (dark *green line*) estimated from X-ray diffraction profiles (Fig. 7) in post-treated cellulose with NaOH aqueous solution.

hydrolysis on amorphous region, which may increase the crystallinity of cellulose II as the acid hydrolysis. The effect of alkaline hydrolysis should be stronger as NaOH concentration is higher. However, on the post-treatment on cellulose II, the decrease of crystallinity was observed at more than 10 % concentration of NaOH. Therefore, it cannot be thought the alkaline hydrolysis is the major factor of increasing crystallinity at the post-treatment. The other important factors that are taken into account in conventional mercerization or regeneration process are the temperature at post-treatment and subsequent neutralization or washing process. These factors are discussed in the following sections.

3.3.2 Effects of temperature on post-treatment

The effect of temperature for constructing Na-cellulose is also important and it was reported that mercerization was promoted preferably by lower temperature [16].According to this report, higher temperature lower the construction of Na-cellulose during mercerization, instead construction of cellulose II is promoted because the disordered structure is thought to be easier to mercerize than the ordered structure. Fig. 3-9 and 3-10 shows the solid state ^{13}C CP/MAS NMR spectra of the hydrated state mercerized and neutralized cellulose II in a 10 % NaOH aqueous solution at room temperature, 60 ℃ and 80 ℃ at hydrated and dried state, respectively. Table 1 shows the CI_{nmr} calculated from the dried state NMR spectra in Fig. 3-10. CI_{nmr} was increased and both rates of the accessible surface and inaccessible surface/amorphous were decreased by 60℃ and 80℃, compared with the room temperature. Higher temperature might be interrupting the construction of the Na-cellulose I at the original crystal part. As the result, high temperature treatment promotes the construction of the cellulose II crystal structure and larger crystal size than lower temperature.

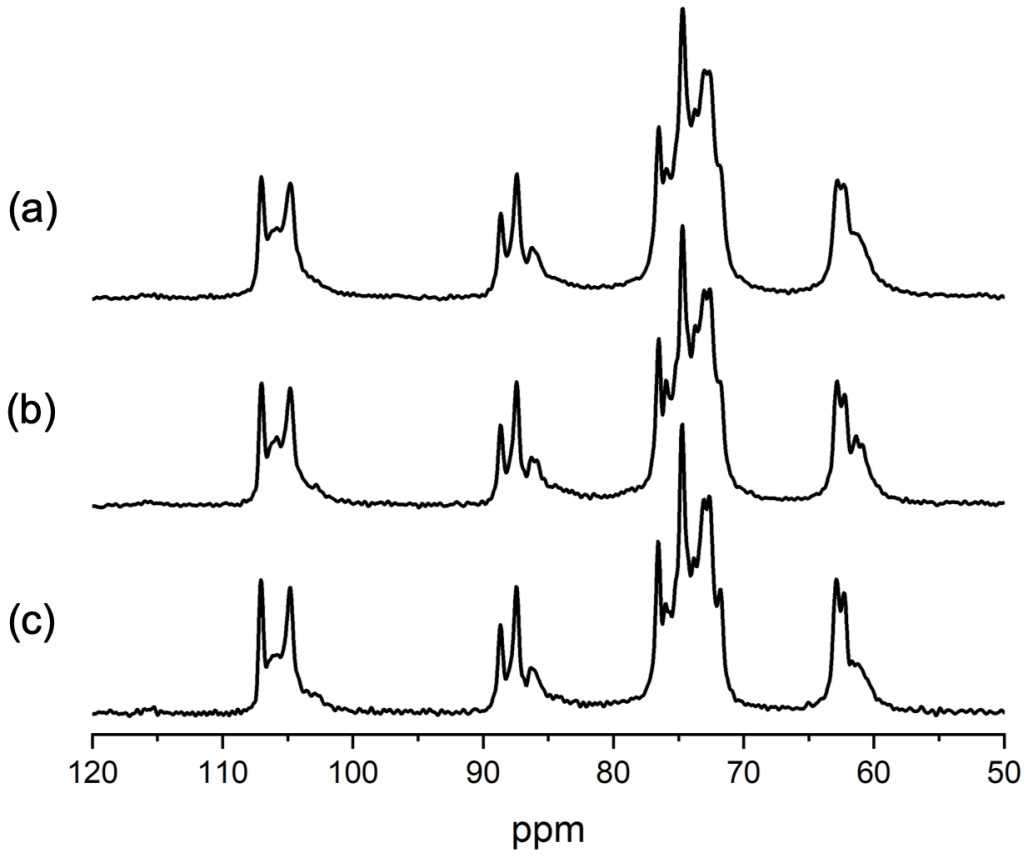

Fig. 3-9. Hydrated state ^{13}C CP/MAS NMR spectra of post-treated cellulose at (a) room temperature., (b) 60 ℃ and (c) 80 ℃. Samples were dried after NaOH was removed from the samples by 20 wt% H_2SO_4 aqueous solution and subsequent deionized water.

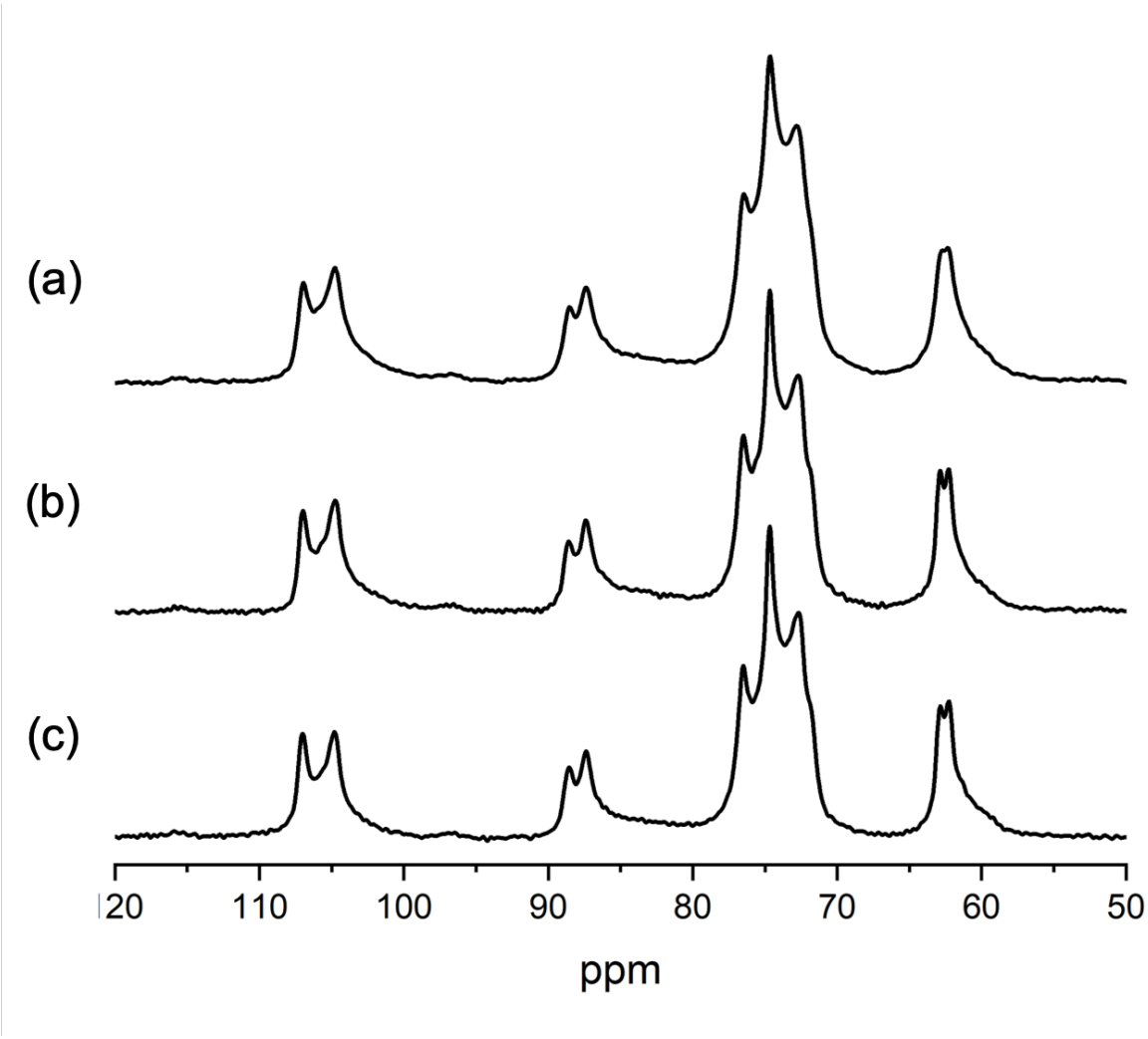

Fig.3-10. Dried state ^{13}C CP/MAS NMR spectra of post-treated cellulose at (a) room temperature., (b) 60 ℃ and (c) 80 ℃. Samples were dried after NaOH was removed from the samples by 20 wt% H_2SO_4 aqueous solution and subsequent deionized water.

Table 1. CI_{nmr}, accessible surface fraction and inaccessible surface (or amorphous) fraction by quantitatively evaluated from the NMR spectra in the post-treated cellulose with 10 % NaOH aqueous solution at various temperature.

Temperature	CI_{nmr} (%)	Accessible Surface Fraction (%)	Inaccessible Surface Fraction (%)
RT	59.1	11.4	29.4
60 ℃	61.8	11.4	26.7
80 ℃	62.7	9.77	27.5

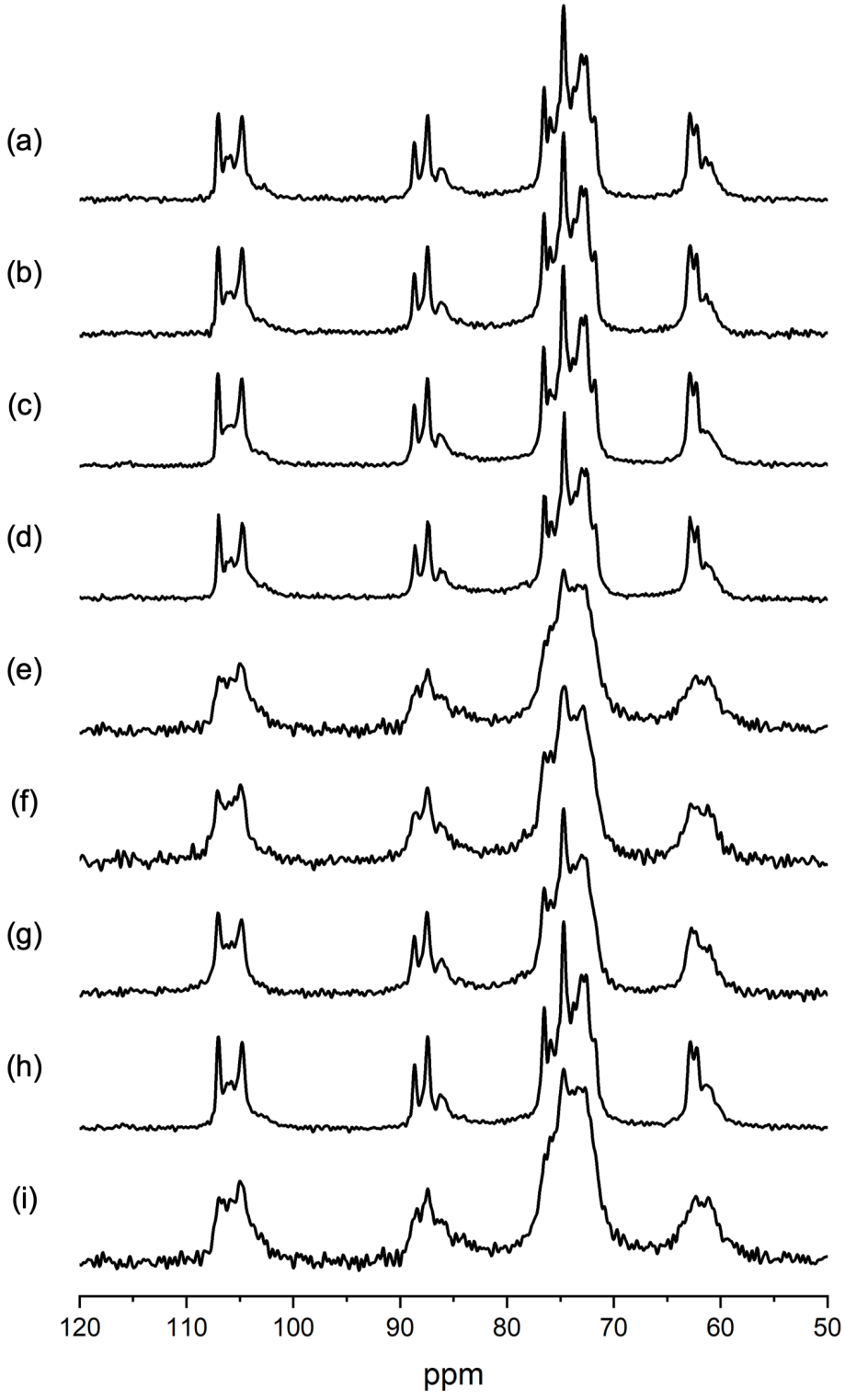

Fig. 3-11. Hydrated state ^{13}C CP/MAS NMR spectra of the post-treated cellulose neutralized with 1 wt% (a), 10 wt % (b) and 20 wt %(c) H_2SO_4 aqueous solution, 1 wt % (d) and 10 wt % (e) HCl aqueous solution, 1 wt % (f) and 20 wt % (g) CH_3COOH aqueous solution, and 1 wt % (h) and 20 wt % (i) H_3PO_4 aqueous solution.

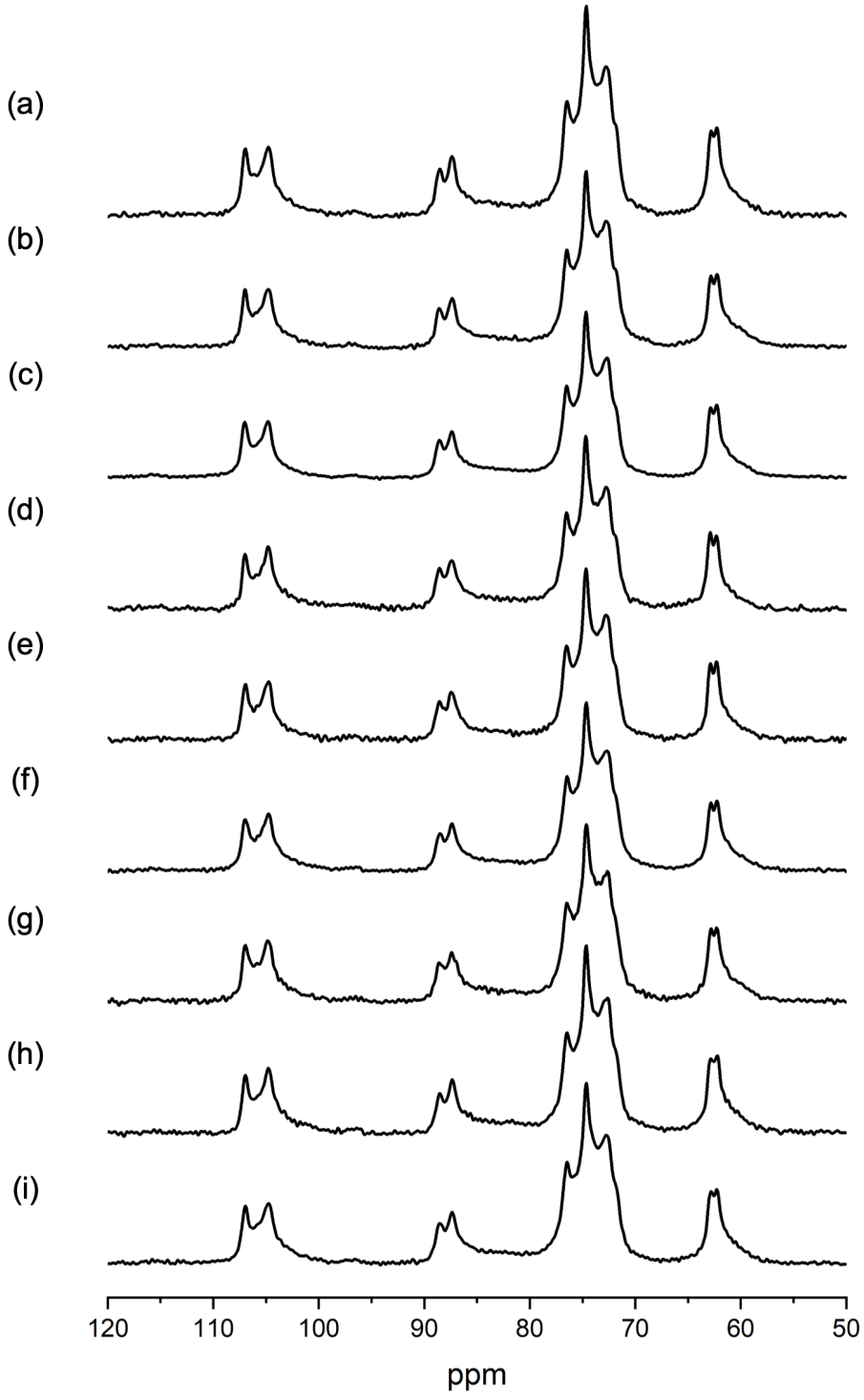

Fig. 3-12. Hydrated state ^{13}C CP/MAS NMR spectra of the post-treated cellulose neutralized with 1 % (a), 10 % (b) and 20 %(c) H_2SO_4 aqueous solution, 1 % (d) and 10 %(e) HCl aqueous solution, 1 % (f) and 20 % (g) CH_3COOH aqueous solution, and 1% (h) and 20 % (i) H_3PO_4 aqueous solution.

Table 2. CI_{nmr}, accessible surface fraction and inaccessible surface(or amorphous) fraction by quantitatively evaluated from the NMR spectra in the post-treated cellulose with 10 % NaOH aqueous solution at 80℃ and neutralized with various acids aqueous solution at room temperature

Acid for Neutralization	Concentration of $Acid_{aq}$ (wt%)	CI_{nmr} (%)	Accessible surface fraction (%)	Inaccessible Surface Fraction (%)
H_2SO_4	1	62.1	11.1	26.8
H_2SO_4	10	62.0	10.3	27.7
H_2SO_4	20	62.7	9.78	27.5
HCl	1	55.3	6.78	37.9
HCl	20	62.7	9.68	27.6
CH_3COOH	1	57.2	10.2	32.5
CH_3COOH	20	61.6	10.1	28.3
H_3PO_4	1	57.0	11.1	31.9
H_3PO_4	20	60.7	11.4	27.9

3.3.3 Effects of acid for neutralization

Na-cellulose was converted to cellulose II during the neutralization process. This process can be altered with different types or concentrations of acids. Fig. 3-11 and 3-12 shows the solid state ^{13}C CP/MAS spectra of the mercerized cellulose neutralized by 20 % sulfuric acid, hydrochloric acid, phosphoric acid, and acetic acid. The results show that the spectra of the samples neutralized by a weak acid (e.g. phosphoric acid and acetic acid) had slightly broader linewidth than when neutralized by a stronger acid (e.g. sulfuric acid and hydrochloric acid). The CI_{nmr} calculated from the NMR spectra of dried post treated cellulose samples shown in Table 2. The CI_{nmr} of the samples neutralized by a strong acid were larger than those with a weak acid. For the neutralization of the NaOH in the mercerization, the required amount of strong acid aqueous solution was less than that of the weak acid, up to pH 7. The final concentrations of the salts generated by the neutralization were more with the strong acids than with the weak acids. It can be thought that the concentration of salts finally generated by

neutralization is correlated with the hydrophobic interaction in solution. It was reported that the kosmotropic salts generally induce a hydrophobic alkyl chain packing on the polymer molecules [17], and also reported in the case of fibroin that β-sheet construction is induced by kosmotropic ions [18]. It can be thought hydrophobic interaction was also induced by kosmotropic salts. It was reported that the hydrophobic interaction has important role for the crystal structure of the cellulose II[5].

Finally, the effect of neutralization temperature was estimated. Fig. 3-13 and 3-14 shows the t solid state ^{13}C CP/MAS spectra of the mercerized cellulose neutralized by 20 % sulfuric acid at room temperature or 80 ℃. The spectra show similar characteristic. C4 fitting was carried out for evaluating the crystallinity and surface fraction. Table 3 shows that the neutralization temperature did not make significant differences, but better crystallinity was obtained by the neutralization at room temperature. Accordingly, neutralization with high concentrations of strong acid could promote the cellulose II crystal assembly at room temperature.

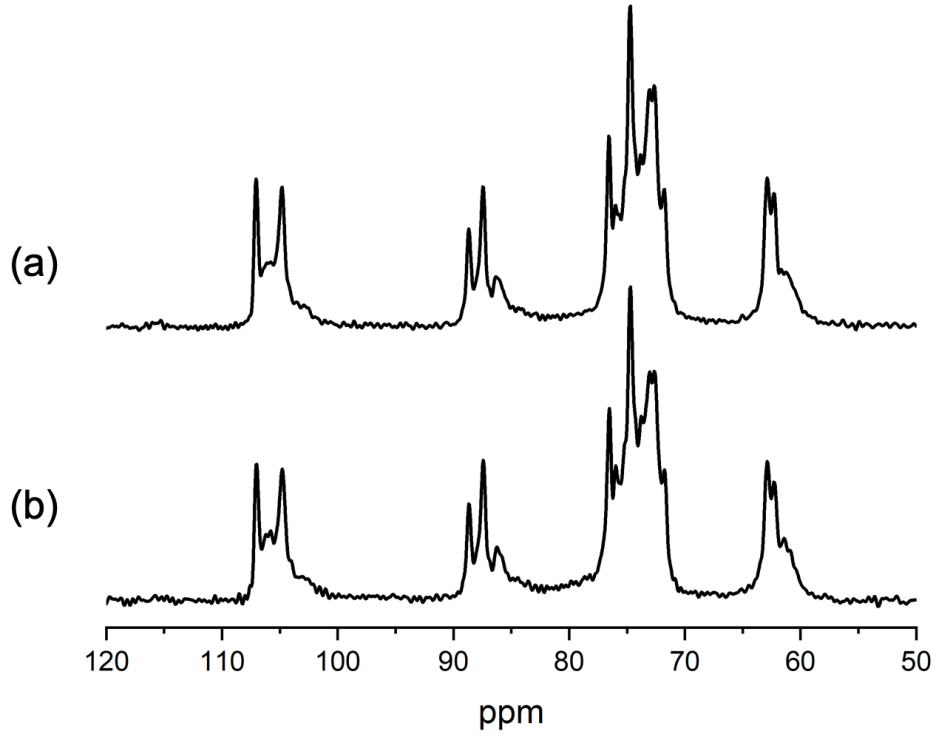

Fig.3-13 Hydrated state ^{13}C CP/MAS NMR spectra of the post-treated cellulose neutralized with (20 % H_2SO_4 at room temperature (a) and 80 ℃ (b).

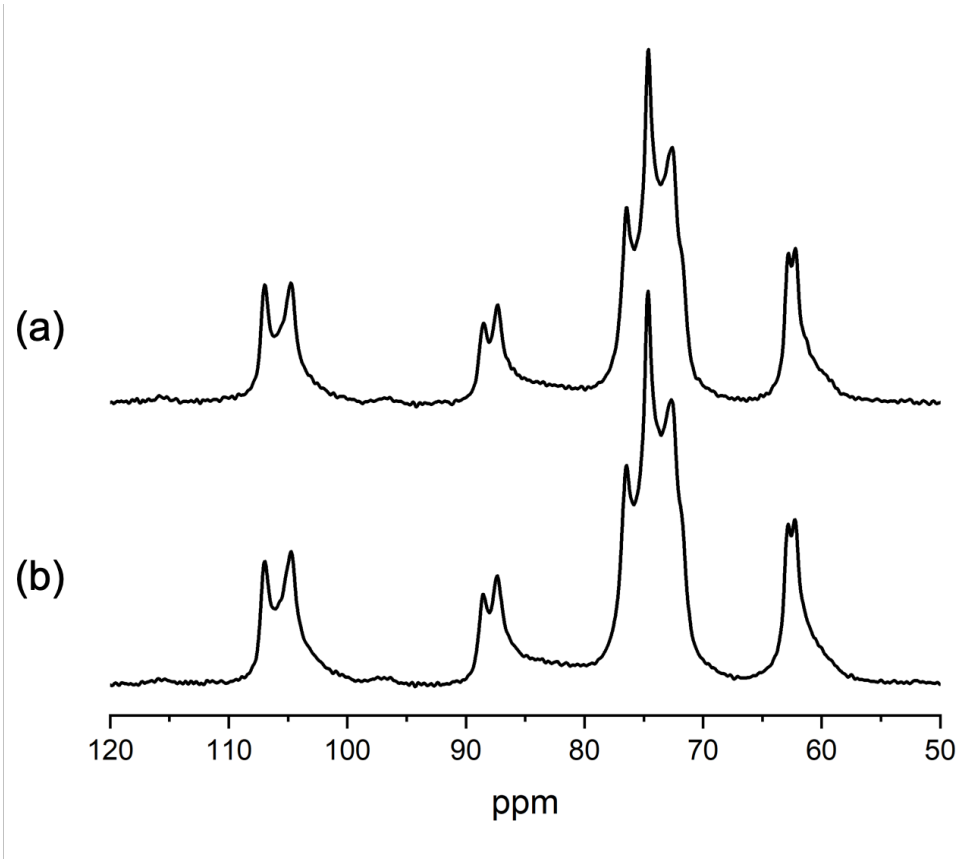

Fig.14 Hydrated state ^{13}C CP/MAS NMR spectra of the post-treated cellulose neutralized with (20 % H_2SO_4 at room temperature (a) and 80 ℃ (b).

Table 3. CI_{nmr}, accessible surface fraction and inaccessible surface (or amorphous) fraction by quantitatively evaluated from the NMR spectra in the post-treated cellulose with 10 % NaOH aqueous solution at 80℃ and neutralized with 20%H_2SO_4 aqueous solution at various temperature.

Neutralization Temperature	CI_{nmr} (%)	Accessible surface fraction (%)	Inaccessible Surface Fraction (%)
RT	62.7	9.78	27.5
80℃	61.9	9.24	28.9

3.3.4. Post-treatment on the regenerated cellulose II

Based on the discussions, regenerated cellulose was post-treated with the optimized condition, i.e., soak with 10 % NaOH aqueous solution with 80 ℃ and subsequent neutralization with 20 % H_2SO_4 aqueous solution. Solid state ^{13}C CP/MAS NMR spectra of regenerated cellulose before and after post-treatment are shown in Fig. 9. From the spectra, it can be clearly seen that the resonance lines became narrower with post-treatment than that before the treatment and the calculated CI_{nmr} improved from 33.0 % to 54.0 % as shown in Table 4.

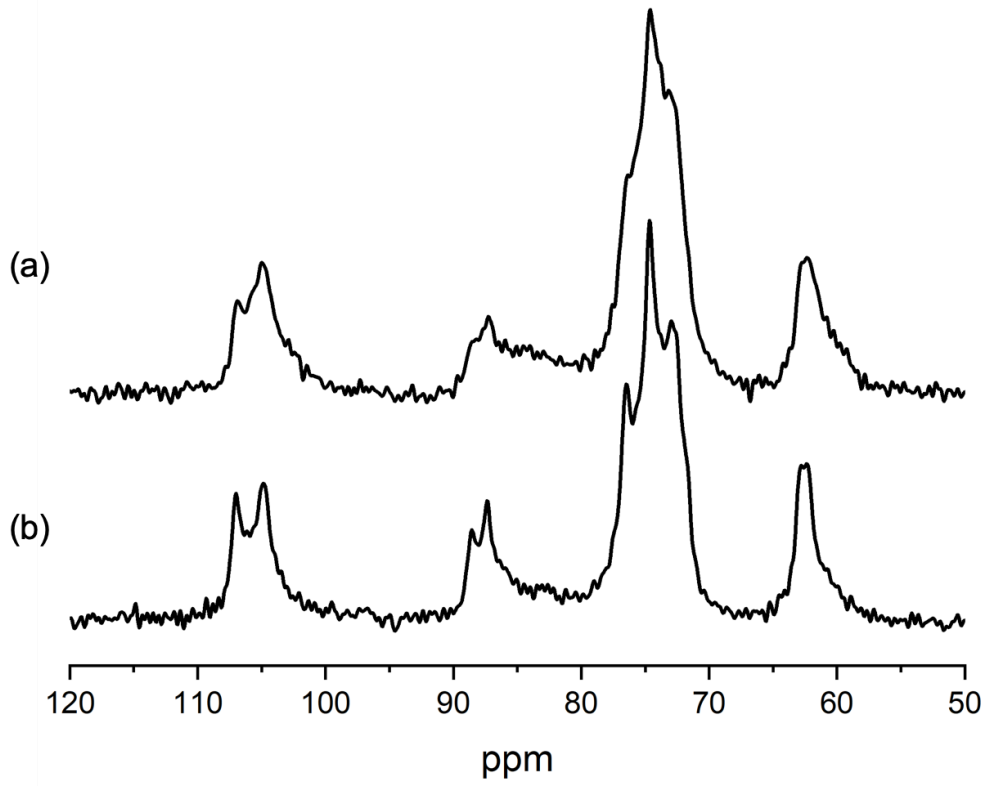

Fig. 10 Dried state ^{13}C CP/MAS NMR spectra of (a) before and (b) after post-treated regenerated cellulose at dried state. All samples were dried after NaOH was removed from the samples by 20 wt% H_2SO_4 aqueous solution and subsequent deionized water.

Table 4. Crystallinity Index, accessible surface fraction and inaccessible surface/amorphous fraction by quantitatively evaluated from the NMR spectra in the rpost-treated regenerated cellulose with 10% NaOH aqueous solution (Fig. 9).

Sample	Crystallinity Index (%)	Accessible Surface Fraction (%)	Inaccessible Surface Fraction (%)
regenerated cellulose	33	11.9	55.1
regenerated cellulose after post-treatment	54	12	34

3.4. Conclusions

The change of crystallinity, crystal size and surface fractions by NaOH post-treatment on the mercerized or regenerated cellulose II were revealed by solid state ^{13}C CP/MAS NMR and XRD experiments. The crystallinity index obtained by solid state ^{13}C CP/MAS NMR shows similar tendency to the crystal size obtained from XRD. Crystallinity was decided to maximized at the post-treatment with 10% NaOH aqueous solution. Decreasing the formation of Na-cellulose in crystal core during post-treatment are important for the crystal size of cellulose II. Moreover, Na-cellulose construction is affected by the concentration of NaOH, treatment temperature, and selection of acid in the subsequent neutralization process. It was discovered that 10 % concentration is the most efficient for decreasing inaccessible surface region and increasing crystal size; further, the high temperature much more decrease the inaccessible surface and increases crystallinity. During neutralization, it is probable that higher polarity of solvent generated by the kosmotropic salt provides a more efficient crystallization process on post-treatment.

Rererences

[1] H. Yang, T. Wang, D. Oehme, L. Petridis, M. Hong, J.D. Kubicki, Structural factors affecting ^{13}C NMR chemical shifts of cellulose: a computational study, Cellulose. 25 (2018) 23–36. doi:10.1007/s10570-017-1549-6.

[2] J. Cai, L. Zhang, J. Zhou, H. Qi, H. Chen, T. Kondo, X. Chen, B. Chu, Multifilament fibers based on dissolution of cellulose in NaOH/urea aqueous solution: structure and properties, Advanced Materials. 19 (2007) 821–825. doi:10.1002/adma.200601521.

[3] J. Široký, R.S. Blackburn, T. Bechtold, J. Taylor, P. White, Attenuated total reflectance Fourier-transform Infrared spectroscopy analysis of crystallinity changes in lyocell following continuous treatment with sodium hydroxide, Cellulose. 17 (2010) 103–115. doi:10.1007/s10570-009-9378-x.

[4] X. Colom, F. Carrillo, Crystallinity changes in lyocell and viscose-type fibres by caustic treatment, European Polymer Journal. 38 (2002) 2225–2230. doi:10.1016/S0014-3057(02)00132-5.

[5] N. Isobe, U.J. Kim, S. Kimura, M. Wada, S. Kuga, Internal surface polarity of regenerated cellulose gel depends on the species used as coagulant, Journal of Colloid and Interface Science. 359 (2011) 194–201. doi:10.1016/j.jcis.2011.03.038.

[6] J. Zhou, L. Zhang, Solubility of Cellulose in NaOH / Urea Aqueous Solution, Polymer Journal. 32 (2000) 866–870.

[7] L. Zhang, Y. Mao, J. Zhou, J. Cai, Effects of coagulation conditions on the properties of regenerated cellulose films prepared in NaOH/Urea aqueous solution, Industrial and Engineering Chemistry Research. 44 (2005) 522–529. doi:10.1021/ie0491802.

[8] M. Wada, M. Ike, K. Tokuyasu, Enzymatic hydrolysis of cellulose I is greatly accelerated via its conversion to the cellulose II hydrate form, Polymer Degradation and Stability. 95 (2010) 543–548. doi:10.1016/j.polymdegradstab.2009.12.014.

[9] C. Chang, B. Duan, L. Zhang, Fabrication and characterization of novel macroporous cellulose-alginate hydrogels, Polymer. 50 (2009) 5467–5473. doi:10.1016/j.polymer.2009.06.001.

[10] D. Massiot, F. Fayon, M. Capron, I. King, S. Le Calvé, B. Alonso, J.O. Durand, B. Bujoli, Z. Gan, G. Hoatson, Modelling one- and two-dimensional solid-state NMR spectra, Magnetic Resonance in Chemistry. 40 (2002) 70–76. doi:10.1002/mrc.984.

[11] G. Zuckerstätter, N. Terinte, H. Sixta, K.C. Schuster, Novel insight into cellulose supramolecular structure through ^{13}C CP-MAS NMR spectroscopy and paramagnetic relaxation enhancement, Carbohydrate Polymers. 93 (2013) 122–128. doi:10.1016/j.carbpol.2012.05.019.

[12] C.M.C. L. Segal, J.J. Creely, A.E. Martin, Jr, An Empirical Method for Estimating the Degree of Crystallinity of Native Cellulose Using the X-Ray Diffractometer, Textile Research Journal. 29 (1959) 786–794. doi:10.1177/004051754701701001.

[13] C.P. Azubuike, H. Rodríguez, A.O. Okhamafe, R.D. Rogers, Physicochemical properties of maize cob cellulose powders reconstituted from ionic liquid solution, Cellulose. 19 (2012) 425–433. doi:10.1007/s10570-011-9631-y.

[14] F. Horii, A. Hirai, R. Kitamaru, Solid-state ^{13}C-NMR study of conformations of oligosaccharides and cellulose - Conformation of CH2OH group about the exo-cyclic C-C bond, Polymer Bulletin. 10 (1983) 357–361. doi:10.1007/BF00281948.

[15] H. Kono, Y. Numata, T. Erata, M. Takai, ^{13}C and1H resonance assignment of mercerized cellulose II by two-dimensional MAS NMR spectroscopies, Macromolecules. 37 (2004) 5310–5316. doi:10.1021/ma030465k.

[16] F. Porro, O. Bédué, H. Chanzy, L. Heux, Solid-state ^{13}C NMR study of Na-cellulose complexes, Biomacromolecules. 8 (2007) 2586–2593. doi:10.1021/bm0702657.

[17] Y. Zhang, P.S. Cremer, Interactions between macromolecules and ions: the Hofmeister series, Current Opinion in Chemical Biology. 10 (2006) 658–663. doi:10.1016/j.cbpa.2006.09.020.

[18] N.A. Oktaviani, A. Matsugami, F. Hayashi, K. Numata, Ion effects on the conformation and dynamics of repetitive domains of a spider silk protein: Implications for solubility and β-sheet formation, Chemical Communications. 55 (2019) 9761–9764. doi:10.1039/c9cc03538a.

Chapter 4. DFT Approach to the Pathway of Conformational Changes of C6-Hydroxymethyl Group

4.1. Introduction

In this chapter, to clarify the irreversibility of Mercerization process, DFT calculations were carried out on a single cellotetraose molecules as a model for a single chain of cellulose, with a focus on the reaction coordinates among various C6 conformations. As already mentioned, during mercerization process, the conformation changes from *tg* to *gt* irreversibly. gt have never been observed in cellulose I crystal core and also tg has never been observed in cellulose II crytal core. On the other hand, in the regeneration process, the C6 conformation changes from *gg* to *gt*, while in the biosynthesis process, it might change from *gg* to *tg*. The second aim of this study is to investigate the C6 conformational changing pathways among *gg*, *tg*, and *gt* states in the regeneration and biosynthesis processes. In those processes single-chain-like state will play an important role as an intermediate. The hydrogen bonding pattern and the following molecular conformations are constructed from dihedral angles of each hydroxyl or hydroxymethyl group. These angles are taken as parameters of molecular potential energy and the obtained relationships between angles and the potential energy surface (PES) were analyzed for the characterization of each C6 conformation, especially about *tg* and *gt* conformations, which relate to cellulose I and II, respectively. Transition processes among *tg*, *gt*, and *gg* were extensively examined while taking into account the hydrogen bonding network.

4.2. Methods

The starting cellotetraose model, which has *tg*-A and B conformations (Figs. 4-1), was optimized by DFT with the ωB97XD functional and 6-31G (d, p) basis set, with the initial coordinate set taken from the X-ray diffractometry data of cellulose Iβ[6]. Subsequently, single-point energy calculations at 6-31G++(d,p) level was carried out . The energy was expressed as a difference from the energy of the *tg*-B type structure at each level. The functional was used for correlating long-range interactions by dispersion forces[7] and a 6-31G (d, p) basis set was used while taking into account polarization of orbitals. The conformations of hydroxyl hydrogens were expressed with dihedral angles as χ_2 (C1'-C2'-O2'-H'), χ_3 (C4''-C3''-O3''-H''), χ_6 (C5-C6-O6-H), and C6 conformation as ω (C4-C5-C6-O6). Note that the dihedral angle χ_2 belongs to the residue adjacent to the residue containing C6, in which the dihedral angles are expressed as χ_6 and ω; χ_3 also belongs to another adjacent residue at the opposite side of χ_2, as shown in Fig. 4-2.

For calculation of each 2D-PES, two dihedral angles (see Table 1) were selected as the coordinates of the PES plot and the remaining angles were fixed at their most probable values during calculation. Each selected set of coordinates correspond to each dihedral angle between -180° to 180° in 10° steps and the zero-energy was indicated as the energy of tg-B type conformation. The potential energies were obtained by the optimization of each structure at various angles set with DFT (ωB97XD/ 6-31G (d, p)). The conformations of other residues were maintained as the initial cellulose I type structure. Single-point energy calculations at 6-31G++(d,p) level was carried out on stable and meta-stable points. In order to confirm that the specific point appeared in the PES plot is a meta-stable state, frequency analyses were also carried out. Gaussian09 was used for DFT calculations.

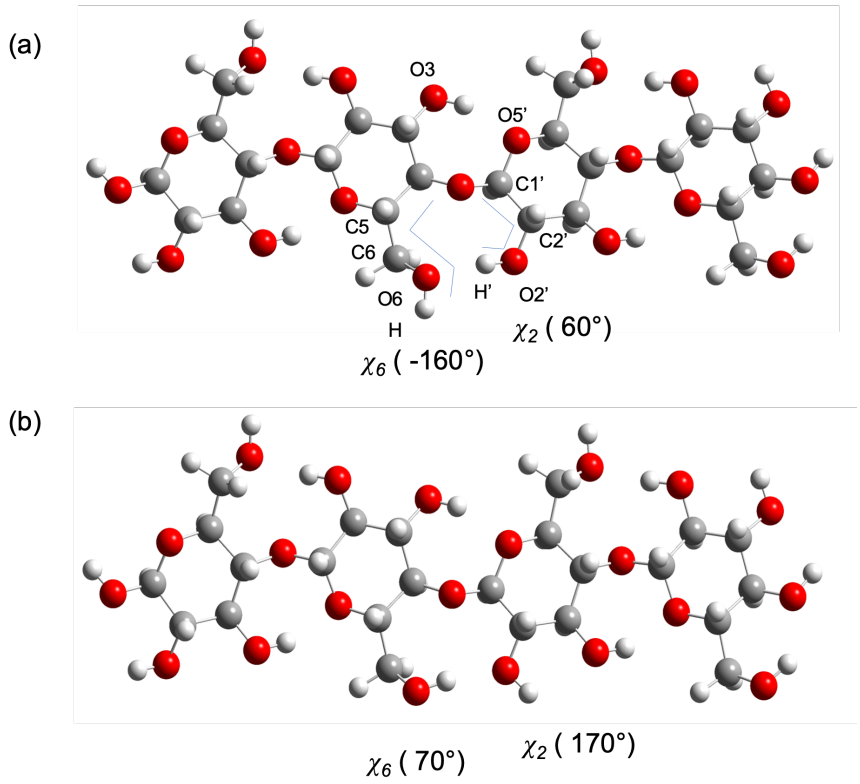

Fig. 4-1. Structure with *tg* conformation: (a) *tg*-A type conformation corresponding to cellulose I crystal structure; (b) *tg*-B type conformation corresponding to surface or amorphous state.

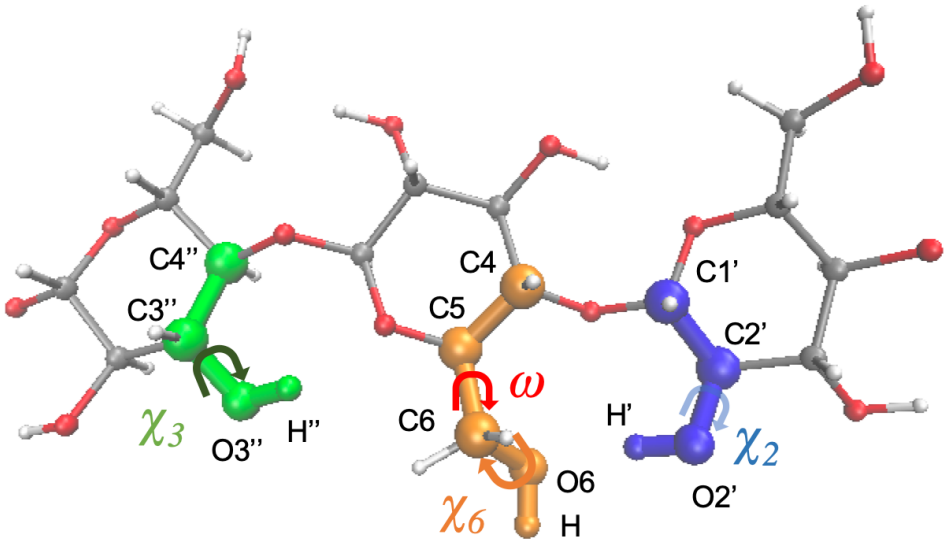

Fig. 4-2. Dihedral angles correspond to each hydroxyl and hydroxymethyl group. Dihedral angle of hydroxyl proton χ_2 corresponds to C1'-C2'-O2'-H', χ_3 corresponds to C4''-C3''-O3''-H'', χ_6 corresponds to C5-C6-O6-H and ω corresponds to C4-C5-C6-O6.

4.3. Results and Discussion

Conformational changes of cellulose molecules should be caused by hydrogen bond breaking because the conformation is maintained by hydrogen bonding. The hydrogen bonds of cellulose I are first broken, followed by a conformational change in order to construct the cellulose II structure. Frequency analysis of an optimized cellotetraose *tg*-A type shows that all modes have positive frequencies, namely, a stable state. Other conformations that have hydrogen bonds between O2' and O6 at *tg* or O3'' and O6 at *gt* also have positive frequencies. In order to elucidate conformational changes, it is necessary to investigate the details of hydrogen bond breaking and reconstruction of the conformation. These changes should appear in PES for (χ_2-χ_6) at *tg* and for (χ_3-χ_6) at *gt*.

4.3.1. Conformation for hydrogen bond breaking from tg

In the *tg* conformation, hydrogen bonds disruption and reconstruction was simulated by DFT calculation. Fig. 3 shows 2D-PES plot with the (χ_2-χ_6) set of variables for parameteters. The local minima at the coordinates (χ_2, χ_6) = (60, -160) indicate *tg*-A type conformation where O6 functions as a proton accepter, and at (χ_2, χ_6) = (-170, 70) indicate *tg*-B type conformation where O6-H functions as a proton donor. The normal mode vibrational analysis revealed that *tg*-A and *tg*-B type structures is surely stable state because they have only real frequency. On the other hand, the O2'-O6 hydrogen bond is breaking, in which several energy minima can be found (Fig. 4). Since the conformation of C6 remains nearly as *tg* (ω-fixed), this meta-stable state without hydrogen bond (O2'-O6) is designated as *tg**. Table 2 shows energy differences among *tg*-A, *tg*-B and *tg**. The *tg** structure found here is not stable when compared with *tg*-A or B type conformations, requiring some additional conformational reconstruction. With careful examination of the local area in the 2D-PES plot of χ_2-χ_6 around *tg**(Fig. 4-5), it was judged to be difficult to reconstruct a hydrogen bond returning to either the *tg*-A or

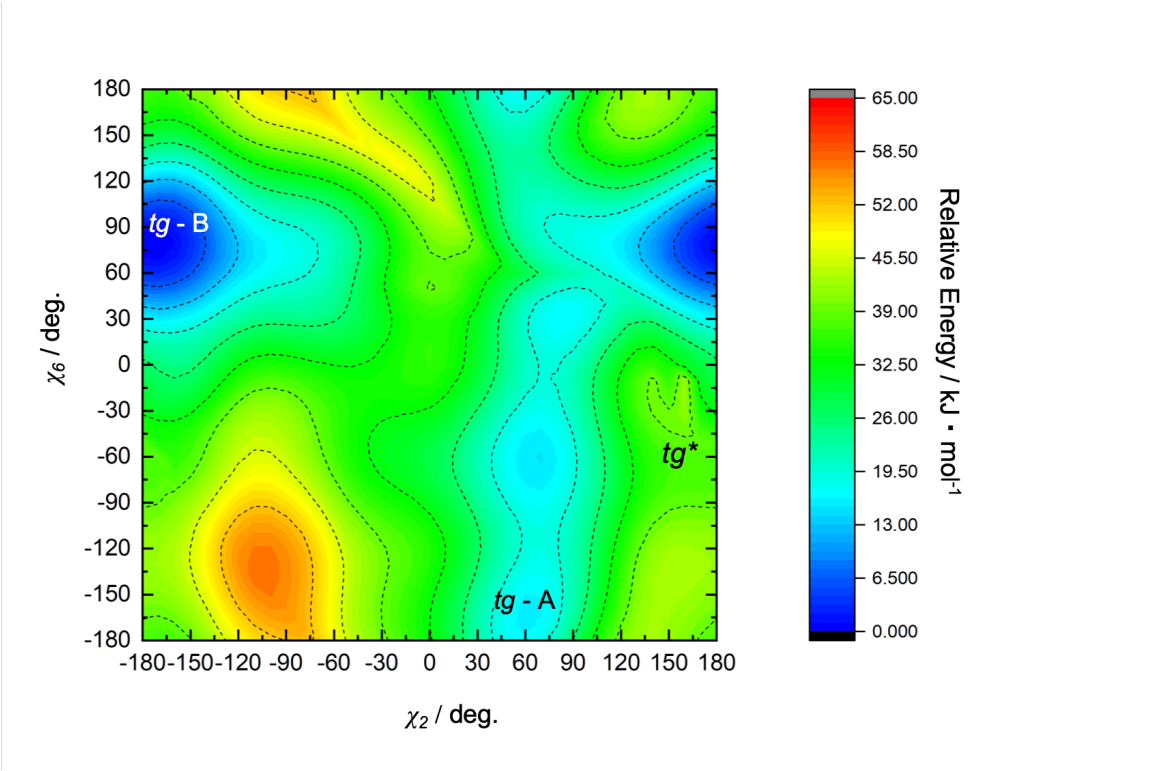

Fig. 4-3. 2D-PES of χ_2 and χ_6 as degrees of freedom for the *tg* conformation. The local minimum at the coordinates: (χ_2, χ_6) = (60, -160) indicates *tg*-A type conformation, (χ_2, χ_6) = (-160, 60) indicates *tg*-B type conformation, and (χ_2, χ_6) = (170, - 70) indicates *tg**.

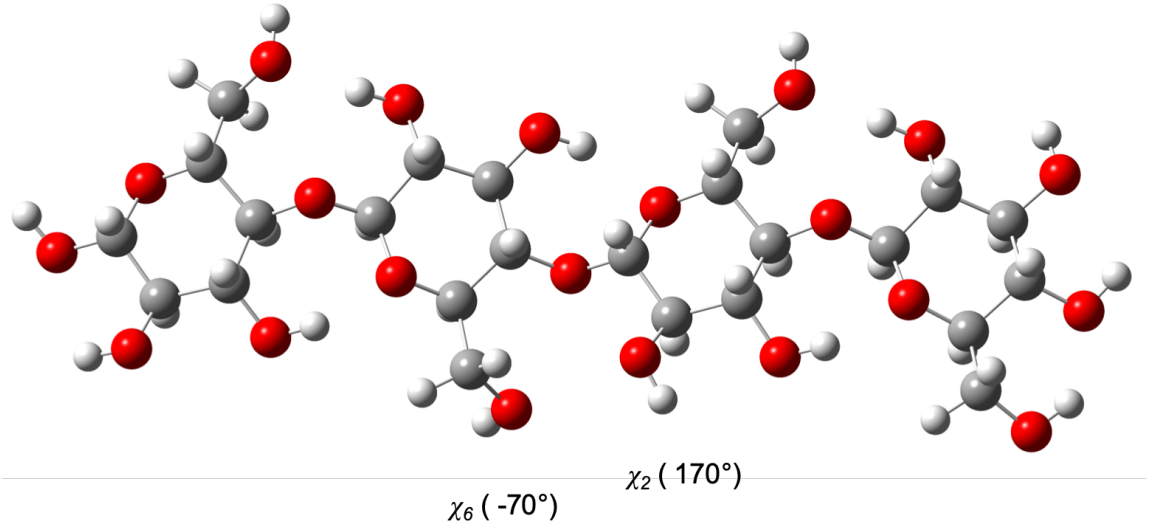

Fig. 4-4. The structure of *tg**, which has no hydrogen bond between O2 and O6.

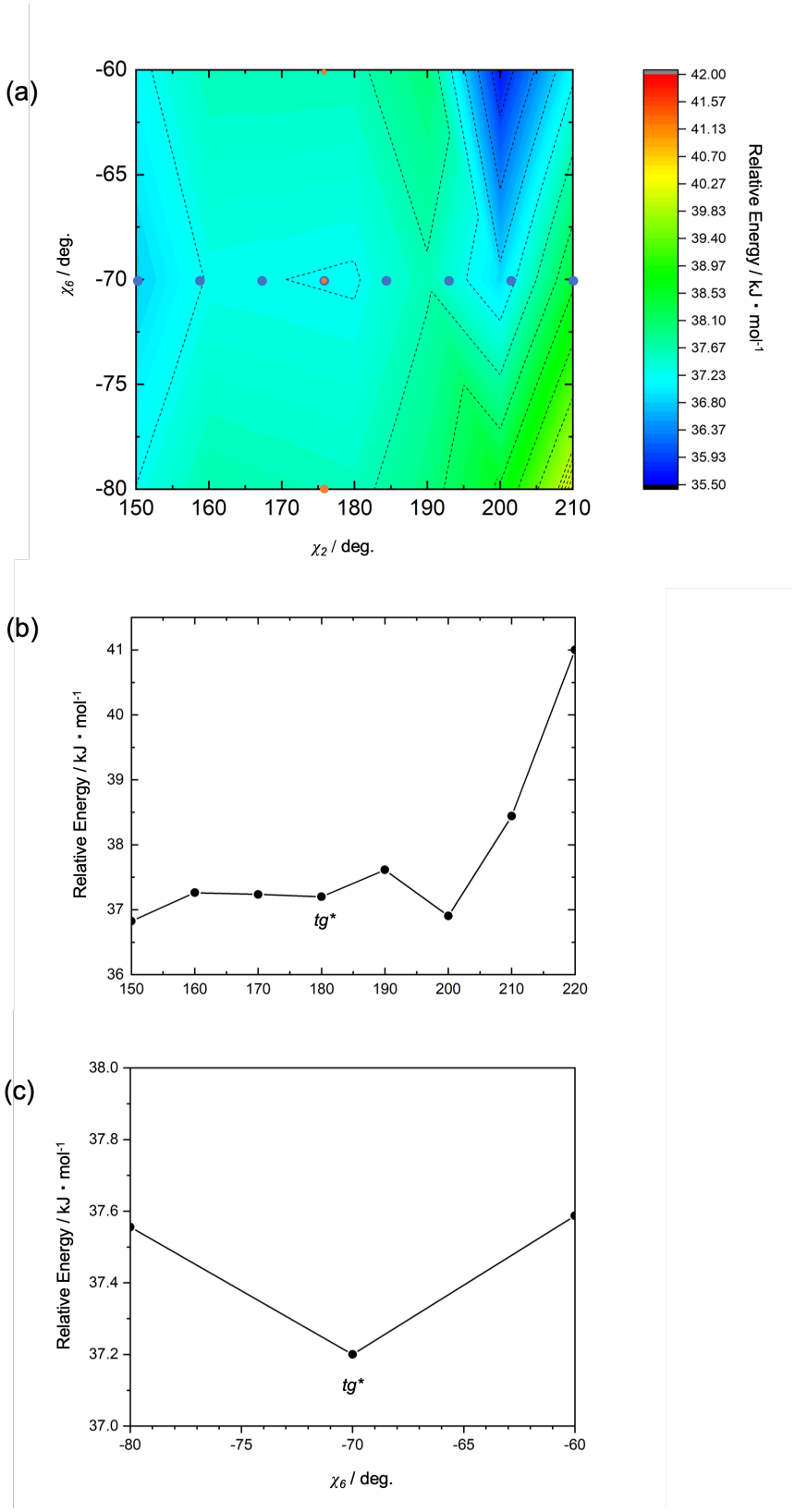

Fig. 4-5. (a) the PES of χ_2 and χ_6 on the range of [150:210] for χ_2 and [-80:-60] for χ_6 . (b) Cross section along χ_2 of (a). (c) Cross section along χ_6 of (a).

B type because *tg** is the local minimum with respect to χ_2 and χ_6. This result suggests that the reconstruction related to C6 conformation should be involved. In fact, the normal mode vibrational analysis revealed that *tg** has positive frequencies for χ_2 and χ_6, and only one mode, the vibration of ω direction, has imaginary frequency corresponding to the conformational change of C6 (Fig. 4-6). The *tg** state is meta-stable for χ_2 and χ_6, but unstable for ω rotation where only C6 conformational changes minimize the potential energy from *tg**. To confirm this C6 conformational change in the energy minimization of *tg**, 2D-PES plots of ω-χ_2 and ω-χ_6 were calculated as shown in Figs. 4-7 and 4-8, respectively. Both plots clearly show that the pathway from *tg** to *gt* has no energy barrier. Fig. 4-9 shows the schematic diagram as an overview of this transition from PES calculations. $\Sigma\Delta\chi_i$ was defined as the relative distance along a reaction path in vector space consisting of χ_2, χ_3 and χ_6 as components. Once the hydrogen bond between O2' and O6 is broken in the *tg* conformation, there will correspond to the transition to the *tg**, the conformational change of C6 leads to the *gt* conformation with a new hydrogen bond between O3' and O6.

The *tg** state has not been found yet experimentally. Experimentally, hydrogen bond breaking of cellulose and C6 conformational changes from *tg* to *gt* will occur when solvent molecules or alkaline ions in solution interact with the cellulose I crystal. The ^{13}C NMR chemical shifts of cellulose C6 with *tg*, *gt*, and *gg* conformations were reported as ~65 ppm, 62–63 ppm, and 61–62 ppm, respectively. In the mercerization process, a complex of Na-cellulose is generated as an intermediate in the *gt* conformation, identified through the ^{13}C NMR chemical shift (62.1 ppm) of C6[8]. The *tg** will have a very short lifetime and could not be found in the dissolution or mercerization process.

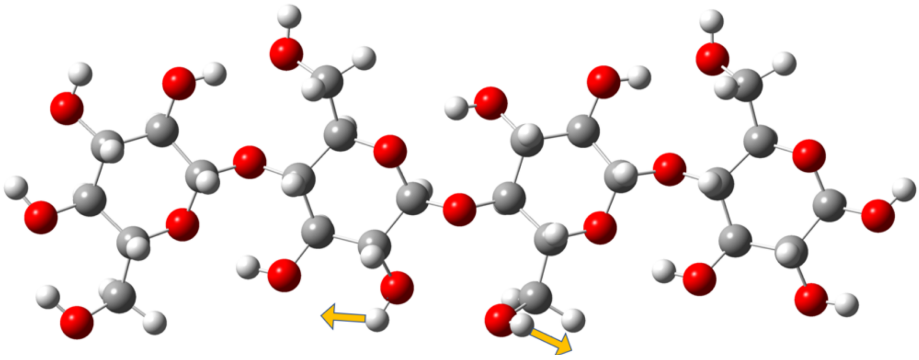

Fig. 4-6. The negative vibrational mode (-20.75 cm^{-1}) in *tg** structure. This mode has, large amplitude stretching of O2'-H and rotation of O6 (ω) as well as slight torsion of inter-anhydroglucose bond.

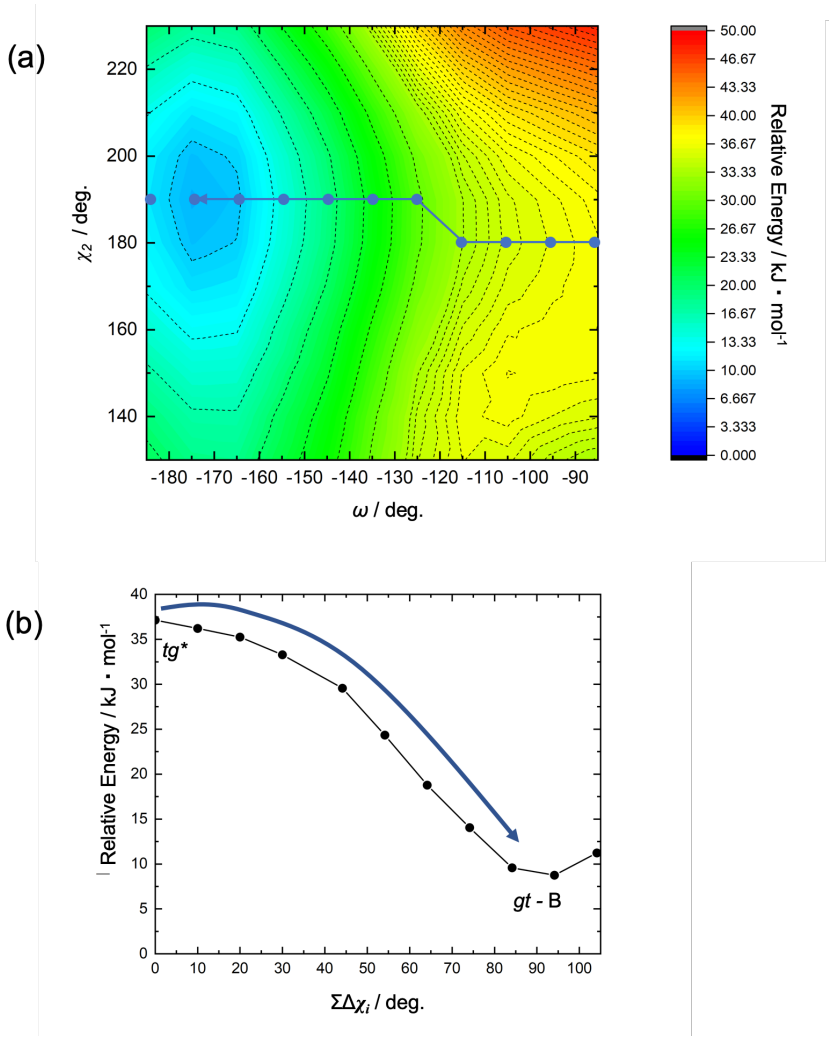

Fig.4-7. (a) The PES of ω-χ_2 (b) The cross section of (a), which correspond to energy minimization pathway from *tg** to *gt*-B.

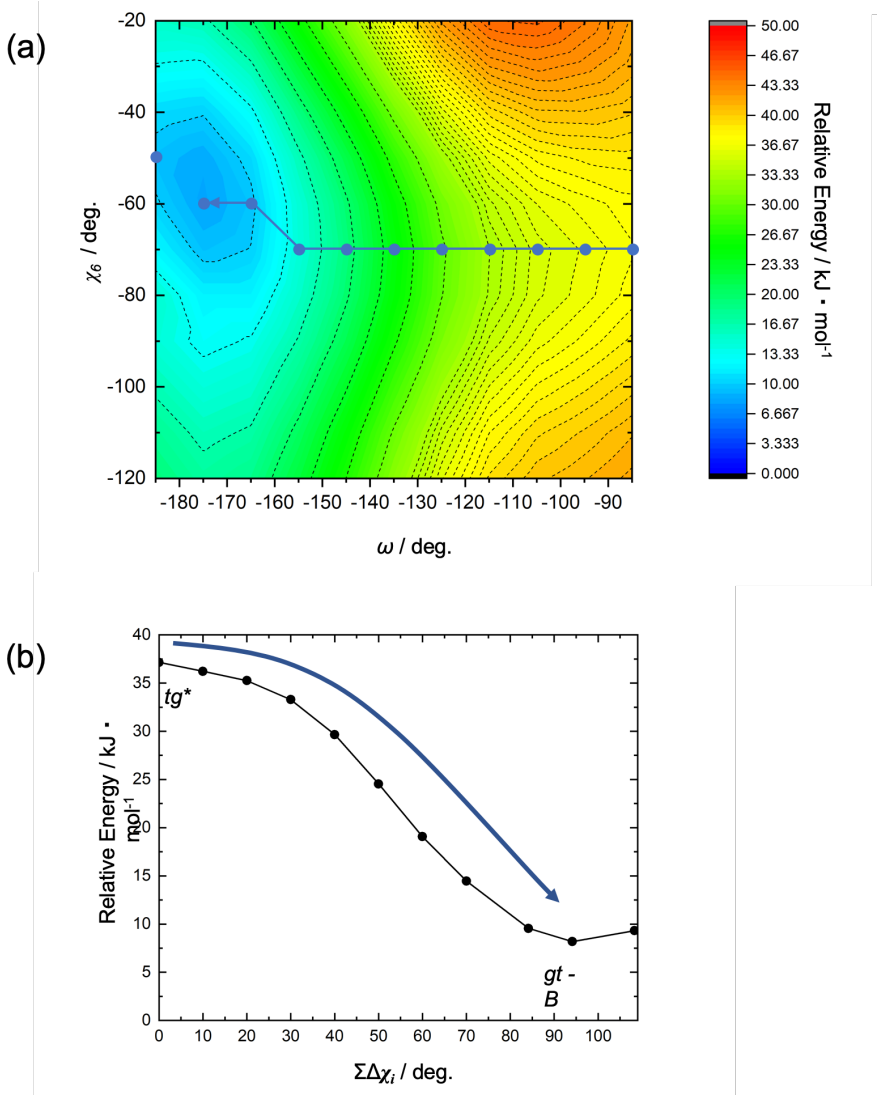

Fig. 4-8. (c) The PES of ω-χ_6 (d) The cross section of (c), which correspond to energy minimization pathway from *tg** to *gt*-B

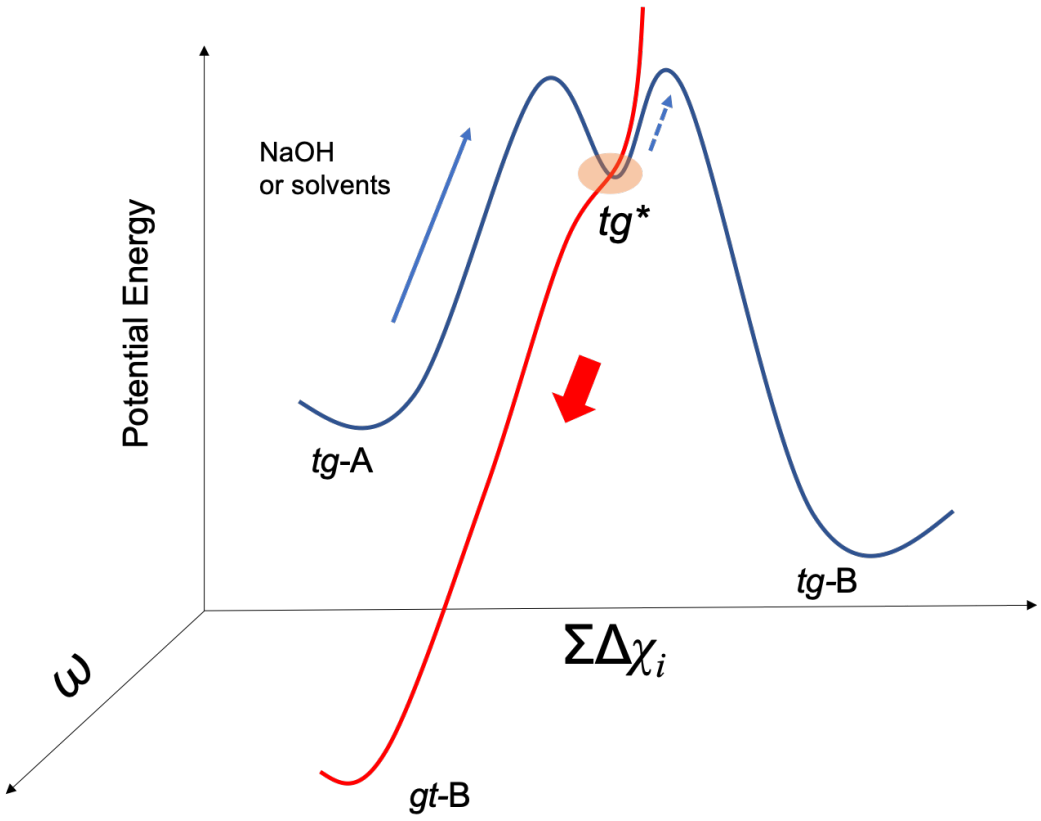

Fig. 4-9. Schematic diagram of C6 conformational transition from *tg* to *gt*. For C6 conformational change, the hydrogen bond between O2' and O6 has to be broken and pass through *tg** as the meta-stable state. At *tg**, energy minimization occurs only along the ω direction.

4.3.2. Hydrogen bond breaking of the gt conformation

Fig.4-10 shows the calculated 2D-PES (χ_3-χ_6) plot (Fig. 4-10). The result shows several energy minima which correspond to *gt*-A (90, 90) and *gt*-B (60, -50) and also meta stable *gt*-B (-170, -50) conformations (Fig. 4-11). In the case of the *gt* conformation, two additional types of hydrogen bond for O3-O6 are possible. The *gt*-A and *gt*-B types are decided whether O6 is a proton acceptor or donor like in the case of *tg*. The meta stable state of *gt*-B, called as *gt*-B (m), has only O6-O3 hydrogen bond, while O5 is not involved in any hydrogen bond. In addition, the point where the hydrogen bond between O3-O6 is broken can be found at around (χ_3, χ_6) = (-150, 70), and the molecular structure is unstable because this point is a saddle point with the imaginary energy gradients along χ_6 toward *gt*-B types. The energy differences among *gt*-A, *gt*-B, *gt*-B(m), *gt** was summarized in table 3. In Fig. 4-12 shows a reaction pathway from *gt** to *gt*-A or *gt*-B. This pathway indicates a different change from that of *tg** where the energy gradient was positive along χ_2 and χ_6. However, as in the case of *gt*, this state is identified as *gt** (Fig. 4-11). Fig. 4-12 and Fig. 4-13 shows the reaction paths as one of the possibilities from *gt** are either from *gt** to *gt*-A or from *gt** to *gt*-B with ω-fixed. In order to confirm whether the same reaction path can be obtained when the ω degree is relaxed, the PES calculations of ω-χ_3 and ω-χ_6 were carried out (Fig. 4-14 and Fig.4-15). The PES plots of ω-χ_3 and ω-χ_6 show that the χ_3 or χ_6 change was preferred relative to ω for energy minimization, which suggests that the C6 conformational change from *gt** will never take place, even after hydrogen bond disruption of the *gt* conformation. This is very different from the case of hydrogen-bond disruption at the *tg* conformation. The *gt* conformation is more stable than *tg* when the hydrogen bond is broken since *gt** don't change into *tg*. The normal mode vibrational analysis (Fig. 4-16) shows that *gt** has positive frequencies for χ_3 and ω, and only one mode, the vibration of χ_6 direction, has a imaginary frequency. Fig. 4-17 shows the schematic diagram of the transition starting from *gt**.

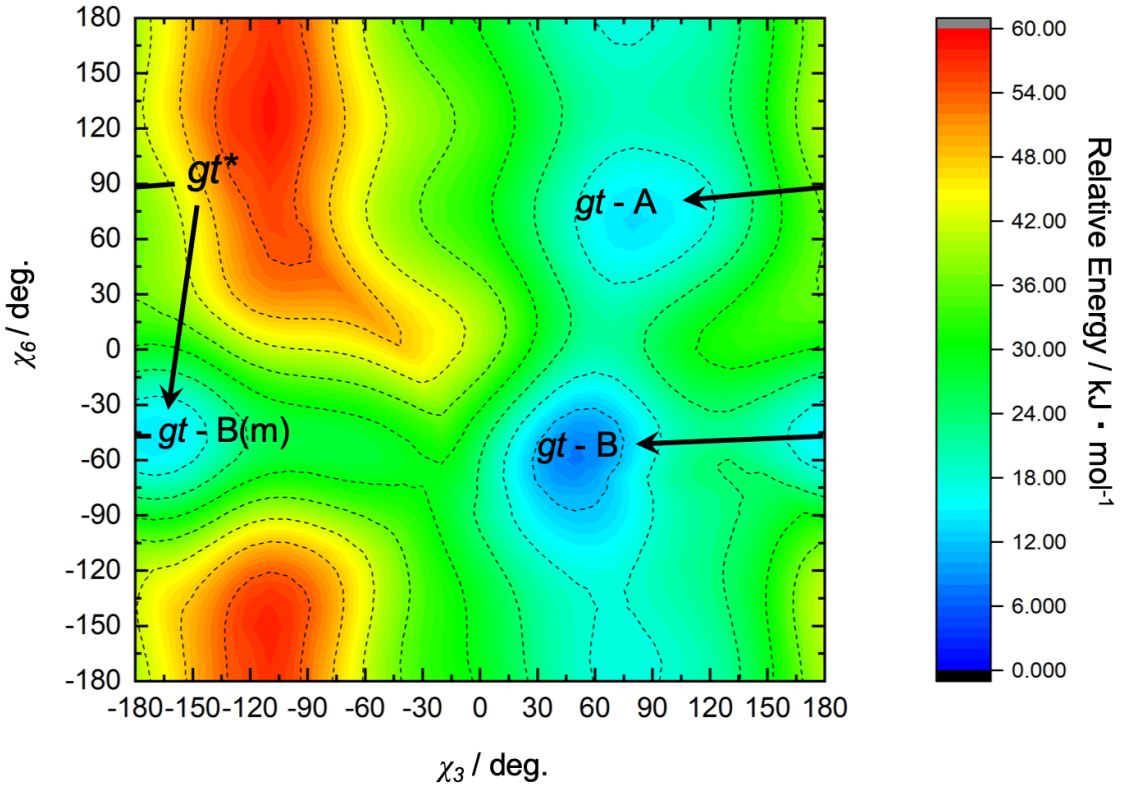

Fig.4-10. 2D-PES of χ_3 and χ_6 as degrees of freedom for the *gt* conformation. The local minimum at the coordinates: (χ_3, χ_6) = (80, 70) indicates *gt*-A type conformation, (χ_3, χ_6) = (50, -60) indicates *gt*-B type conformation, (χ_3, χ_6) = (-170, -50) indicates *gt*-B (m) confirmation, and (χ_3, χ_6) = (-150, 70) indicates *gt** confirmation.

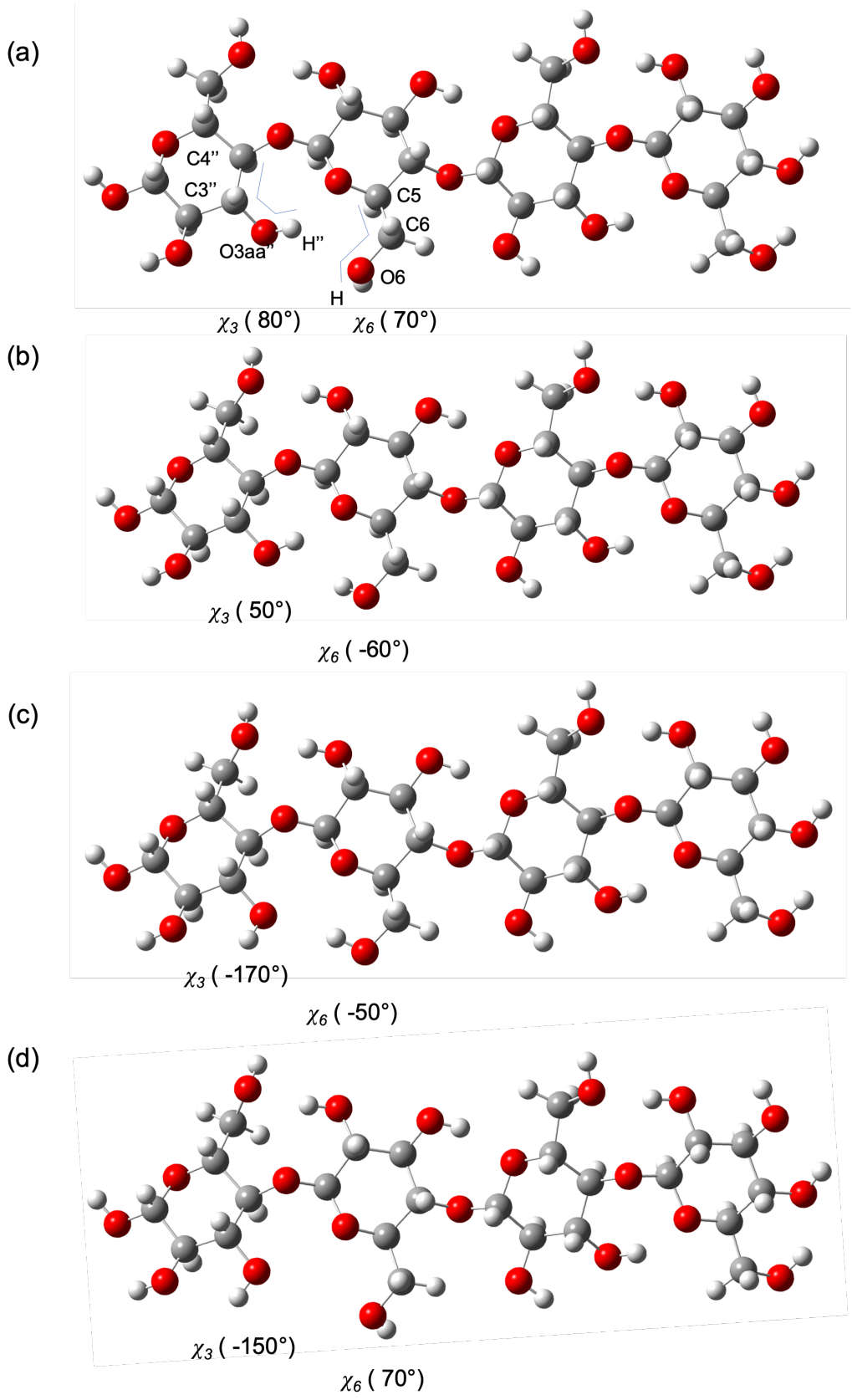

Fig.4-11. (a) Structure of *gt*-A type. (b) Structure of *gt*-B type. (c) Structure of gt-B (m) type. (d) Structure of *gt**.

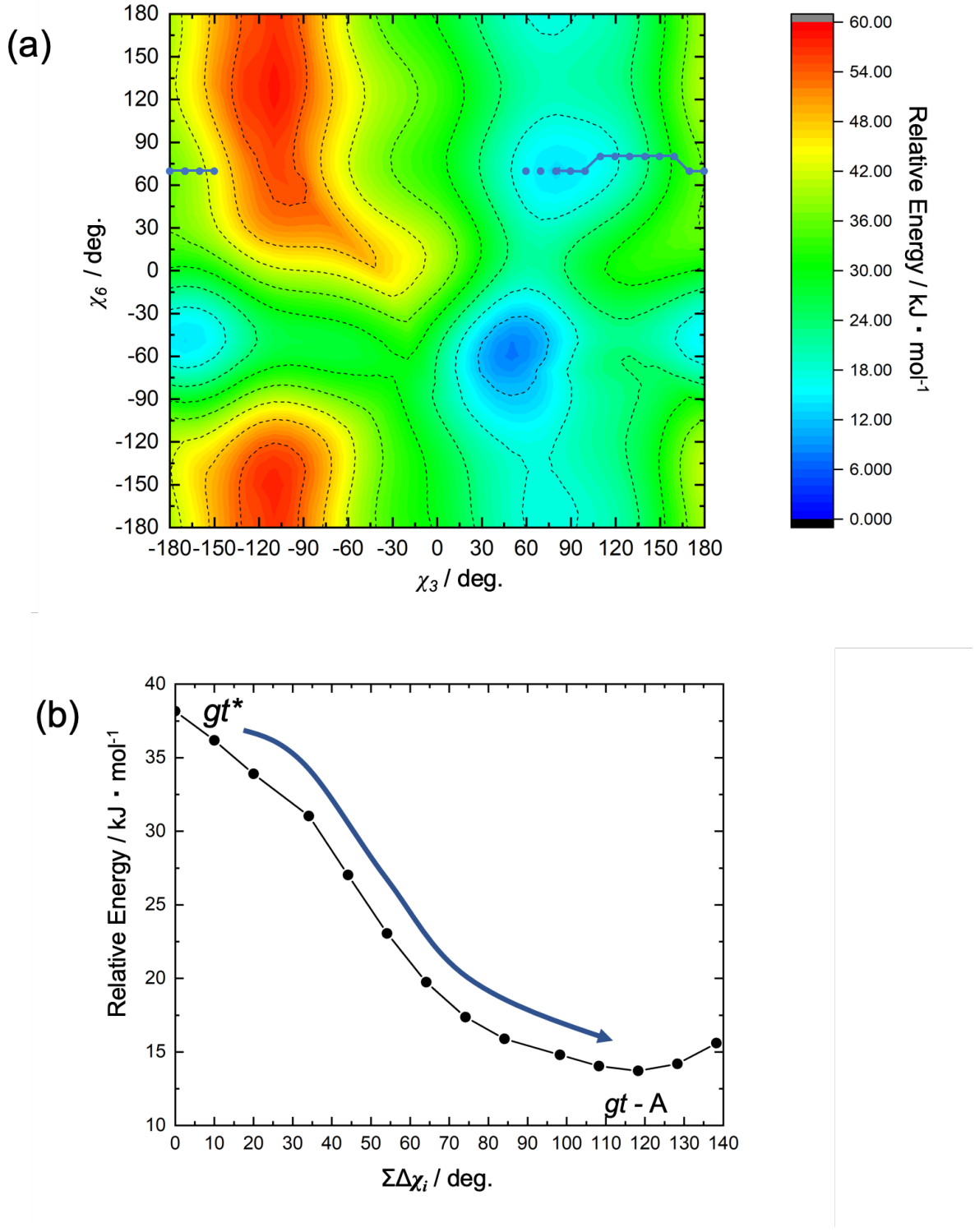

Fig.4-12. (a)The PES of χ_2 and χ_6 with energy minimization pathway from *gt** to *gt*-A (b) The cross section of (a) which correspond to energy minimization pathway from *gt** to *gt*-A

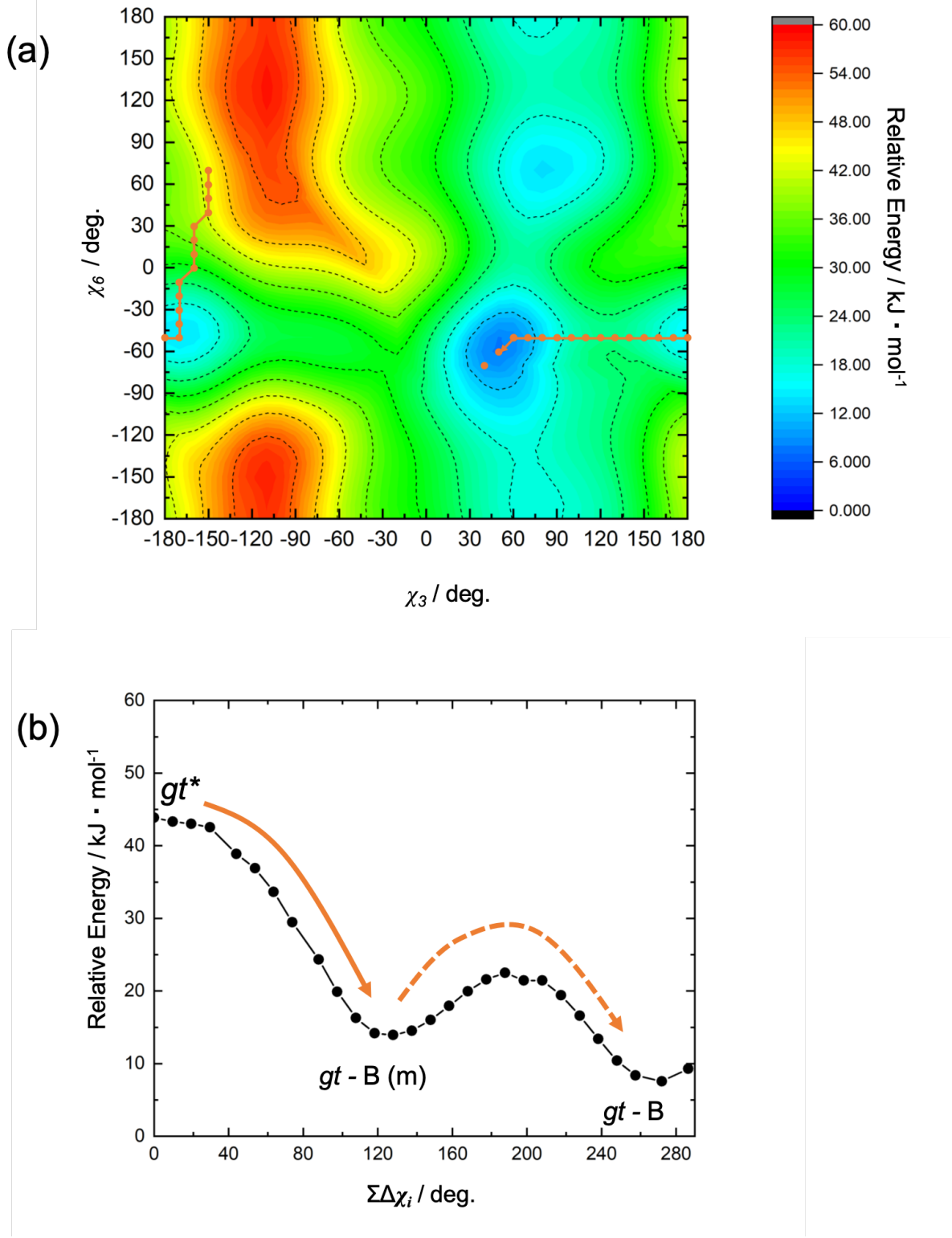

Fig.4-13. (a)The PES of χ_2 and χ_6 with energy minimization pathway from *gt** to *gt*-B(m) and *gt*-B (b) The cross section of (a) which correspond to energy minimization pathway from *gt** to *gt*-B

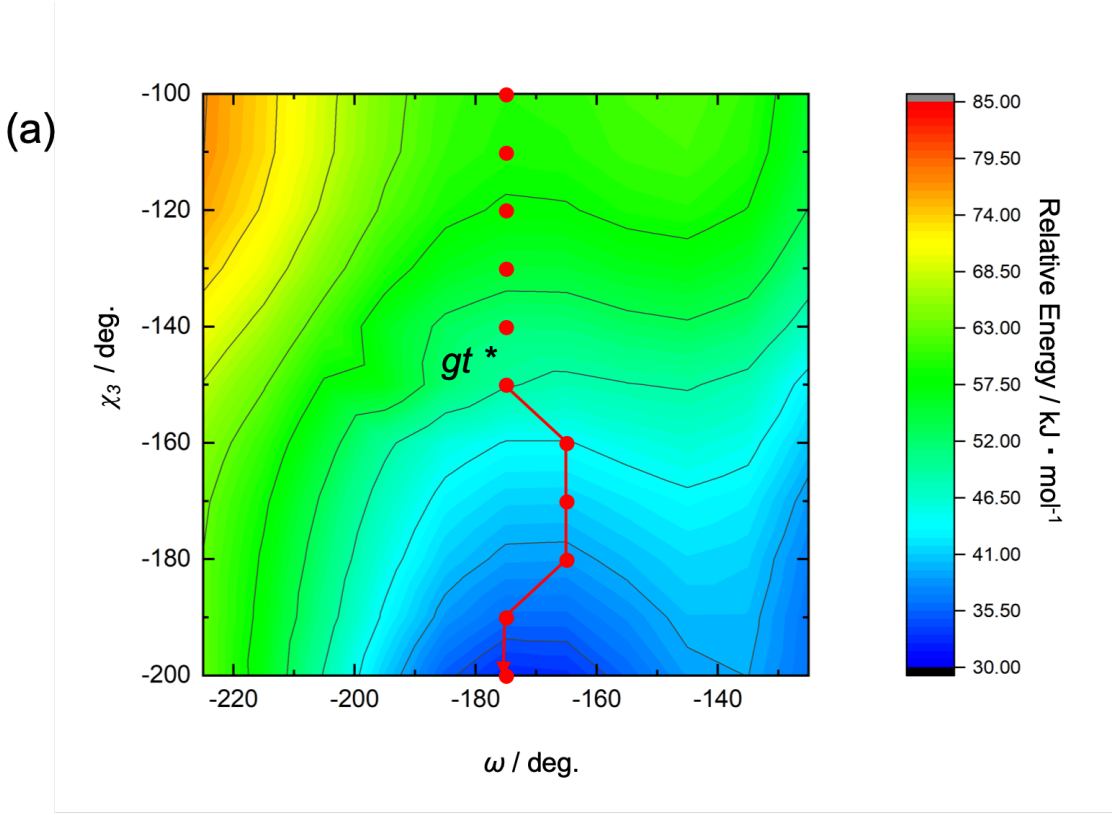

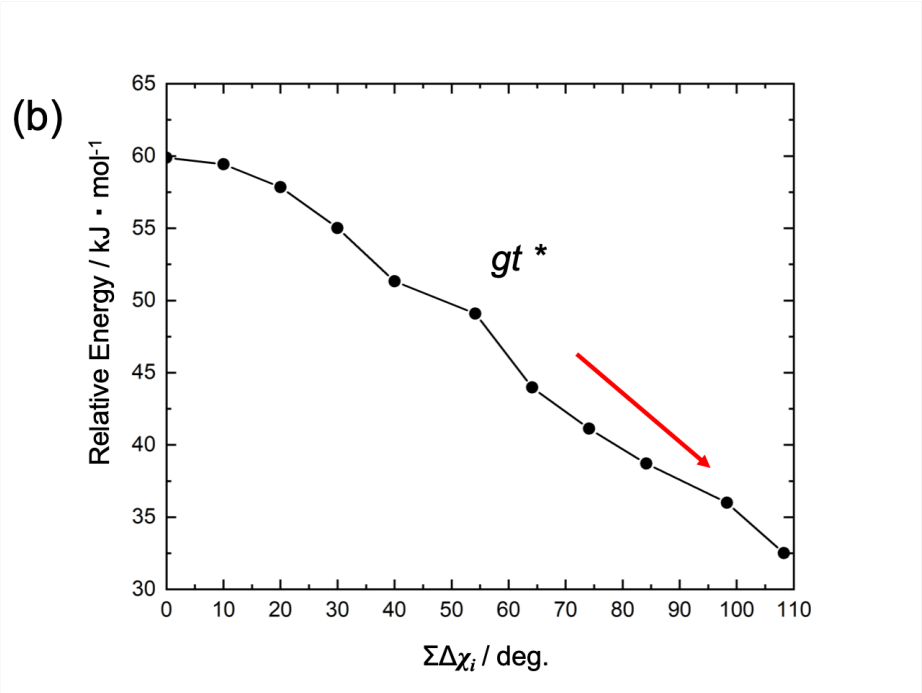

Fig.4-14. (a) The PES of ω-χ_3 at *gt* (b) The cross section of (a), which correspond to energy minimization pathway from *gt** to *gt*-A.

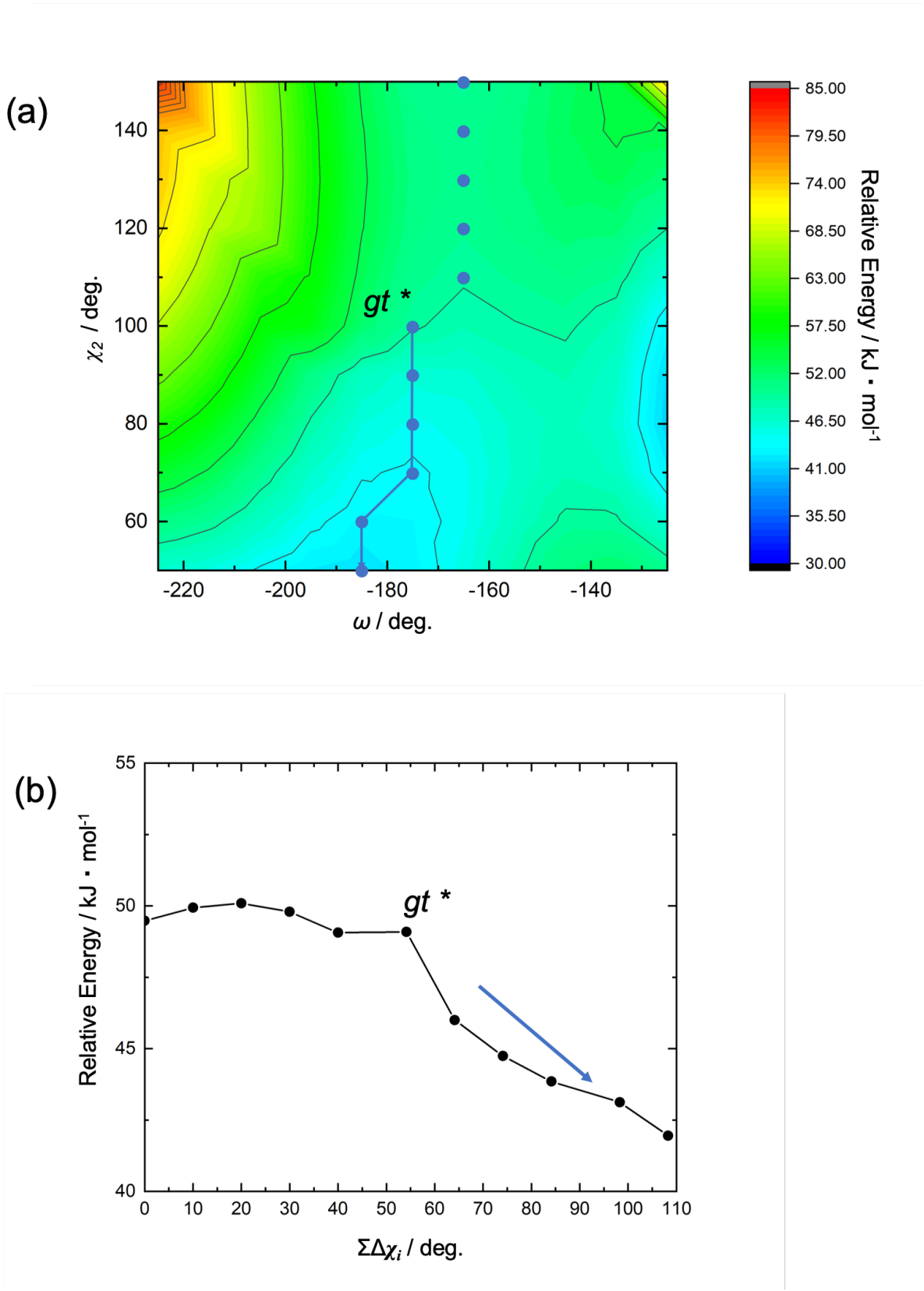

Fig. 4-15. (a) The PES of ω-χ_6 at *gt* (b) The cross section of (a), which correspond to energy minimization pathway from *gt** to *gt*-B

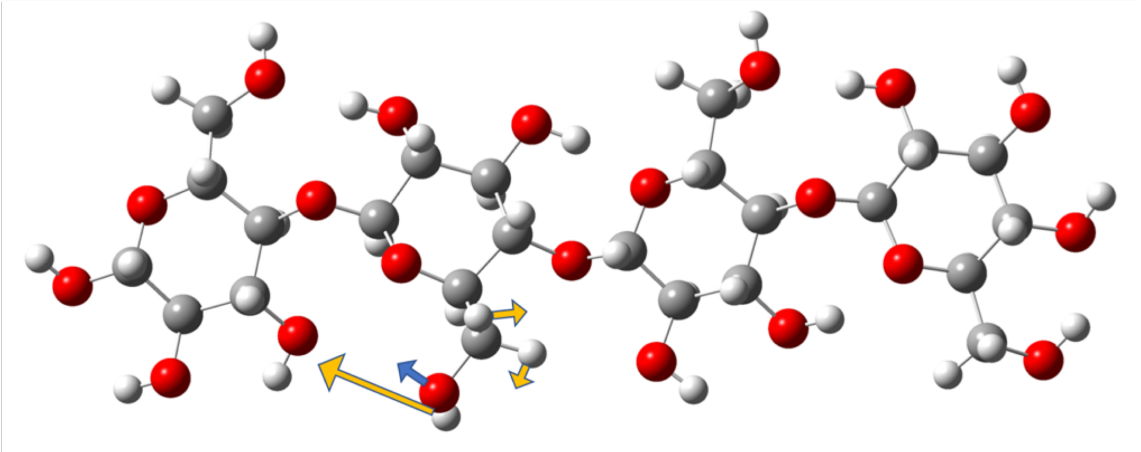

Fig.4-16. The negative vibrational mode (-18.68 cm^{-1}) in *gt** structure. This mode has a large amplitude rotation of O6-H (χ_6).

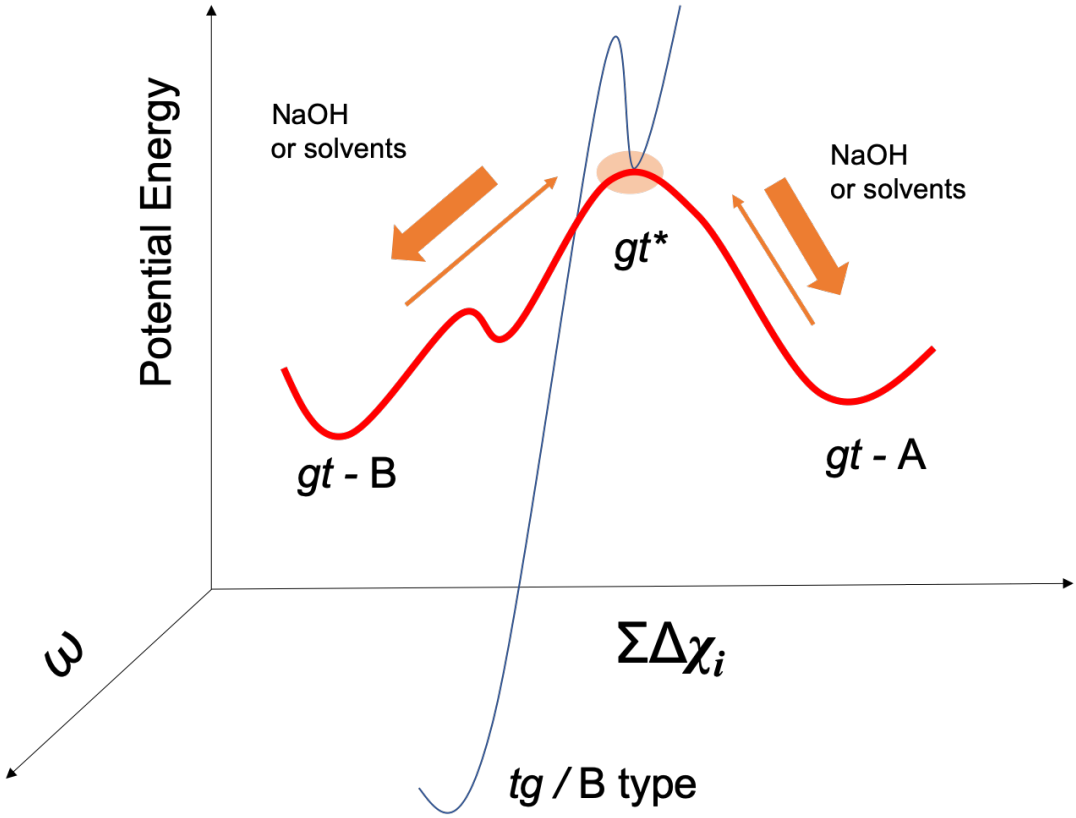

Fig.4-17. chematic diagram of hydrogen bond reconstruction of the *gt* conformation. For the C6 conformational change, the hydrogen bond between O3 and O6 has to be broken and pass through *gt** as the meta-stable state. Even though the hydrogen bond reconstruction is preferred, the C6 conformation changes to *tg*.

4.3.3. Pathway to the tg or gt conformation from gg

The previous PES analyses show that the *tg** or *gt** state of cellulose molecules without hydrogen bonds between O6 and O2' or O3'' will eventually generate *gt* , and it might be very rare or impossible to construct *tg* as a stable state. However, any cellulose produced by biological systems (e.g., plants or algae) has the structure of cellulose I and its C6 conformation is *tg*. Therefore, the possible pathways that can transform cellulose to the *tg* conformation should be explored. According to ^{13}C NMR studies, the C6 chemical shift of dissolved cellulose has been reported as 61 ppm corresponding to *gg*. Several modeling studies have reported on the conformations of cellulose and cellulose synthetase BcsB and BcsD, in which cellulose in BcsB [9] or BcsD [10] has a *gg* conformation. Therefore, it is appropriate to assume that the crystallization process will starts from the *gg* conformation in the biosynthetic process. ω-χ_2 PES was calculated with χ_6 fixed to the position that is a similar value to the *tg*-A type (χ_6 = 160 °; Fig. 4-18). The result shows that the most stable state in the *gg* conformation is the state without hydrogen bonds for (O2'-O6) (*gg*-free). However, the metastable point corresponding to the *gg* conformation with O2-O6 hydrogen bonds (ω = 60 °) was also found, designated as *gg** (Figs. 4-19). Even with the *gg* conformation, the molecule might have a weak hydrogen bond (O2'-O6) with slight steric distortion. The energy differences between *gg*-free and *gg** are summarized in table 4. The *gg** state is energetically meta-stable and ω can change from *gg** to *tg* along the pathway with similar activation energy from *gg** to *gg*-free (Fig. 4-20 and Fig.4-21). In order to generate the *tg* conformation, the hydrogen bond (O2'-O6) has to be constructed before the C6 conformational change, since there will be another possible pathway from the *gg*-free to the *gt* conformation, otherwise the conformation will transform to *gt*. Accordingly,

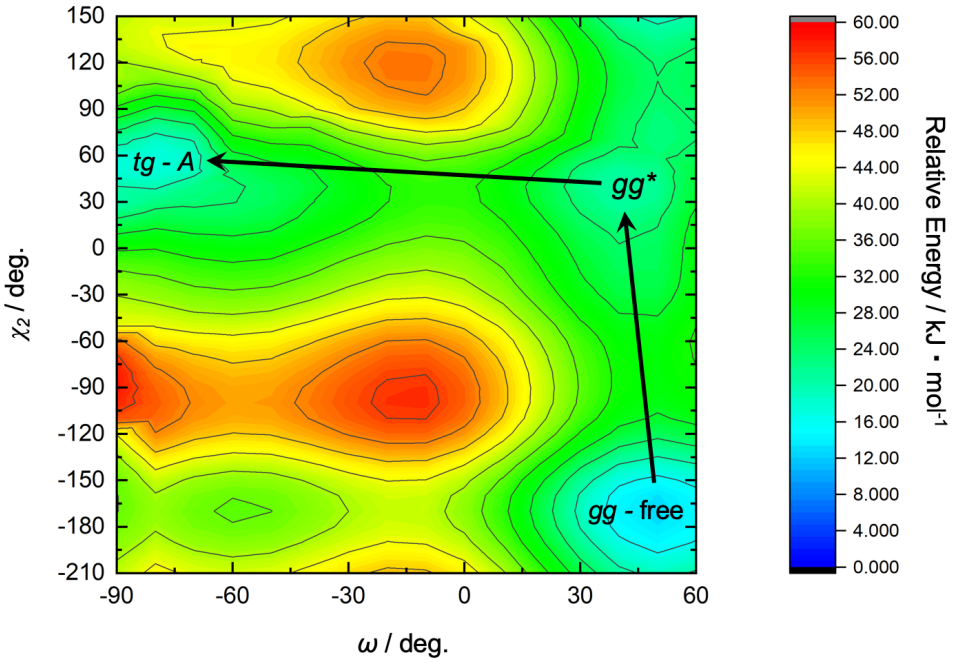

Fig.4-18. 2D-PES of ω and χ_2 as degrees of freedom for the *gg* conformation. The local minimum at the coordinates: (ω, χ_2) = (50, -180) indicates *gg*-free, (ω, χ_2) = (-80, 60) indicates the *tg*-A type conformation, and (ω, χ_2) = (40, 50) indicates *gg**.

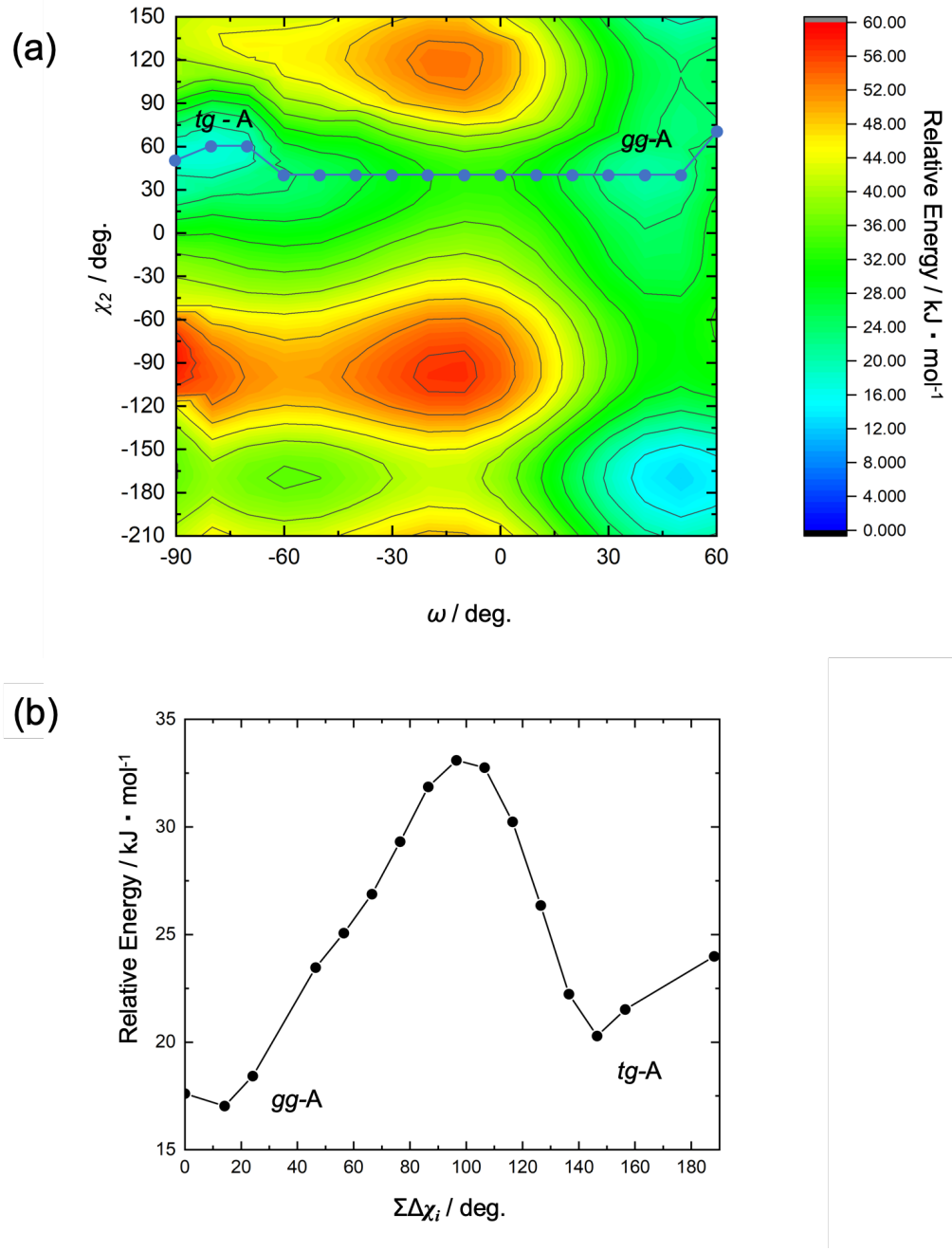

Fig.4-19. (a) The PES of ω-χ_3 (b) The cross section of (a), which correspond to energy minimization pathway from *gt** to *gt*-A.

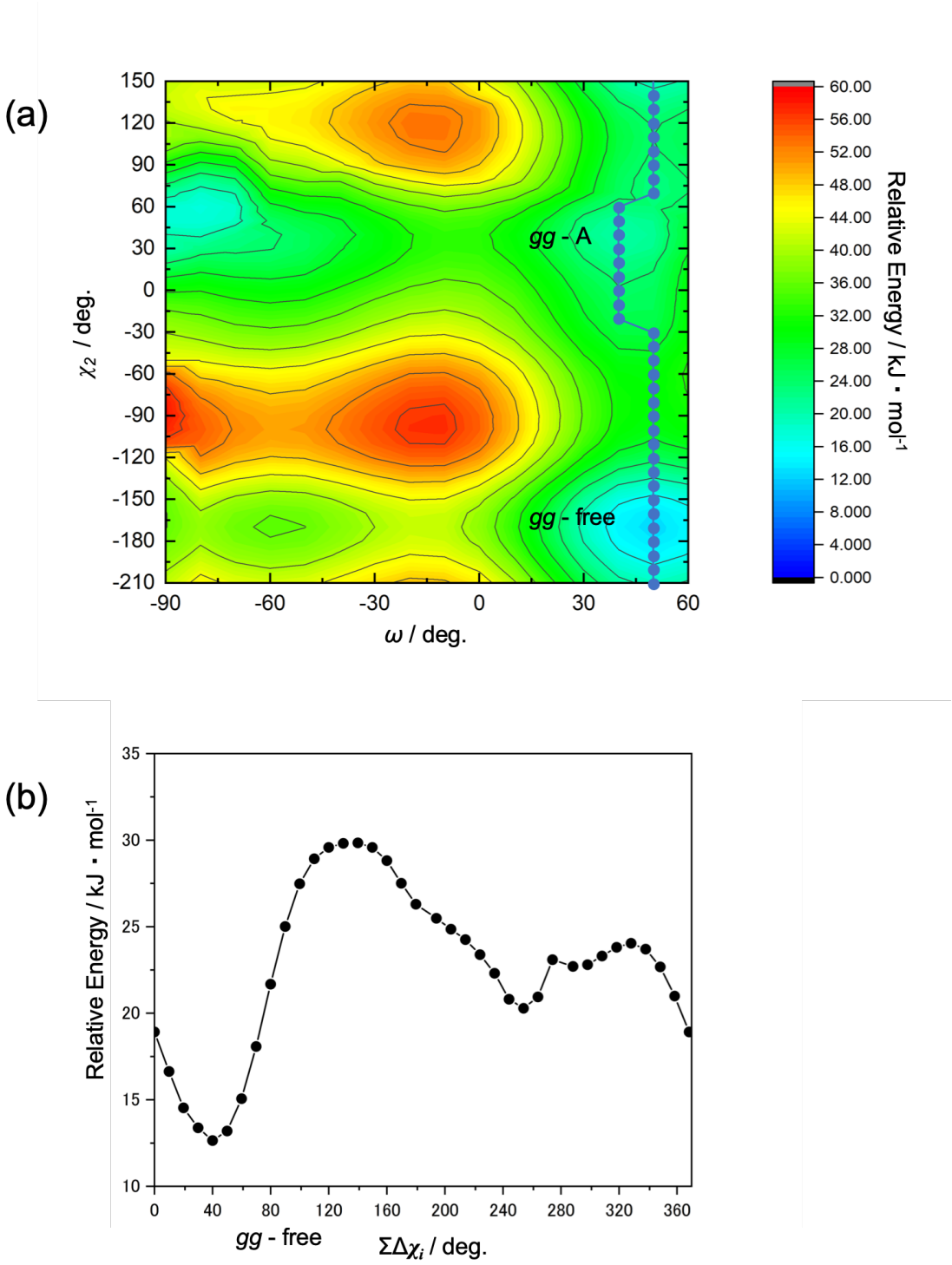

Fig.4-20. (a) The PES of ω-χ_6 (b) The cross section of (a), which correspond to energy minimization pathway from *gt** to *gt*-B

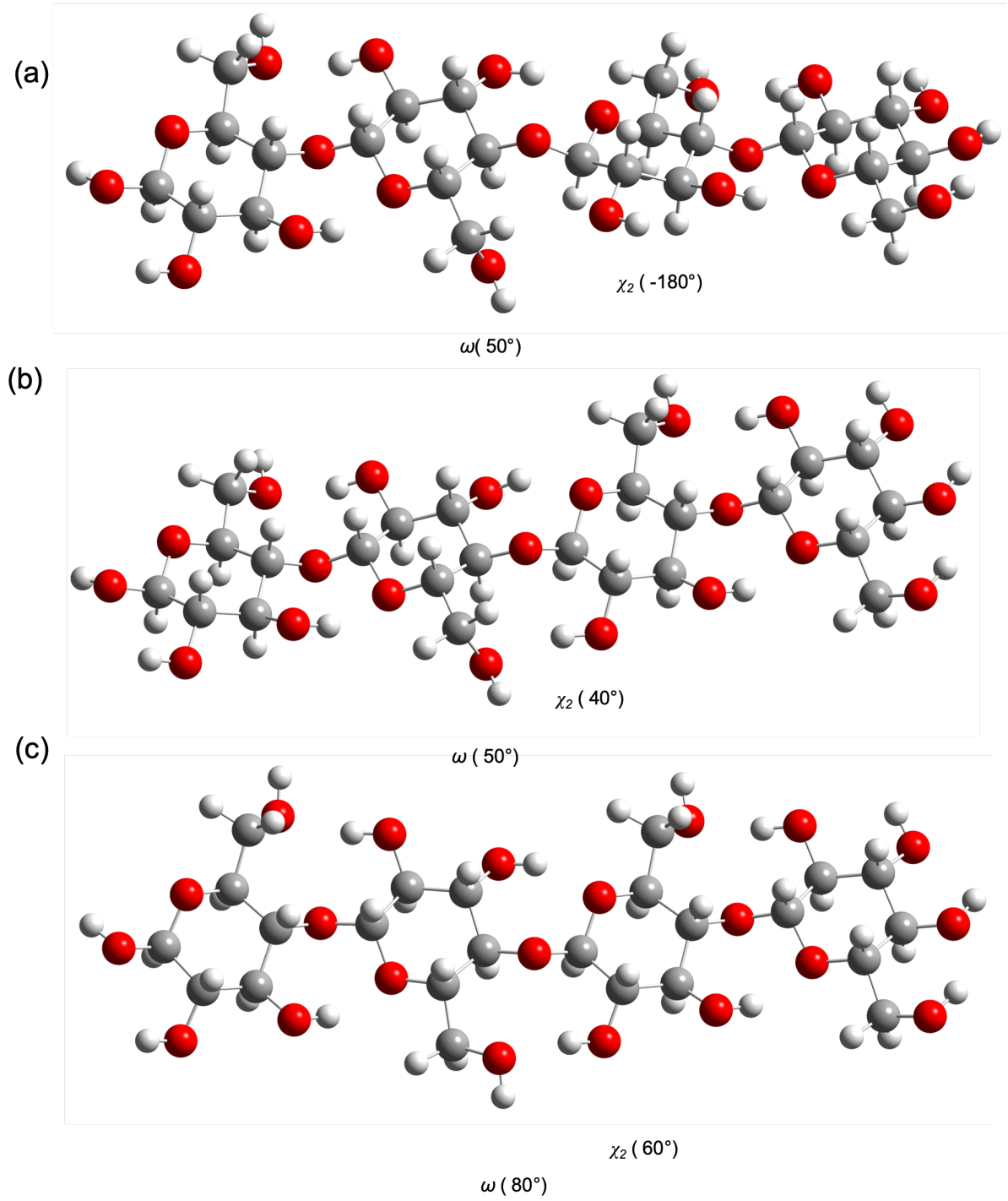

Fig.4-21. he structures which correspond to *gg*-free (a), *gg*-free, (b) gg*, and *tg*-A (c).

in biological systems during cellulose synthesis or crystallization, an initial *gg*-free cellulose may receive some stereochemical force to construct the *gg** state or to inhibit a path from *gg*-free to *gt*. At the moment, since the precise mechanisms of cellulose synthesis by enzymes are uncertain, it cannot be stated clearly the mechanism of *tg* generation. However, the present study based on DFT calculations of the simple cellotetraose model could provide insight into the mechanism which can produce cellulose I with the *tg* conformation.

4.3.4. The change of hydroxyl conformation and hydrogen bond in cello-trtraose with Na ion

It has been reported in the research of mercerization mechanism, Na-cellulose is thought to be constructed [11]. Thus, Na ion has a key role to convert C6 conformation from *tg* to *gt*. For C6 conformational change, hydrogen bonds disruption especially related to O6-H can be thought to be needed. The 1D PES of Cello-tetraose model accompanied by a Na^+ ion was conducted by DFT calculation with χ_2 as a parameter. Fig. 4-22 shows the 1D PES of the model along χ_2 direction. Initial structure, which was cellotetraose-*tg*-A type structure accompanied by Na^+ ion, was unstable than that of *tg** type structure interacted with Na^+. Fig.4-23 shows structural change along the PES shown in Fig. 4-22. Transition state was shown as the peak top of the pes line. The normal mode vibrational analysis revealed that the structure which corresponds to the structure of peak top has only one mode of imaginary frequency corresponding to the hydrogen bond construction or disruption. The energy difference was summarized in Fig. 4-24. Therefore, Na ion can disrupt the O2-O6 hydrogen bonds and stabilize the unstable *tg** state. For elucidation of Na+ ion removement, another calculation is thought to be needed.

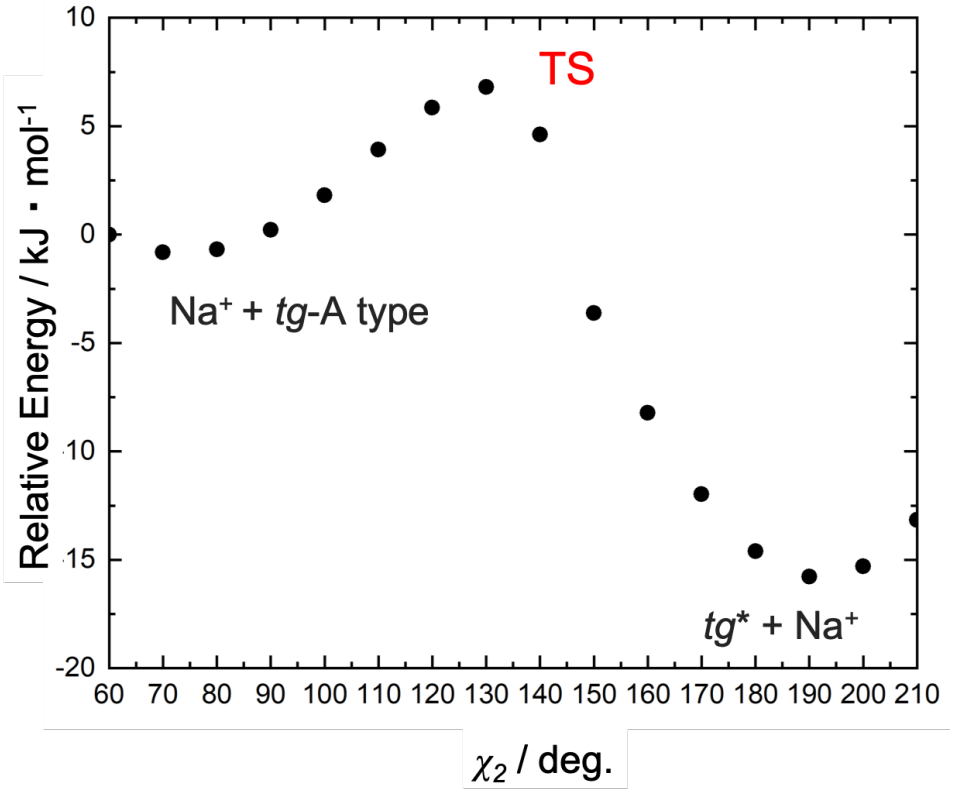

Fig. 4-22. 1D PES of χ_2 on tg-A + Na^+ ion model

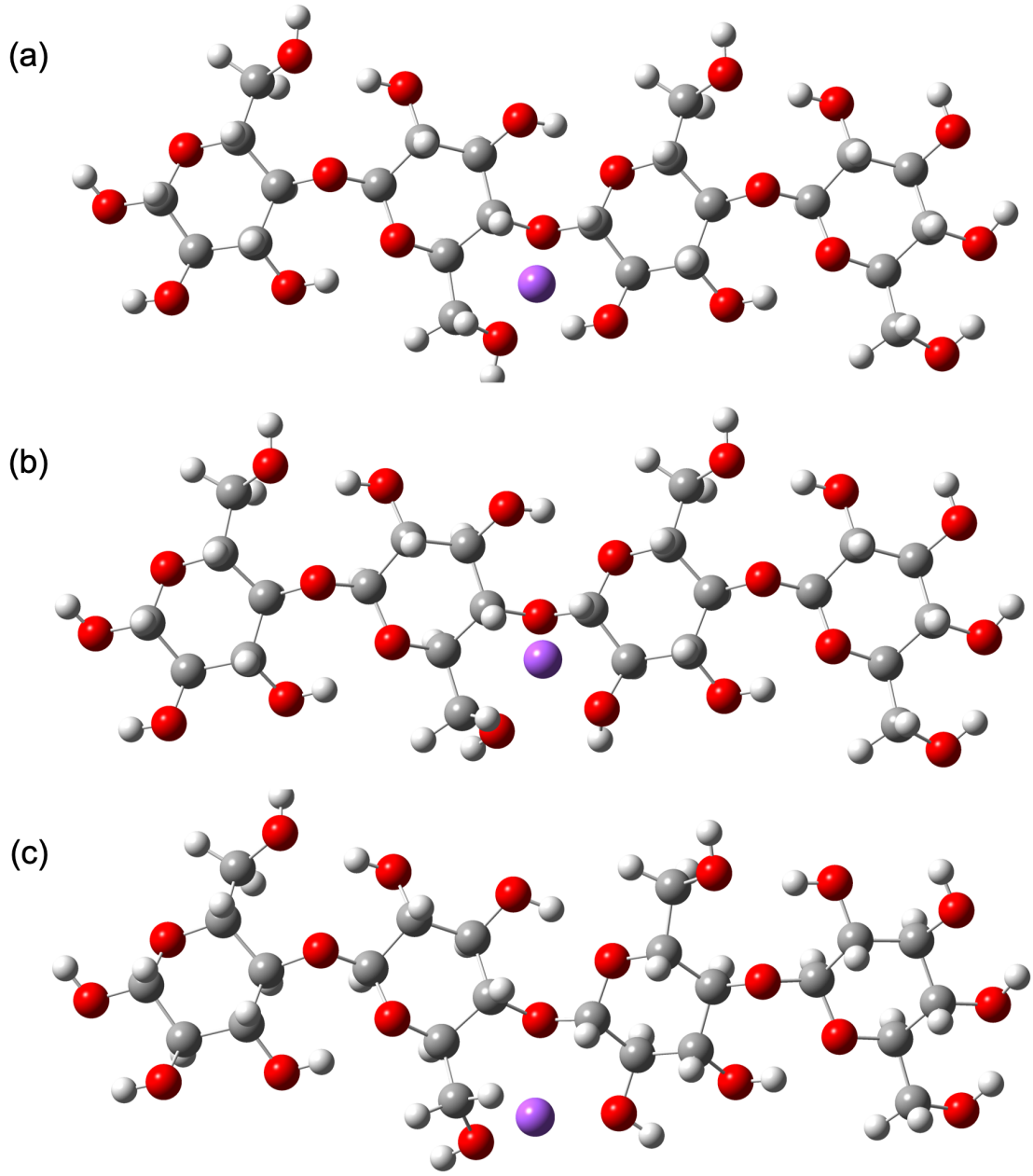

Fig.4-23.The change of the conformation on 1D PES of χ_2 on tg-A + Na^+ ion model as shown in Fig.4-22. (a) initial structure (b) the structure correspond to transition state and (c) most stable structure

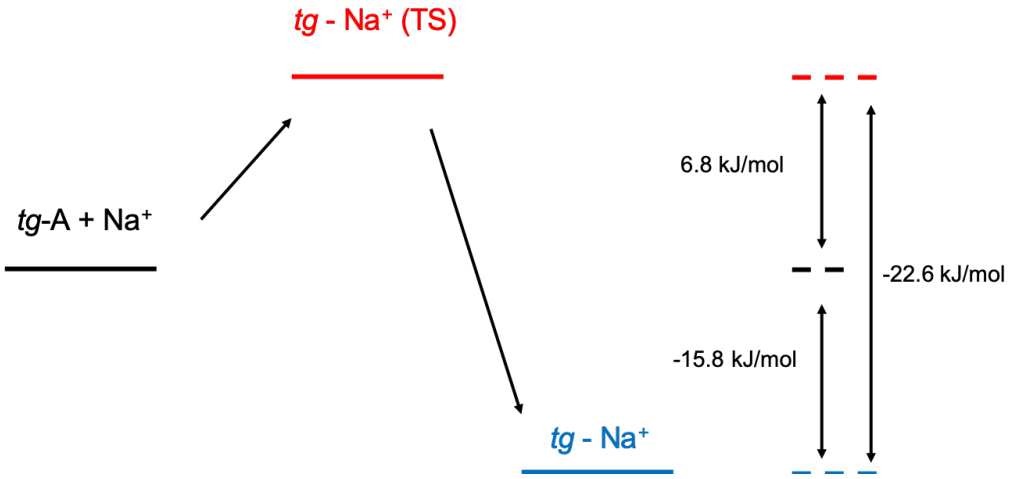

Fig.4-24. Energy diagram of 1D PES of χ_2 on tg-A + Na^+ ion model

4.4. Conclusions

PES calculations by DFT on the simple cellotetraose molecule as the model of cellulose focusing on the conformation of C6 and intra-molecular hydrogen bonding were carried out. The result clarified the mechanisms of the transitions among three kinds of C6 conformations of single-chain cello-trtraose, namely *gg*, *gt*, and *tg*. The hydrogen bond disruption of (O2'-O6) plays an important role in the transition from *tg* to *gt*. In particular, this work could provide important view related to cellotetraose that may give insight into the mechanism of *tg* generation in biological systems in which the process relies on hydrogen bond construction between (O2'-O6) before conformational changes. Based on this result, it is suggested that there might be the specific interactions between cellulose molecule and cellulose synthetase complex before crystallization process. Further computational approaches such as QM and MD on the more extended molecules are proceeding and will be published near future.

Rererences

[1] F. Horii, A. Hirai, R. Kitamaru, Solid-state ^{13}C-NMR study of conformations of oligosaccharides and cellulose - Conformation of CH2OH group about the exo-cyclic C-C bond, Polymer Bulletin. 10 (1983) 357–361. doi:10.1007/BF00281948.

[2] Y. Nishiyama, G.P. Johnson, A.D. French, V.T. Forsyth, P. Langan, Neutron Crystallography , Molecular Dynamics , and Quantum Cellulose I, Biomacromolecules. 9 (2008) 3133–3140. doi:10.1021/bm800726v.

[3] P. Chen, Y. Nishiyama, J.L. Putaux, K. Mazeau, Diversity of potential hydrogen bonds in cellulose I revealed by molecular dynamics simulation, Cellulose. 21 (2014) 897–908. doi:10.1007/s10570-013-0053-x.

[4] P. Langan, Y. Nishiyama, H. Chanzy, A revised structure and hydrogen-bonding system in cellulose II from a neutron fiber diffraction analysis, Journal of the American Chemical Society. 121 (1999) 9940–9946. doi:10.1021/ja9916254.

[5] H. Miyamoto, M. Umemura, T. Aoyagi, C. Yamane, K. Ueda, K. Takahashi, Structural reorganization of molecular sheets derived from cellulose II by molecular dynamics simulations, Carbohydrate Research. 344 (2009) 1085–1094. doi:10.1016/j.carres.2009.03.014.

[6] Y. Nishiyama, P. Langan, H. Chanzy, Crystal Structure and Hydrogen-Bonding System in Cellulose Iβ from Synchrotron X-ray and Neutron Fiber Diffraction, Journal of the American Chemical Society. 124 (2002) 9074–9082. doi:10.1021/ja0257319.

[7] J. Da Chai, M. Head-Gordon, Long-range corrected hybrid density functionals with damped atom-atom dispersion corrections, Physical Chemistry Chemical Physics. 10 (2008) 6615–6620. doi:10.1039/b810189b.

[8] F. Porro, O. Bédué, H. Chanzy, L. Heux, Solid-state ^{13}C NMR study of Na-cellulose complexes, Biomacromolecules. 8 (2007) 2586–2593. doi:10.1021/bm0702657.

[9] J.L.W. Morgan, J.T. McNamara, J. Zimmer, Mechanism of activation of bacterial cellulose synthase by cyclic di-GMP, Nature Structural and Molecular Biology. 21 (2014) 489–496. doi:10.1038/nsmb.2803.

[10] S.-Q. Hu, Y.-G. Gao, K. Tajima, N. Sunagawa, Y. Zhou, S. Kawano, T. Fujiwara, T. Yoda, D. Shimura, Y. Satoh, M. Munekata, I. Tanaka, M. Yao, Structure of bacterial cellulose synthase subunit D octamer with four inner passageways, Proceedings of the National Academy of Sciences. 107 (2010) 17957–17961. doi:10.1073/pnas.1000601107.

[11] T. Okano, A. Sarko, Intermediates and a Possible Mercerization Mechanism, Jouranal of Applied Polymer Science. 30 (1985) 325–332.

Chapter 5. Concluding Remarks

Chapter 2

The change of the crystallinity, surface structure fraction and the ratio of cellulose I and II by mercerization was analyzed using solid state ^{13}C CP/MAS NMR measurement. Two types of surface model was applied; one model was defined as inner and outer surface distinguished by C6 conformation and other model was defined as accessible and inaccessible surface. Both model shows non-crystalline surface region increased during mercerization; the decrease of cellulose I resulted in not increasing of cellulose II but increasing of non-crystalline region. It was implied that non-crystalline region was located surrounding crystal core.

Chapter 3

For improving the crystallinity of cellulose II, post-treatment by low concentration NaOH aqueous solution was applied for mercerized cellulose. The change of crystallinity, surface fraction and crystal size was analyzed based on solid state ^{13}C CP/MAS NMR measurement and X-ray diffraction study. The change of Crystallinity Index obtained from solid state ^{13}C CP/MAS NMR was good agreement with that of crystal size obtained by X-ray diffraction. Increasing crystal size coincided with decreasing inaccessible surface. Moreover, the change enhanced by high-temperature NaOH treatment and also neutralization by strong acids consisted by cosmotropic anion. These results indicates crystallization of cellulose II is independent from mercerization or regeneration of cellulose, which is correspond to the transition from cellulose I to II and surface structure is strongly related to the crystallinity of cellulose.

Chapter 4

C6 conformational change was examined by DFT calculation of cello-tetraose model. *tg* conformation, which corresponds to the C6 conformation of cellulose I, is preferentially changes to *gt*, which corresponds to the C6 conformation of cellulose II via transition state *tg**. For constructing tg, one possible pathway was shown; *gg* conformation constructs a hydrogen bond between O2 and O6 with certain torsion and subsequently rotating C6

conformation to *tg*. The pathway has a energy barrier and some other driving force is needed. Moreover, the stability of the C6 conformation depend on surrounding environment. More large-scale modeling or simulation is needed for further understanding of C6 conformational change directly explaining the mechanism of crystal transition or crystallization. However, the obtained result in this chapter can gives the basis of these simulation.

As summarized above, the author gave insights into the construction of less crystalline cellulose II structure and difficulty of the constructing the conformation correspond to cellulose I. In addition, solid state NMR approach for elucidating surface structures of cellulose crystal is effective for crystallinity evaluation. Conventionally, cellulose II was thought to be difficult to highly crystalline. However, even cellulose II materials can construct high mechanical properties. For elucidating the crystal or hierarchical structure transition mechanism, structural analysis and computational simulation is required. The author believes that the research explained here is the basis for the elucidation research and can construct part of the basis of them.

Acknowledgements

I would like to express my great appreciation to Associate Professor Tomoki Erata (Hokkaido University) for his continuous guidance and encouragement in the entire work of this work. I wish to special thanks to Assosiate Professor Shin-ichiro Sato and Associate Professor Kenji Tajima, (Hokkaido University) for continuous constructive suggestion and discussion. I would like to acknowledge Professor Mutsumi Takagi, Assistant Professor Masashi Fujiwara (Hokkaido University) for their valuable advice and encouragement.

I would like to acknowledge Dr. Toshifumi Hiraoki (Hokkaido University) for valuable advice and experimental construction regarding NMR techniques, Professor Thomas Rosenau, Dr. Markus Bacher (University of Natural Resources and Life Sciences, Vienna) and Porfessor Hiroyuki Kono (Tomakomai National College of Technology) for valuable advice and experimental methods and analysis construction regarding NMR techniques.I would like to thank The High Brilliance X-ray Laboratory, Hokkaido University for allowing the utilization of their X-ray diffractometer.

I would like to Ms. Ayaka Makino and Yuki Kugo for continuous cooperation and assistance for the work. I would also like to thanks to the members in this laboratory for their assistance.